Durham E-Theses

Antibacterial Functional Surfaces

SAMANTHA NOHEMI BARRIENTOS-PALOMO

How to cite:

Use policy

Antibacterial Functional Surfaces

Samantha Nohemi Barrientos-Palomo

PhD Thesis

Department of Chemistry

Durham University

2021

Declaration

The work described in this thesis was undertaken at Durham University Chemistry Department between October 2015 and June 2019. It is the original work of the author except where otherwise stated or acknowledged and has not been submitted for a degree in this or in any other university.

Statement of Copyright

Acknowledgments

I want to thank Chemistry Stores, and the Electronics, Glassblowing, and Mechanical Workshops, for all their help and support, which played a key role in each experimental chapter.

The work in this thesis was carried out in the Chemistry lab CG098 and the Biology lab CG229.

List of Collaborative Publications

1.- Ritchie, A. W.; Cox, H. J.; **Barrientos-Palomo, S. N.**; Sharples, G. J.; Badyal, J. P. S. Bioinspired Multifunctional Polymer–Nanoparticle–Surfactant Complex Nanocomposite Surfaces for Antibacterial Oil–Water Separation. *Colloids Surf. A* **2019**, *560*, 352–359.

2.- Wilson, M.; **Barrientos-Palomo, S. N.**; Stevens, P. C.; Mitchell, N. L.; Oswald, G.; Nagaraja, C. M.; Badyal, J. P. S. Substrate-Independent Epitaxial Growth of the Metal–Oganic Framework MOF-508a. *ACS Appl. Mater. Interfaces* **2018**, *10(4)*, 4057–4065.

3.- Gürsoy, M.; Harris, M. T.; Downing, J. O.; **Barrientos-Palomo, S. N.**; Carletto, A.; Yaprak, A. E.; Karaman, M.; Badyal, J. P.S. Bioinspired Fog Capture and Channel Mechanism Based on the Arid Climate Plant *Salsola crassa*. *Colloids Surf. A* **2017**, *529*, 195–202.

Abstract

Development of antibacterial surfaces is a technological strategy of great importance in different healthcare and economic spheres, due to the versatility of using a variety of bulk materials with customised surface functionality. Currently, these antibacterial functionalised materials are needed given the antimicrobial resistance has become a major threat for the healthcare and food-production sectors worldwide. This thesis presents introductory discussion about what antibacterial surfaces are and why they are important, explains experimental techniques used, and proposes three different approaches of antibavcterial coatings whose chemical properties were studied and corelated to their corresponding antibacterial activities.

The first proposed approach is the surface immobilisation of chitosan on pulsed plasma deposited poly(glycidyl methacrylate) coatings, where amine and hydroxyl groups of chitosan undergo nucleophilic substitution with epoxide groups of the plasma deposited films leading to surface tethering of the biopolymer. These cloths were effective at killing *Staphylococcus aureus* and *Escherichia coli*.

The second approach is the atomised spray plasma deposition of poly(acrylic acid) coating, that displayed high antibacterial efficiency against *E. coli* which is attributed to the high retention of the functional carboxyl group and its easiness to be deprotonated in aqueous media.

The third proposed approach is the atomised spray plasma deposition of metallosurfactant/polymer coatings that showed high antibacterial efficiency against *S. aureus* and *E. coli* within minutes of interaction time, due to the antibacterial properties of metallosurfactants where metal ions were complexed with cationic or non-anionic with doubly hydrophobic alkyl chain surfactants. An estimation of the possible antibacterial mechanism is discussed by testing different mutant *E. coli* strains. Furthermore, these samples showed antibacterial activity after reuse from one antibacterial test to another for several times after rinse with water.

The work concludes with an overall discussion and conclusion about the three experimental approaches, and with corresponding appendices showing detailed data from antibacterial test results.

Table of Contents

List of Schemes

List of Figures

List of Tables

1. Introduction

1.1. Antibacterial Surfaces

1.1.1. Introduction

Antimicrobial resistance (AMR) is a major threat for the healthcare and food-production sectors worldwide.[1] AMR has been worsening during the last decades due to the emergence of drug-resistant microorganisms, in part due to inappropriate usage of antibiotics in human and animal health.[2,3] This has resulted in higher medical costs and increasing mortality, due the lack of new antimicrobial agents to treat these so-called "superbugs".[4,5] There will be consequences for multiple different sectors regarding AMR, if new antimicrobial agents or approaches are not developed. For healthcare, the current antimicrobial agents may not be effective for certain human infections over the next 30 years with the costs linked to bacterial infection estimated to be 3.1% GDP (ranging from 2.3% in all Organisation for Economic Co-operation and Development, Europe Union, and European Economic Area countries, to 10% in Sub-Saharan Africa in the absolute resistance scenario),[6] and it is estimated that antimicrobial resistance will be the cause of a total of 350 million deaths, according to the World Health Organization (WHO).[7] To overcome this problem, different approaches have been employed to mitigate the spread of multi-drug resistant bacterial diseases propagated through contaminated surfaces due to biofilm formation. The work presented in this thesis proposes three different approaches for the immobilisation of antibacterial agents onto surfaces by applying diverse precursors and techniques, which can be adapted to a variety of uses.

1.1.2. Antibacterial Resistance

Antibacterial resistance is a natural evolutionary process in bacteria, driven by mutation of antibiotic targets within cells, transmission of resistance traits between strains and species and other environmental factors. Where

antibiotics are in regular use, either in their environment or in their host (e.g., humans, animals or plants), a selective pressure is imposed whereby only resistant organisms can survive and proliferate.[8–11] Consequently, bacteria naturally evolve mechanisms or enzymatic alterations to resist antimicrobial agents.[12,13] Bacteria are able to develop resistance through different routes, including the following mechanisms: (a) modifications to block entry of antibiotics by altering porins on the bacterial cell wall, sometimes leading to antibiotic degradation before it reaches the periplasmic space; (b) mutation of penicillin binding proteins (PBPs), by changing their active sites, diminishing sensitivity towards penicillins, cephalosporins, and other β-lactams; (c) enzymatic inhibition: bacteria produce enzymes to deactivate the antibiotic; (d) alteration of the target molecule: producing a decreased affinity of the antibiotic; (e) efflux pumps: some Gram-negative bacteria have the capacity to pump out antibiotics preventing an effective antibiotic concentration inside the bacterial cell; Figure 1. 1.[12–15]
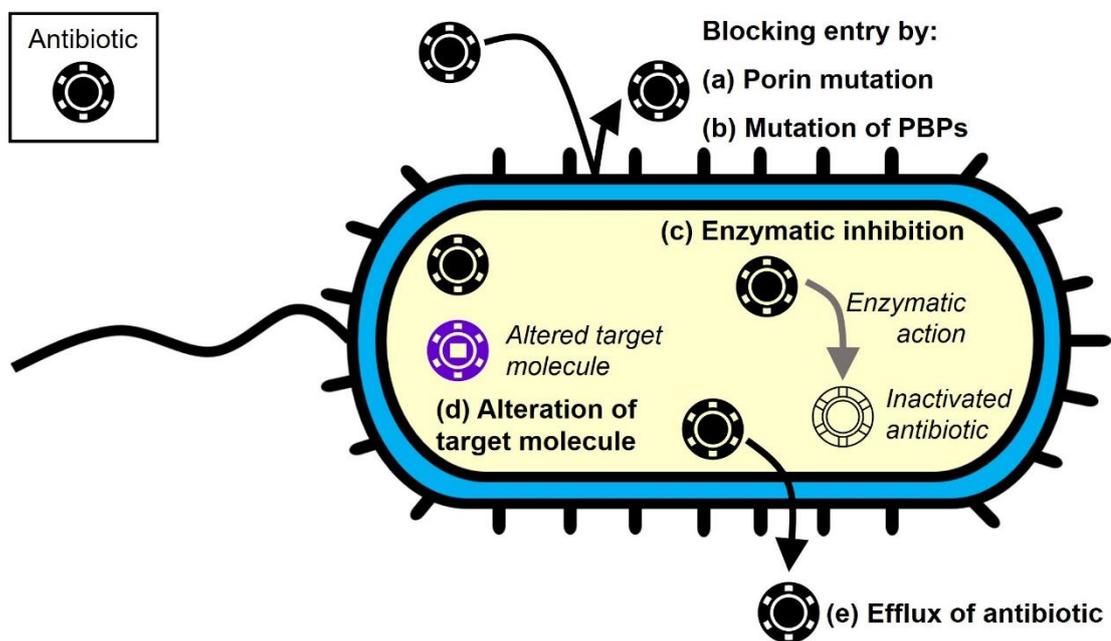
Figure 1. 1: Mechanisms of antibiotic resistance in bacteria: (a) blocking entry of antibiotic into the bacterial cell by porin mutation; (b) blocking entry of antibiotic into the bacterial cell by mutation of PBPs; (c) enzymatic inhibition; (d) alteration of target molecule; (e) efflux pumps.[13] Figure adapted from Tortora et al.[12]

Furthermore, the frequent use of antimicrobial agents against microbial infections or contamination has led drug-resistant microorganisms to survive or multiply despite being exposed to antimicrobial agents in doses equal or higher than recommended, making them ineffective, reducing infection treatment options.[9,16–19] Therefore, in order to successfully manage bacterial infection, it is important to promote public awareness, and global surveillance, funds, and coalition to achieve genuine action. This could include preventing the spread of infections with proper sanitation, reducing antibiotic use, investing in new and alternative antimicrobials, accurately check bacterial susceptibility to antibiotics and determine their ability to suppress and to kill bacteria, so the chemical agents are not used irresponsibly, as well as to recognise and support scientists working in this field.[2,20] For instance, in the United Kingdom (UK), the Advisory Committee on Dangerous Pathogens (ACDP) provides advice to workers and others at risk from exposure to dangerous pathogens (i.e., biological or infectious agents) in the workplace or through workplace activities.[21] ACDP lists biological agents per hazard groups, from low risk to high risk. However, institutions worldwide have different hazard classification, depending on geography, the incidence of microorganisms, their vectors, associated diseases and levels of hygiene.[22]

Nevertheless, apart from the aforementioned main antibiotic resistance mechanisms of individual bacteria, the formation of bacterial biofilms increases the antibacterial resistance even more by physically obstructing antibacterial agent penetration inside the bacterial cell.[12] Thus, the susceptibility of biofilms to antimicrobial agents should be tested against biofilm-associated organisms simulating conditions *in vivo*, rather than standard microdilution testing that relies upon the response of planktonic bacteria instead of surface-associated structures.[23] Therefore, new and alternative strategies are needed to limit infections and contamination on surfaces, which are of high importance for biomedical, commercial, and industrial fields, and domestic use.

1.1.3. Biofilms

Bacteria rarely live in isolated single-species colonies, and if they grew in a uniform monolayer, nutrients would not be able to reach the lower depths of the film, and toxic wastes could accumulate. Instead, they collaborate to live in macroscopic communities known as biofilms, which are complex structures whose morphology and physicochemical composition vary depending on the type or microbes present, strains, surface involved, and environmental conditions.[24–26] Chemically, biofilms are composed of an exopolysaccharide matrix (i.e., glycocalyx[27]), containing organised bacterial microcolonies with functional heterogeneity, proteins, teichoic acids, and extracellular DNA,[24] allowing aggregation and cell-to-cell communication between cells, and form synergistic microconsortia, with their interactions and gradients.[27] The biofilms' morphology can consist of amorphous, mushroom- or pillar-like structures separated by water-filled spaces that expose bacteria to a continuous flow of nutrients, developing an extracellular digestive system that also allows the excretion of waste through the current flow.[27,28] These physical and chemical features protect biofilms from degradation, desiccation, ultraviolet (UV) radiation, host humoral responses, antibiotics, and other chemicals which are sufficiently toxic to damage free bacterial cells.[23,24,29,30] This means that bacteria in nature are more resistant to antimicrobial agents than if it were an isolated single bacterium-type colony, so antimicrobial agents that effectively work for a single cell may not work for the same kind of bacteria when found in a biofilm.

Biofilms appear when a single bacterium attaches to an organic or inorganic surface, although they can be made up of more than one bacterial species.[31] They have production cycles that generally comprise five steps: (a) attachment of single planktonic bacteria onto a surface by physicochemical forces such as hydrophobic, electrostatic, and van der Waals; (b) transition from reversible to irreversible attachment by secreted extracellular polymers; (c) early development of biofilm complex, by producing molecules on the bacterial cell surface that recognise adhesive molecules in the matrix, leading to agglomeration and development of the

biofilm matrix; (d) biofilm growth from microcolonies into a mature adhesive matrix that traps nutrients from the environment to continue the life-cycle, whose structure is specific for each bacteria species; and (e) dispersion of single cells from the biofilm to restart the cycle on a fresh surface and increase the biofilm extension.[24,32] Figure 1. 2.
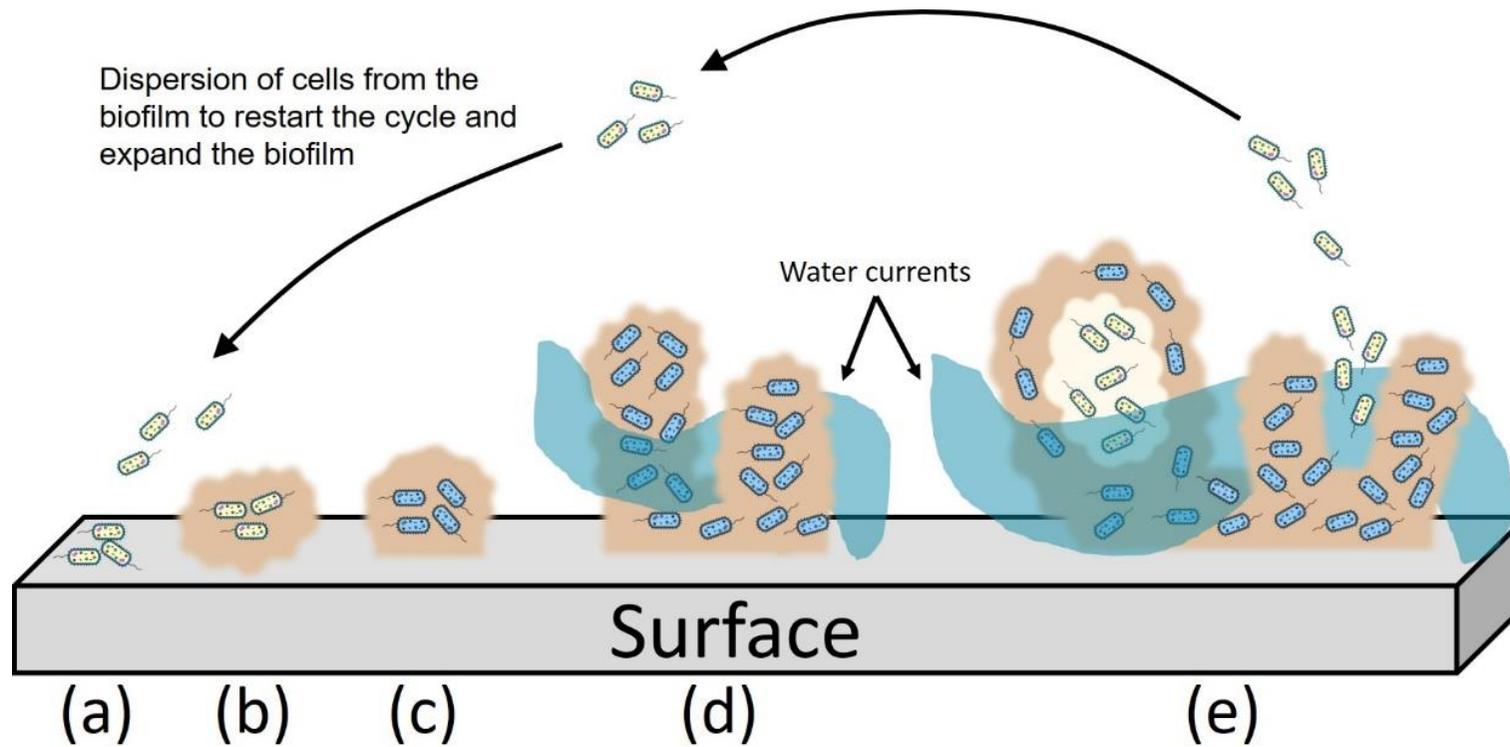
Figure 1. 2: Steps of biofilm formation: (a) attachment of single bacteria cells; (b) transition from reversible to irreversible attachment; (c) early development of biofilm complex; (d) biofilm growth into a mature adhesive matrix; (e) dispersion of single cells to restart the biofilm cycle.[12,24] Figure adapted from Tortora et al.[12] Biofilms are expressions of bacterial group behaviour. Cell density alters gene expression in bacterial cells in a process known as quorum sensing, which is the ability of bacteria to communicate and coordinate behaviour, so they secrete a signalling chemical (i.e., inducer) to the surrounding medium in order to attract more bacterial cells and promote biofilm-forming behaviours.[12,23]

As expected, the aforementioned physicochemical features of biofilms promote resistance to antimicrobial agents.[33,34] The mechanisms of resistance in the biofilm implies the physical exclusion of the antimicrobial agent at the time the cell density increases and individual bacteria in the biofilm improve their antimicrobial resistance.[32] When pathogens form biofilms on tissues (e.g., organs, mouth, bones) or surfaces disturbing their proper functionality (e.g., medical devices, lenses, pipes), this can result in infection or disease for humans, plants, animals, pipes, and biomedical devices, because bacterial biofilms exhibit a significantly decreased susceptibility (10–1000 times[32,35]) to antimicrobial agents, compared to isolated bacteria.[24,32,36,37] Approximately 70% of human bacterial infections are estimated to involve biofilms.[12]

1.2. Antibacterial Emerging Approaches and Technology

Different approaches have been proposed to combat infections caused by bacterial biofilms,[24,38] given that they can interact with non-living matter surfaces in hospitals (e.g., bedrails, medical instrumentation, biomedical devices, catheters, etc.), homes (e.g., kitchens and toilets), and other public spaces (e.g., public toilets, restaurants, libraries, etc.) colonising them and making the bacteria within these complexes much more difficult to eradicate.[9,28]

Furthermore, various microorganisms relevant to public health represent a problem due to the infections and diseases they cause when forming biofilms. For instance, in the medical field, *E. coli*-containing biofilms can cause biliary tract infections, bacterial prostatitis and infections in urinary catheters,[39] while *S. aureus*-containing biofilms can grow on contact lenses,[40] mechanical heart valves, arteriovenous shunts, protheses and orthopaedic devices, representing a leading cause of nosocomial infections together with *S. epidermidis*.[41,42] In addition, varied infections and diseases also occur in both animals and humans due to the presence of biofilms in

non-medical areas such as water supplies and food products.[43] Overall, up to 80% of microbial infections in humans are related to biofilms.[39,44]

These diseases represent a critical problem due to their increment and reappearing, in addition to the emerging infectious diseases (EIDs) (i.e., bacterial diseases are not static[27]) which are infections that either appeared or evolved, and are increasing in incidence;[45,46] however, EIDs depend on different factors to emerge,[12] Figure 1. 3. The risk that those factors present depends on the geographical location of study because the environmental characteristic of a place directly affect the incidence of certain infectious diseases.[9,47] For instance, some regions in the world report specific resistant strains (e.g., *Mycobacterium tuberculosis*), while other countries report specifically insect-borne, bacterial-, and sexually transmitted infections, and AMR in general as major concerns, independently of the practices undertaken and structures designed to address the AMR issue.[48,49]
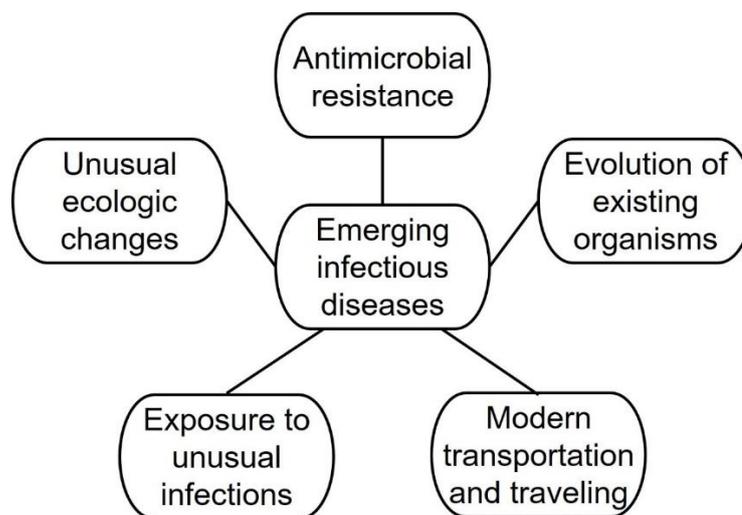
Figure 1. 3: Factors that contribute to the emergence of an infectious disease.[12]

To address the antimicrobial resistance problem, there has been some research to find efficient antimicrobial agents, approaches, and medical procedures, such as international action plans,[50–52] novel antibiotics and vaccines,[53–55] metals,[56,57] metal complexes,[58,59] novel materials,[60] nanomaterials,[61] application of plant-derived antimicrobials,[62–64] alternative therapies,[33,65,66,] rapid antibiotic susceptibility tests to avoid the widespread

overuse and misuse of antibiotics,[67–69] application of electromagnetic fields,[70] and antimicrobial surfaces.[71–75]

It is worthy of mention that the use of materials coated with immobilised antimicrobial agents, applying different techniques, is a field that is rapidly expanding, and flexibility is required to adapt to the specific needs of the application.[76] Thus, this thesis presents the synthesis and processing of antibacterial coatings, that offer alternatives to overcome infections occurring on everyday surfaces due to biofilm formation.

1.2.1. Antibacterial Surfaces

The concept of "antibacterial surface" corresponds to the surface of any material or agent that works to kill, prevent, or limit the growth and proliferation of bacteria. Antibacterial surfaces are considered important strategies to prevent the formation of intractable biofilms, rather than to develop an approach to remedy already colonised surfaces, and prevent infections derived from biofilm contamination.[77]

Given the current situation, several research groups are working on the development of intelligent materials to overcome and prevent infections caused by biofilms.[78] Regardless of the processing technique employed, antibacterial coatings are aimed at generating materials with bioactive properties, while retaining mechanical properties and enhancing features of the bulk material; those coatings must satisfy mechanical, tribological and chemical characteristics that make them compatible with the bulk material.[75] Furthermore, antibacterial coatings can be classified as antibacterial agent release, bacteria repelling, and contact killing coatings.[75]

The classification of antibacterial coatings is made according to the way the coatings interact with and against bacteria.[79,80] Therefore, antibacterial agent release coatings, as its name suggests, leach antibacterial agents to the surrounding environment over time, killing bacteria on top and around the treated surface,[75] such as the antibacterial coatings in Chapter 5. Bacteria repelling coatings are surfaces that resist bacteria attachment and possess

antimicrobial properties due to their complex topography rather than containing antimicrobials, without compromising cell compatibility for biomedical applications.[75]

Finally, contact killing coatings are developed either by creating nanostructured patterns that induce bacterial cell death by mechanical means,[81] or by immobilising antibacterial agents onto surfaces, which directly interact with pathogenic bacteria without releasing the bioactive agents,[82] such as the antibacterial coatings in Chapter 3 and Chapter 4. Nevertheless, these contact-killing antibacterial coatings have different antibacterial mechanisms due to their particular surface chemistry or physical nanopattern which lead to specific interactions against bacterial species.[81] On one hand, for the case of immobilised antibacterial agents onto surfaces, the mechanism of antibacterial activity will vary depending on the chemistry of these antimicrobial agents and the interacting bacterial species themselves, because chemical surface changes allow different interactions against bacteria;[83] for instance, specific agents (e.g., charged molecules,[84–87] metal ions,[88] functional polymers,[89] or combination of them) either kill or repel bacteria due to the nature of their characteristic functional groups, whilst antimicrobial complexes (e.g., antimicrobial peptides[90–92]) with non-specific antibacterial mechanism reach multiple targets of bacterial cells, resulting in a versatile approach to prevent diverse bacterial growth on surfaces. On the other hand, up to date there is no standardised antibacterial mechanism of nanopatterned surfaces due to the differences among specific geometric parameters at the nanoscale and, consequently, their antibacterial activity will depend on the elasticity of each particular bacterial cell wall species when they interact with these surfaces.[81–94]

Antimicrobial coatings represent useful strategies to prevent pathogens becoming resistant by supporting existing hygiene procedures and avoiding antibiotic-resistant bacterial attachment or development on surfaces, since high-touch surfaces are associated with infections.[95–98] Furthermore, the development of antimicrobial surfaces is not limited to bacterial infections (e.g., *Staphylococcus aureus* MRSA[99]), but also diseases caused by other type of pathogenic microorganisms, such as the fungal pathogen, *Candida auris*,[100] influenza[101] and Ebola viruses,[102] and more recently, SARS-CoV-

2,[103,104] which was declared as the cause of the COVID-19 pandemic by the WHO in March 2020.[105] Finally, it is noteworthy to mention that antimicrobial coatings should be carefully designed and studied under relevant environments (i.e., in laboratory and on site), so they do not promote the spread of AMR instead of eliminating infectious microorganisms,[96] or processed to remain either permanently adhered to the bulk material or not, depending on their final application (e.g., wound dressings, contact lenses or prosthesis such as breast implants).[40]

1.2.2. Plasma Processing of Antibacterial Surfaces

The current need for versatile antibacterial materials has had an impact in all branches of surface science research, where plasma science and engineering has been relevant in the field of antibacterial surfaces and coatings due to the observed decrease of materials performance when they get contaminated by microorganisms, and the corresponding consequences to human health.[74,106]

Antimicrobial coatings fabricated using plasma surface modification or surface functionalisation techniques are of great importance in different industrial and health-care sectors because the surface changes made occur on the topmost layer of materials without altering their bulk characteristics;[106] the processing of plasma coatings takes place under a controlled reactive environment which has an overall ambient temperature, making it amenable for a variety of solid substrate materials requiring physicochemical changes on their surface.[107]

For the case of plasma surface functionalisation, the application of a plasma treatment has a limited efficacy since antimicrobial action is usually a complex mechanism which is beyond of being affected by a single chemical group.[107] On the other hand, plasma polymers offer a variety of functionalities for different antibacterial approaches including being used as carrier matrices for antimicrobial agents such as nanoparticles or metal ions,

or as interlayers for further covalent surface immobilisation of antimicrobial organic compounds, and as covalently grafted antibacterial coatings which offer a permanent surface chemical composition functioning for long periods of time.[107,108] All these is particularly useful for metals[109] and inert materials such as polypropylene, polyethylene, or polytetrafluoroethylene, which are widely used in the medical and food sectors.[110–113]

The versatility of plasma surface applications rely on their ease of deposition, good adherence on most solid substrate materials while providing with reactive chemical surface groups.[107] Overall, plasma processing provides with a variety of options to either functionalise or modify a solid substrate, whose antibacterial mechanism of the tunned antibacterial surfaces will depend on their physical and chemical features.[72,114,115.]

1.3. Thesis Scope

Humans can acquire bacterial infectious diseases through different routes, such as, the respiratory tract, oral cavity and digestive system, eyes, skin and genitourinary system; acquiring such infections is not only restricted to physical contact with other people or animals but also may be transmitted indirectly through objects.[9] Since we are surrounded by different surfaces, it is critical to maintain high hygiene standards to prevent infectious diseases,[9] and maintain high cleaning standards in places such as hospitals and work environments.[2] However, broad-spectrum antibacterial surfaces may augment these procedures for a range of healthcare and commercial applications (e.g., in biomedical and industrial settings) to restrict and eliminate bacterial pathogen growth as planktonic cells and also within biofilms.[75,95,116] Furthermore, although regularly used materials lack or have low antibacterial properties, they are still preferred due to their bulk properties. Hence, this present research focuses on the immobilisation of antimicrobial agents onto different surfaces in order to prevent bacterial growth, while taking advantage of the bulk material properties.

The aim of this work is to test and understand, by experimental means:

- The physicochemical features, and antibacterial efficiency of the proposed coatings (i.e., immobilised chitosan, atomised spray plasma deposited (ASPD) poly(acrylic acid), and ASPD (metallosurfactant / polymer) coatings), to determine whether they are capable of preventing bacterial colonisation, thus limiting the spread of infections and,
- Estimate the antibacterial mechanism of ASPD (metallosurfactant / polymer) coatings in chapter 5 by testing these coatings against Gram-negative *Escherichia coli* mutant strains.
- To evaluate the effectivity of the proposed coatings and make the corresponding comparisons as antibacterial surfaces.

1.4. References

(1) Marshall, B. M.; Levy, S. B. Food Animals and Antimicrobials: Impacts on Human Health. *Clin. Microbiol. Rev.* **2011**, *24*, 718–733.

(2) O'Neill, J. Tackling Drug-Resistant Infections Globally: Final Report and Recommendations; Review on Antimicrobial Resistance. Wellcome Trust and UK Government ed.: London, 2016.

(3) D'Costa, V. M.; King, E. C.; Kalan, L.; Morar, M.; Sung, W. W. L.; Schwarz, C.; Froese, D.; Zazula, G.; Calmels, F.; Debruyne, R.; Golding, G. B.; Poinar, H. N.; Wright, G. D. Antibiotic Resistance is Ancient. *Nature* **2011**, *477*, 457–461.

(4) Peterson, E.; Kaur, P. Antibiotic Resistance Mechanisms in Bacteria: Relationships Between Resistance Determinants of Antibiotic Producers, Environmental Bacteria, and Clinical Pathogens. *Frontier Micobiol.* **2018**, *9*, 1–21.

(5) Kahlmeter, G.; Brown, D. F. J.; Goldstein, F. W.; MacGowan, A. P.; Mouton, J. W.; Österlund, A.; Rodloff, A.; Steinbakk, M.; Urbaskova, P.; Vatopoulos, A. European Harmonization of MIC Breakpoints for Antimicrobial Susceptibility Testing of Bacteria. *J. Antimicrob. Chemother.* **2003**, *52*, 145–148.

(6) Taylor, J.; Hafner, M.; Yerushalmi, E.; Smith, R.; Bellasio, J.; Vardavas, R.; Bienkowska-Gibbs, T.; Rubin, J. Estimating the Economic Costs of Antimicrobial Resistance: Model and Results. 1st Ed.; RAND Europe: Cambridge, 2014.

(7) World Health Organization: Antimicrobial Resistance. https://www.who.int/westernpacific/health-topics/antimicrobial-resistance (accessed Oct 04, 2020).

(8) World Health Organization. Online Q&A: What is Antimicrobial Resistance? https://www.who.int/features/qa/75/en/ (Accessed October 26, 2020).

(9) CDC Centers for Disease Control and Prevention. *Antibiotic Resistance Threats in the United States 2019*, 1st ed.; U. S. Department of Health and Human Services: Atlanta, 2019.

(10) Casewell, M.; Friis, C.; Marco, E.; McMullin, P.; Phillips, I. The European Ban on Growth-Promoting Antibiotics and Emerging Consequences for Human and Animal Health. *J. Antimicrob. Chemother.* **2003**, *52*, 159–161.

(11) Stekel, D. First Report of Antimicrobial Resistance Pre-Dates Penicillin. *Nature* **2018**, *562*, 192.

(12) Tortora, G. J.; Funke, B. R; Case, C. L. Microbiology An Introduction, 12th ed.; Pearson Education, Inc.: New York, 2016.

(13) De Sousa Oliveira, K.; De Lima, L. A.; Cobacho, N. B.; Dias, S. C.; Franco, O. L. Mechanisms of Antibacterial Resistance: Shedding Some Light on These Obscure Processes? In *Antibiotic Resistance: Mechanisms and New Antimicrobial Approaches*; Kon, K.; Rai, M., Ed.; Academic Press, Elsevier Inc.: London, United Kingdom, 2016.

(14) Haenni, M.; Moreillon, P. Mutations in Penicillin-Binding Protein (PBP) Genes and in Non-PBP Genes during Selection of Penicillin-Resistant Streptococcus gordonii. Antimicrob. *Agent Chemotherapy*, **2006**, *50*, 4053–4061.

(15) Reygaert, W. An Overview of the Antimicrobial Resistance Mechanisms of Bacteria. *Microbiol.* **2018**, *4*, 482–501.

(16) World Health Organization. Health Topics: Drug Resistance. http://www.who.int/topics/antimicrobial_resistance/en/ (Accessed January 17, 2017).

(17) World Health Organization. *Global Report on Antimalarial Drug Efficacy and Drug Resistance: 2000–2010*; World Health Organization: Geneva, 2010.

(18) DeMars, Z.; Biswas, S.; Amachawadi, R. G.; Renter, D. G.; Volkova, V. V. Antimicrobial Susceptibility of Enteric Gram Negative Facultative Anaerobe Bacilli in Aerobic Versus Anaerobic Conditions. *PLoS ONE.* **2016**, *11*, e0155599.

(19) Taylor, J.; Hafner, M.; Yerushalmi, E.; Smith, R.; Bellasio, J.; Vardavas, R.; Bienkowska-Gibbs, T.; Rubin, J. Estimating the Economic Costs of Antimicrobial Resistance: Model and Results. 1st Ed.; RAND Europe: Cambridge, 2014.

(20) Bonev, B.; Hooper, J.; Parisot, J. Principles of Assessing Bacterial Susceptibility to Antibiotics Using the Agar Diffusion Method. *J. Antimicrob. Chemother*. **2008**, *61*, 1295–1301.

(21) Health and Safety Executive. Advisory Committee on Dangerous Pathogens (ACDP). http://www.hse.gov.uk/aboutus/meetings/committees/acdp/ (Accessed Mar 23, 2017).

(22) Felmingham, D.; Grüneberg, R. N. The Alexander Project 1996–1997: Latest Susceptibility Data from this International Study of Bacterial Pathogens from Community-Acquired Lower Respiratory Tract Infections. *J. Antimicrob. Chemother*. **2000**, *45*, 191–203.

(23) Miller, M. B.; Bassler, B. L. Quorum Sensing in Bacteria. *Annu. Rev. Microbiol*. **2001**, *55*, 165–199.

(24) Beoletto, V. G.; Oliva, M. M.; Marioli, J. M.; Carezzano, M. E.; Demo, M. S. Antimicrobial Natural Products Against Bacterial Biofilms. In *Antibiotic Resistance: Mechanisms and New Antimicrobial Approaches*; Kon, K.; Rai, M., Ed.; Academic Press, Elsevier Inc.: London, United Kingdom, 2016.

(25) Berlanga, M.; Guerrero, R.; Living Together in Biofilms: The Microbial Cell Factory and Its Biotechnological Implications. *Microb Cell Fact*. **2016**, *15*, 165.

(26) Ljungh, Å.; Yanagisawa, N.; Wadström, T. Using The Principle of Hydrophobic Interaction to Bind and Remove Wound Bacteria. *J. Wound Care* **2006**, *15*, 175–180.

(27) Considine, G. D.; Kulik, P. H. Van *Nostrand's Scientific Encyclpedia*, 10th Ed.; John Wiley and Sons Inc.: New Jersey, 2008; Vol. 1.

(28) Davies, D. G.; Parsek, M. R.; Pearson, J. P.; Iglewski, B. H.; Costerton, J. W.; Greenberg, E. P. The Involvement of Cell-to-Cell Signals in the Development of a Bacterial Biofilm. *Science*. **1998**, *280*, 295–298.

(29) Flemming, H.-C.; Wingender, J. The Biofilm Matrix. *Nature Rev. Microbiol*. **2010**, *8*, 623 –633.

(30) Olson, M. E.; Ceri, H.; Morck, D. W.; Buret, A. G.; Read, R. R. Biofilm Bacteria: Formation and Comparative Susceptibility to Antibiotics. *Can. J. Vet. Res.* **2002**, *66*, 86–92.

(31) Mah, T.-F. C.; O'Toole, G. A. Mechanisms of Biofilm Resistance to Antimicrobial Agents. *Trends Microbiol.* **2001**, *9*, 34–39.

(32) Van Houdt, R.; Michiels, C. W. Role of Bacterial Cell Surface Structures in Escherichia coli Biofilm Formation. *Res. Microbiol.* **2005**, *156*, 626–633.

(33) Donlan, R. M. Biofilm Formation: A Clinically Relevant Microbiological Process. *Clin. Infect. Dis.* **2001**, *33*, 1387–1392.

(34) Ciofu, O.; Rojo-Molinero, E.; Macia, M. D.; Oliver, A. Antibiotic Treatment of Biofilm Infections. *APMIS* **2017**, *125*, 304–319.

(35) Prosser, B. L. T.; Taylor, D.; Dix, B. A.; Cleeland, R. Method of Evaluating Effects of Antibiotics on Bacterial Biofilm. *Antimicrob. Agents Chemother.* **1987**, *31*, 1502–1506.

(36) McDevitt, C. A.; Ogunniyi, A. D.; Valkov, E.; Lawrence, M. C.; Kobe, B.; McEwan, A. G.; Paton, J. C. A Molecular Mechanism for Bacterial Susceptibility to Zinc. *PLoS Pathog.* **2011**, *11*, e1002357.

(37) Tawakoli, P. N.; Ragnarsson, K. T.; Rechenberg, D. K.; Mohn, D.; Zehnder, M. Effect of Endodontic Irrigants on Biofilm Matrix Polysaccharides. *Int. Endontic. J.* **2017**, *50*, 153–160.

(38) Khan, H. A.; Ahmad, A.; Mehboob, R. Nosocomial Infections and Their Control Strategies. *Asian Pac. J. Trop. Biomed.* **2015**, *5*, 509–514.

(39) Costerton, J. W.; Stewart, P. S.; Greenberg, E. P. Bacterial Biofilms: A Common Cause of Persistent Infections. *Am. Assoc. Adv. Sci.* **1999**, *284*, 1318–1322.

(40) Salwiczek, M.; Qu, Y.; Gardiner, J.; Strugnell, R. A.; Lithgow, T.; McLean, K. M.; Thissen, H. Emerging Rules for Effective Antimicrobial Coatings. *Trends Biotechnol.* **2014**, *32*, 82–90.

(41) Khatoon, Z.; McTiernan, C. D.; Suuronen, E. J.; Mah, T.-F.; Alarcon, E. I. Bacterial Biofilm Formation on Implantable Devices and Approaches to Its Treatment and Prevention. *Helyon* **2018**, *4*, e01067.

(42) Vaishampayan, A.; Ahmed, R.; Wagner, O.; De Jong, A.; haag, R.; Kok, J.; Grohmann, E. Transcriptomic Analysis of Stress Response to Novel Antimicrobial Coatings in a Clinical MRSA Strain. *Mater. Sci. Eng., C* **2021**, *119*, 111578.

(43) Tasneem, U.; Yasin, N.; Nisa, I.; Shah, F.; Rasheed, U.; Momin, F.; Zaman, S.; Qasim, M. Biofilm Producing Bacteria: A Serious Threat to Public Health in Developing Countries. *J. Food Sci. Nutr.* **2018**, *1*, 25–31.

(44) Olson, M. E.; Ceri, H.; Morck, D. W.; Buret, A. G.; Read, R. R. Biofilm Bacteria: Formation and Comparative Susceptibility to Antibiotics. *Can. J. Vet. Res.* **2002**, *66*, 86–92.

(45) Podolsky, S. H.; The Evolving Response to Antibiotic Resistance (1945–2018). *Palgrave Commun.* **2018**, *4*, 1–8.

(46) Loftus, M.; Stewardson, A.; Naidu, R.; Coghlan, B.; Jenney, A.; Kepas, J.; Lavu, E.; Munamua, A.; Peel, T.; Sahai, V.; Tekoaua, R.; Tudravu, L.; Zinhite, J.; Cheng, A.; Rafai, E.; Peleg, A. Antimicrobial Resistance in The Pacific Island Countries and Territories. *BMJ Global Health* **2020**, *5*, e002418.

(47) Klein, E. Y.; Tseng, K. K.; Pant, S.; Laxminarayan, R. Tracking Global Trends in The Effectiveness of Antibiotic Therapy Using the Drug Resistance Index. *BMJ Global Health* **2019**, *4*, e001315.

(48) World Health Organization. Worldwide Country Situation Analysis: Response to Antimicrobial Resistance. WHO Press., Geneva: 2015.

(49) Smith, R. D.; Coast, J. Antimicrobial Resistance: A Global Response. *Bull. W. H. O.* **2002**, *80*, 126–133.

(50) Strategies and Action Plans on Antimicrobial Resistance. European Centre for Disease Prevention and Control: An Agency of The European Union. https://www.ecdc.europa.eu/en/publications-data/directory-guidance-prevention-and-control/antimicrobial-resistance-strategies (Accessed: November 05, 2020).

(51) White, A.; Hughes, J. M. Critical Importance of A One Health Approach to Antimicrobial Resistance. *EcoHealth* **2019**, *16*, 404–409.

(52) Centers for Disease Control and Prevention. Antibiotic / Antimicrobial Resistance (AR / AMR): The AMR Challenge. https://www.cdc.gov/drugresistance/intl-activities/amr-challenge.html (Accessed: November 05, 2020).

(53) Baker, S. J.; Payne, D. J.; Rappuoli, R.; Gregorio, E. D. Technologies to Address Antimicrobial Resistance. *PNAS* **2018**, *115*, 12887–12895.

(54) Annunziato, G. Strategies to Overcome Antimicrobial Resistance (AMR) Making Use of Non-Essential Target Inhibitors: A Review. *Int. J. Mol. Sci.* **2019**, *20*, 5844.

(55) Laws, M.; Shaaban, A.; Rahman, K. M. Antibiotic Resistance Breakers: Current Approaches and Future Directions. *FEMS Microbiol. Rev*. **2019**, *43*, 490–516.

(56) Lemire, J. A.; Harrison, J. J.; Turner, R. J. Antimicrobial Activity of Metals: Mechanisms, Molecular Targets and Applications. *Nature* **2013**, *11*, 371–384.

(57) Turner, R. J. Metal-Based Antimicrobial Strategies. *Microb. Biotechnol.* **2017**, *10*, 1062–1065.

(58) Kaur, G.; Garg, P.; Kaur, B.; Chaudhary, G. R.; Kumar, S.; Dilbaghi, N.; Hassan, P. A.; Gawali, S. L. Cationic Double Chained Metallosurfactants: Synthesis, Aggregation, Cytotoxicity, Antimicrobial Activity and Their Impact on The Structure of Bovine Serum Albumin. *Soft Matter* **2018**, *14*, 5306–5318.

(59)Shurygina, I. A.; Shurygin, M. G.; Sukhov, B. G. Nanobiocomposites of Metals as Antimicrobial Agents. In *Antibiotic Resistance: Mechanisms and New Antimicrobial Approaches*; Kon, K.; Rai, M., Ed.; Academic Press, Elsevier Inc.: London, United Kingdom, 2016.

(60) Hall, T. J.; Azoidis, I.; Barroso, I. A.; Hughes, E. A. B.; Grover, L. M. Formulation of An Antimicrobial Superabsorbent Powder that Gels *in situ* to Produce Reactive Oxygen. *Mater. Sci. Eng., C* **2021**, *118*, 111479.

(61) Vimbela, G. V.; Ngo, S. M.; Fraze, C.; Yang, L.; Stout, D. A. Antibacterial Properties and Toxicity from Metallic Nanomaterials. *Int. J. Nanomed.* **2017**, *12*, 3941–3965.

(62) Chávez-González, M. L.; Rodríguez-Herrera, R.; Aguilar, C. N. Essential Oils: A Natural Alternative to Combat Antibiotics Resistance. In *Antibiotic Resistance: Mechanisms and New Antimicrobial Approaches*; Kon, K.; Rai, M., Ed.; Academic Press, Elsevier Inc.: London, United Kingdom, 2016.

(63) Upadhyay, A.; Karumathil, D. P.; Upadhyaya, I.; Bhattaram, V.; Venkitanarayanan, K. Controlling Bacterial Antibiotic Resistance Using Plant-Derived Antimicrobials. In *Antibiotic Resistance: Mechanisms and New Antimicrobial Approaches*; Kon, K.; Rai, M., Ed.; Academic Press, Elsevier Inc.: London, United Kingdom, 2016.

(64) Barbosa, F.; Pinto, E.; Kijjoa, A.; Pinto, M.; Sousa, E. Targeting Antimicrobial Drug Resistance with Marine Natural Products. *Int. J. Antimicrob. Agents.* **2020**, *56*, 106005.

(65) Preciado, G. M.; Michel, M. M.; Villarreal-Morales, S. L.; Flores-Gallegos, A. C.; Aguirre-Joya, J.; Morlett-Chávez, J.; Aguilar, C. N.; Rodríguez-Herrera, R. Bacteriocins and Its Use for Multidrug-Resistant Bacteria Control. In *Antibiotic Resistance: Mechanisms and New Antimicrobial Approaches*; Kon, K.; Rai, M., Ed.; Academic Press, Elsevier Inc.: London, United Kingdom, 2016.

(66) Bragg, R. R.; Boucher, C. E.; Van der Westhuizen, W. A.; Lee, J.-Y.; Coetsee, E.; Theron, C.; Meyburgh, L. The Potential Use of Bacteriophage Therapy as A Treatment Option in A Post-Antibiotic Era. In *Antibiotic Resistance: Mechanisms and New Antimicrobial Approaches*; Kon, K.; Rai, M., Ed.; Academic Press, Elsevier Inc.: London, United Kingdom, 2016.

(67) Jeong, H. Y.; Kim, E.-G.; Han, S.; Lee, G. Y.; Han, S.; Jin, B.; Lim, T.; Kim, H. C.; Kim, T. S.; Kim, D.; Kwon, S. Rapid Antibiotic Susceptibility Test: Commercialization of Life Saving MEMS Devices. *Micro Electro Mechanical Systems (MEMS),* 2017 *IEEE 30th International Conference on.*

(68) Whitchurch, C. B.; Tolker-Nielsen, T.; Ragas, P. C.; Mattick, J. S. Extracellular DNA Required for Bacterial Biofilm Formation. *Science.* **2002**, *295*, 1487.

(69) Park, J.-M.; Kim, J.-I.; Noh, J.-Y.; Kim, M.; Kang, M.-J.; Pyun, J.-C. Hypersensitive Antibiotic Susceptibility Test Based on a β-Lactamase Assay with a Parylene-Matrix Chip. *Enzyme Microb. Technol.* **2017**, *97*, 90–96.

(70) Wu, T. F.; Tseng, S. Y.; Hung, J. C. Generation of Pulsed Electric Fields for Processing Microbes. *IEEE Trans. Plasma Sci.* **2004**, *32*, 1551–1562.

(71) Torres Dominguez, E.; Nguyen, P. H.; Hunt, H. K.; Mustapha, A. antimicrobial Coatins for Food Contact Surfaces: Legal Framework, Mechanical Properties, and Potential Applications. *Compr. Rev. Food Sci. Food Saf.* **2019**, *18*, 1825–1858.

(72) Bazaka, K.; Jacob, M. V.; Chrzanowski, W.; Ostrikov, K. Anti-Bacterial Surfaces: Natural Agents, Mechanisms of Action, and Plasma Surface Modification. *RSC Adv.* **2015**, *5*, 48739–48759.

(73) Yu, Q.; Wu, Z.; Chen, H. Dual-Function Antibacterial Surfaces for Biomedical Applications. *Acta Biomater.* **2015**, *16*, 1–13.

(74) Hasan, J.; Crawford, R. J.; Ivanova, E. P.Antibacterial Surfaces: The Quest for A New Generation of Biomaterials. *Trends Biotechnol.* **2013**, *31*, 295–304.

(75) Cloutier, M.; Mantovani, D.; Rosei, F. Antibacterial Coatings: Challenges, Perspectives, and Opportunities. *Trends Biotechnol.* **2015**, *33*, 637–652.

(76) Arciola, C. R.; Campoccia, D.; Ehrlich, G. D.; Montanaro, L. Biofilm-Based Implant Infections in Orthopaedics. in *Biofilm-Based Healthcare-Associated Infections*; Donelli, G., Ed.; Springer: Switzerland, 2015.

(77) Webb, h. K.; Crawford, R. J.; Ivanova, E. P. Introduction to Antibacterial Surfaces. In *Antibacterial Surfaces*; Ivanova, E. P.; Crawford, R. J., Ed.; Springer: Switzerland, 2015.

(78) Ahmed, W.; Zhai, Z.; Gao, C. Adaptive Antibacterial Biomaterial Surfaces and Their Applications. *Mater. Today Bio* **2019**, *2*, 100017.

(79) Pham, V. T. H.; Bhadra, C. M.; Truong, V, K.; Crawford, R. J.; Ivanova, E. P. Designing Antibacterial Surfaces for Biomedical Implants. In *Antibacterial Surfaces*; Ivanova, E. P.; Crawford, R. J., Ed.; Springer: Switzerland, 2015.

(80) Vasilev, K. Nanoengineered Antibacterial Coatings and Materials: A Perspective. *Coat.* **2019**, *9*, 654.

(81) Linklater, D. P.; Ivanova, E. P. Nanostructured Antibacterial Surfaces – What Can Be Achieved? *Nano Today* **2022**, *43*, 101404.

(82) Kaur, R.; Liu, S. Antibacterial Surface Design – Contact Kill. *Prog. Surf. Sci.* **2016**, *91*, 136–153.

(83) Li, W.; Thian, E. S.; Wang, M.; Wang, Z.; Ren, L. Surface Design for Antibacterial Materials: From Fundamentals to Advanced Strategies. *Adv. Sci.* **2021**, *8*, 2100368.

(84) Ishihara, K.; Ziats, N. P.; Tierney, B. P.; Nakabayashi, N.; Anderson, J. M. Protein Adsorption from Human Plasma is Reduced on Phospholipid Polymers. *J. Biomed. Mater. Res.* **1991**, *25*, 1397–1407.

(85) Chen, R.; Shi, C.; Xi, Y.; Zhao, P.; He. H. Fabrication of Cationic Polymer Surface through Plasma Polymerization and Layer-by-Layer Assembly. *Mater. Manut. Processes* **2020**, *35*, 221–229.

(86) Chen, S.; Li, L.; Zhao, C.; Zheng, J. Surface Hydratation: Principles and Applications Toward Low-Fouling/Nonfouling Biomaterials. *Polymer* **2010**, *51*, 5283–5293.

(87) Campoccia, D.; Montanaro, L.; Arciola, C. R. A Review of The Biomaterials Technologies for Infection-Resistant Surfaces. *Biomaterials* **2013**, *34*, 8533–8554.

(88) Ning, C.; Wang, X.; Li, L.; Zhu, Y.; Li, M.; Yu, P.; Zhou, L.; Zhou, Z.; Chen, J.; Tan, G.; Zhang, Y.; Wang, Y.; Mao, C. *Chem. Res. Toxicol.* **2015**, *28*, 1815–1822.

(89) Hamzah, N.; Leo, C. P. Membrane Distillation of Saline with Phenolic Compound Using Superhydrophobic PVDF Membrane Incorporated with TiO$_2$ Nanoparticles: Separation, Fouling and Self-Cleaning Evaluation. *Desalination* **2017**, *418*, 79–88.

(90) Wang, J.; Dou, X.; Song, J.; Lyu, Y.; Zhu, X.; Xu, L.; Li, W.; Shan, A. Antimicrobial Peptides: Promising Alternatives in The Post Feeding Antibiotic Era. *Med. Res. Rev.* **2019**, *39*, 831–859.

(91) Kim, M. K.; Zhao, A.; Wang, A.; Brown, Z. Z.; Muir, T. W.; Stone, H. A.; Bassler, B. L. Surface-Attached Molecules Control *Staphylococcus aureus* Quorum Sensing and Biofilm Development. *Nat. Microbiol.* **2017**, *2*, 1–12.

(92) Batoni, G.; Maisetta, G.; Esin, S. Antimicrobial Peptides and Their Interaction with Biofilms of Medically Relevant Bacteria. *Biochim. Biophys. Acta* **2016**, *1858*, 1044–1060.

(93) Linklater, D. P.; Juodkazis, S.; Ivanova, E. P. Nanofabrication of Mechano-Bactericidal Surfaces. *Nanoscale* **2017**, *9*, 16564–16585

(94) Linklater, D. P.; Baulin, V. A.; Juodkazis, S.; Crawford, R. J.; Stoodley, P.; Ivanova, E. P. Mechano-Bactericidal Actions of Nanostructured Surfaces. *Nature* **2021**, *19*, 8–22.

(95) Singha, P.; Locklin, J.; Handa, H. A Review of the Recent Advances in Antimicrobial Coatings for Urinary Catheters. *Acta Biomaterialia.* **2017**, *50*, 20–40.

(96) Pietsch, F.; O'Neill, A. J.; Ivask, A.; Jenssen, H.; Inkinen, J.; Kahru, A.; Ahonen, M.; Scghreiber, F. Selection of Resistance by Antimicrobial Coatings in The Healthcare Setting. *J. Hosp. Infect.* **2020**, *160*, 115–125.

(97) Konai, M. M.; Bhattacharjee, B.; Ghosh, S.; Haldar, J. Recent Progress in Polymer Research to Tackle Infections and Antimicrobial Resistance. *Biomacromolecules* **2018**, *19*, 1888–1917.

(98) Tallet, L.; Gribova, V.; Ploux, L.; Vrana, N. E.; Lavalle, P. New Smart Antimicrobial Hydrogels, Nanomaterials, and Coatings: Earlier Action, More Specific, Better Dosing? *Adv. Healthcare Mater.* **2020**, *10*, 2001199.

(99) Oie, S.; Suenaga, S.; Sawa, A.; Kamiya, A. Association between Isolation Sites of Methicillin-Resistant *Staphylococcus aureus* (MRSA) in Patients with MRSA-Positive Body Sites and MRSA Contamination in Their Surrounding Environmental Surfaces. *Jpn. J. Infect. Dis.* **2007**, *60*, 367–369.

(100) CDC Centers for Disease Control and Prevention. Morbidity and Mortality Weekly Report (MMWR): Investigation of the First Seven Reported Cases of *Candida auris*, a Globally Emerging Invasive, Multidrug-Resistant Fungus – United States, May 2013-August 2016. https://www.cdc.gov/mmwr/volumes/65/wr/mm6544e1.htm?s_cid=mm6544e1_w&c_cid=journal_search_promotion_2018 (Accessed, November 02, 2020).

(101) Bean, B.; Moore, B. M.; Sterner, B.; Peterson, L. R.; Gerding, D. N.; Balfour, Jr., H. H. Survival of influenza Viruses on Environmental Surfaces. *J. Infect. Dis.* **1982**, *146*, 47–51.

(102) Sagripanti, J.-L.; Rom, A. M.; Holland, L. E. Persistence in Darkness of Virulent Alphaviruses, Ebola Virus, and Lassa Virus Deposited on Solid Surfaces. *Arch. Virol.* **2010**, *155*, 2035–2039.

(103) Rawlinson, S.; Ciric, L.; Cloutman-Green, E. COVID-19 Pandemic – Let's Not Forget Surfaces. *J. Hosp. Infect.* **2020**, *105*, 790–791.

(104) Seo, G.; Lee, G.; Kim, M. J.; Baek, S.-H.; Choi, M.; Ku, K. B.; Lee, C.-S.; Jun, S.; Park, D.; Kim, H. G.; Kim, S.-J.; Lee, J.-O.; Kim, B. T.; Park, E. C.; Kim, S. I. Rapid Detection of COVID-19 Causative Virus (SARS-CoV-2) in Human Nasopharyngeal Swab Specimens Using Field-Effect Transistor-Based Biosensor. *ACS Nano* **2020**, *14*, 5135–5142.

(105) World Health Organization. WHO Director-General's Opening Remarks at The Media Briefing on COVID-19 - 11 March 2020. https://www.who.int/dg/speeches/detail/who-director-general-s-opening-remarks-at-the-media-briefing-on-covid-19---11-march-2020 (Accessed: November 01, 2020).

(106) Nikiforov, A.; Ma, C.; Choukorov, A.; Palumbo, F. Plasma Technology in Antimicrobial Surface Engineering. *J. Appl. Phys.* **2022**, *131*, 011102.

(107) Vasilev, K.; Griesser, S. S.; Griesser, H. J. Antibacterial Surfaces and Coatings Produced by Plasma Techniques. *Plasma Process. Polym.* **2011**, *8*, 1010–1023.

(108) Schäfer, J.; Fricke, K.; Mika, F.; Pokorná, Z.; Zajícková, L.; Foest, R. Liquid Assisted Plasma Enhanced Chemical Vapour Deposition with a Non-Thermal Plasma Jet at Atmospheric Pressure. *Thin Solid Films* **2017**, *630*, 71–78.

(109) Safety of Metals and Other Materials Used in Medical Devices. https://www.fda.gov/medical-devices/products-and-medical-procedures/safety-metals-and-other-materials-used-medical-devices (accessed May 05, 2022).

(110) Lei, J.; Yang, L.; Zhan, Y.; Wang, Y.; Ye, T.; Li, Y.; Deng, H.; Li, B. Plasma Treated Polyethylene Terephthalate/Polypropylene Films Assembled with Chitosan and Various Preservatives for Antimicrobial Food Packing. *Colloids Surf. B* **2014**, *114*, 60–66.

(111) FDA in Brief: FDA Publishes Material Safety Data to Promote Safer, More Effective Medical Devices. https://www.fda.gov/news-events/press-announcements/fda-brief-fda-publishes-material-safety-data-promote-safer-more-effective-medical-devices (accessed May 05, 2022).

(112) FDA: CFR - Code of Federal Regulations Title 21. https://www.accessdata.fda.gov/scripts/cdrh/cfdocs/cfcfr/cfrsearch.cfm?fr=872.3680 (accessed May 05, 2022)

(113) FDA Recognized Consensus Standards. https://www.accessdata.fda.gov/scripts/cdrh/cfdocs/cfstandards/detail.cfm?standard__identification_no=38209 (accessed May 05, 2022).

(114) Qiu, H.; Si, Z.; Luo, Y.; Feng, P.; Wu, X.; Hou, W.; Zhu, Y.; Chan-Park, M. B.; Xu, L.; Huang, D. The Mechanisms and The Applications of Antibacterial Polymers in Surface Modification of Medical Devices. *Front. Bioeng. Biotechnol.* **2020**, *8*, 910.

(115) Ma, C.; Nikiforov, A.; De Geyter, N.; Morent, R.; Ostrikov, K. (K.). Plasma for Biomedical Decontamination: from Plasma-Engineered to Plasma-Active Antimicrobial Surfaces. *Curr. Opin. Chem. Eng.* **2022**, *36*, 100764.

(116) Mahadik, S. A.; Pedraza, F.; Vhatkar, R. S. Silica Based Superhydrophobic Coating for Long-Term Industrial and Domestic Applications. *J. Alloys Compd.* **2016**, *663*, 487–493.

2. Experimental Techniques

2.1. Plasma Treatment

2.1.1. Plasma: Theoretical Background

Plasma is known as the fourth state of matter, and it is found in a fully or partially ionised gas form. Plasma is composed of electrons, ions, excited molecules, radicals, energetic photons, atoms, molecules, fragments, and neutral species, and their corresponding concentration depends on the ionisation degree of plasma.[1–3] In nature, more than 99% of the universe is in fully ionised plasma state.[4,5] In research laboratories, humanmade plasmas are generated by applying enough energy from electrical discharges (direct current, radiofrequency or microwave discharges) into a gas or precursor vapour (i.e. a non-conducting medium), the applied electric fields strip out an electron from the molecule leading to ionisation of the gas. Therefore, plasma can be classified according to their ionisation degree: full, partial, or weak.[2,6,7]

Fully ionised plasmas exist in natural forms such as stars, aurora borealis, or humanmade plasmas such as thermonuclear fusion plasmas. These are in complete thermodynamic equilibrium—the temperature of electrons and ions are the same as to the plasma temperature due to the high energy and temperature conditions, and thus, unable to be used for plasma material processing. Partially ionised plasmas are in local thermodynamic equilibrium (thermal plasmas)—it may be possible that under certain conditions, the electron and ion temperatures are equal to the plasma in a local volume of Debye length dimension; or weakly ionised plasmas in non-local thermodynamic equilibrium (cold plasmas) in which the plasma temperature remains at room temperature whereas the electron temperature (T_e) is ~10^4–10^5 K. For the case of cold plasmas, the energetic electrons are the source of energy for the material processing and surface functionalisation while the overall plasma temperature remains at room temperature, minimising potential surface damage for thermal irradiation.[7,8]

Plasma technology and materials processing require optimisation of plasma equipment which relies on several physical parameters such as electron temperature, ionisation degree, Debye length, and plasma sheath, that affect the plasma reactivity and efficiency:[2]

- Electron temperature: in non-local equilibrium plasmas (cold plasmas), the electron temperature is much higher than the ion (T_i) or plasma temperatures (T_p): ($T_e \gg T_i \approx T_p$); therefore, electrons are the most energetic particles in the plasma, which gain the kinetic energy from the applied electric field, and transfer their kinetic energy to other particles through inelastic collisions which can lead to the ionisation process. The mean kinetic energy of the electrons is 2–4 eV for cold plasmas in material processing.[2]

- Ionisation degree: the ionisation degree (α) parameter defines the density of charged particles in the plasma phase—the electron density (n_e), and the ion density (n_i) are equal ($n_e \approx n_i$)—in respect of the total amount of particles (n_n) in the gas. In cold plasmas, the typical ionisation degree is ~10^{-4}–10^{-7}, Equation 2. 1.[2,9]

$$\alpha = \frac{n_e}{n_e + n_n}$$

Equation 2. 1

- Debye length: the Debye length is the microscopic scale unit where a significant charge density exists, causing local concentration of positive and negative electric charges. At scales larger than the Debye length, quasineutrality exists in the plasma phase where there is an equilibrium between electron and ion densities ($n_e \approx n_i$).[2]

- Plasma sheath: the plasma sheath is a region which develops a negative potential relative to the plasma bulk close to any surface. The most energetic electrons reach the wall surface where the plasma is confined, developing a negative potential and repelling the less

energetic electrons. Then, the ions which reach the surface are accelerated towards the surface by the gradient potential. Once the electron and ion fluxes reach a flux equilibrium at the wall surface, the wall surface develops a positive potential where $n_i \gg n_e$.[2,10]

The non-equilibrium behaviour of cold plasmas implies that there are different temperatures and ranges of energy for each of the individual species present in the plasma phase, representing an advantage for potential chemical reaction pathways, where electrons provide with the energy (enthalpy) to promote such reactions which are not possible by conventional chemistry procedures.[6]

2.1.1.1. Plasma chemistry

Plasma chemistry is about the chemical reactions occurring in the plasma phase (gas phase), and at the plasma–surface interface when a solid surface is exposed to plasma.[2] For any of these chemical reactions, the electron energy plays an important role because electrons distribute their energy through collisions with other species, producing different reaction pathways in the plasma phase and at the plasma–surface interface, providing with the energy to facilitate the chemical treatment on the surface.[10]

2.1.1.2. Chemical Reactions in The Gas Phase of Plasma

Electrons in the plasma get their energy from the external electromagnetic field so they can sustain the plasma state. Electrons transfer energy to heavy species by energetic inelastic collisions leading to different types of

reactions, being excitation, ionisation, dissociation, and recombination, the main reactions found in the gas phase of plasma.[2]

Excitation: Collisions between electrons (e⁻) and neutral species (M_2), where the core level electron of the latter absorbs kinetic energy, and it is excited to a higher energy state, i.e., producing an excited species (M_2*),

- Equation 2. 2.[2]

$$e^- + M_2 \rightarrow e^- + M_2^*$$ Equation 2. 2

However, this excited state of the molecule last for a short period before the excited electron falls back to its ground state, emitting electromagnetic radiation energy.[10]

- Ionisation: Collisions occurring during ionisation reactions lead to the production of positive or negative, atomic or molecular ions (M_2^+) which maintain the plasma state by producing more electrons through the ionisation process, Equation 2. 3.[2,10]

$$e^- + M_2 \rightarrow M_2^+ + 2e^-$$ Equation 2. 3

Collisions of electrons with electronegative particles can produce anionic molecules. However, in the plasma processing, the anionic molecules are neglected from the chemical reactions because they are repelled by the negative potential formed on the plasma sheath at any surface.[2]

- Dissociation: Inelastic collisions between an electron and a molecule (e.g., M or N) can cause dissociation without leading to ionisation. The dissociation of the molecule occurs through its vibrational or electronic excitation, Equation 2. 4 and Equation 2. 5.[2]

$$e^- + M_2 \rightarrow 2M + e^- \qquad \text{Equation 2. 4}$$

$$e^- + MN \rightarrow e^- + M + N \qquad \text{Equation 2. 5}$$

- Recombination: These kinds of reactions can occur between electrons and ions (atoms or molecules) due to their opposite charges, and between heavy species. When electrons and ions recombine, there is a release of a photon. For example, recombination of an argon ion (Ar^+) with an electron, produces a radiative recombination reaction, releasing releases a photon (hv), considering Plank's constant (h) and the radiation frequency (v), Equation 2. 6.[2]

$$e^- + Ar^+ \rightarrow Ar + hv \qquad \text{Equation 2. 6}$$

2.1.1.3. Chemical Reactions at the Plasma–Surface Interface

The chemical reaction mechanisms at the plasma–surface interface are different from those in the plasma phase. The chemical pathways of these reactions are mainly radical–radical reactions, and ion bombardment, which are accelerated in the plasma sheath towards the surface due to the formed negative potential; the main reactions at the plasma–surface interface are adsorption, recombination, and polymerisation.[2]

Adsorption occurs when radicals (R) and neutral species (M) from the plasma phase reach a solid surface; they can be adsorbed on the surface and remain in solid state. Then, other neutral species or radicals found in the

plasma phase as well as on the surface, can react with the adsorbed species to combine and form polymers.[2]

2.1.1.4. Plasma Polymerisation

Plasma polymerisation is the formation of polymeric materials under the influence of partially ionised plasmas.[11] A plasma polymer is a crosslinked macromolecular structure where the main repetitive functional group is randomly distributed through it, in comparison with well-ordered conventional polymers.[4]

Plasma polymerisation approach can be carried out not only with common polymerisable precursors but also with organic compounds without a polymerisable structure, where the resulting films display their own physical and chemical properties due to their corresponding deposition mechanisms, and tuning of experimental conditions.[12,13] Plasma polymerisation allows the production of ultrathin pin-hole free polymer coatings, whose chemical composition and physical features depends on the precursor and tunning of plasma conditions. A key external parameter to optimise the plasma deposition conditions is the Yasuda parameter, used to control the energy-per-molecule ratio (W/F) and, therefore, affecting the precursor flow rate (F), working pressure, applied power (W), and reactor configuration, so at the end it could be possible to fabricate a polymer coating with optimised physical (e.g., mechanical and electrical properties, roughness) and chemical (i.e., functional group retention) features.[14]

During plasma polymerisation, gas phase and gas-solid phase reactions take place through inelastic collision processes to form a plasma polymer which is frequently processed as a thin film coating on a solid substrate, Figure 2. 1.[13] Plasma polymerisation allows modification of solid surfaces with practically no alteration of its bulk properties, despite the nature of the

substrate; thus, plasma polymerisation is a substrate-independent and room temperature process.
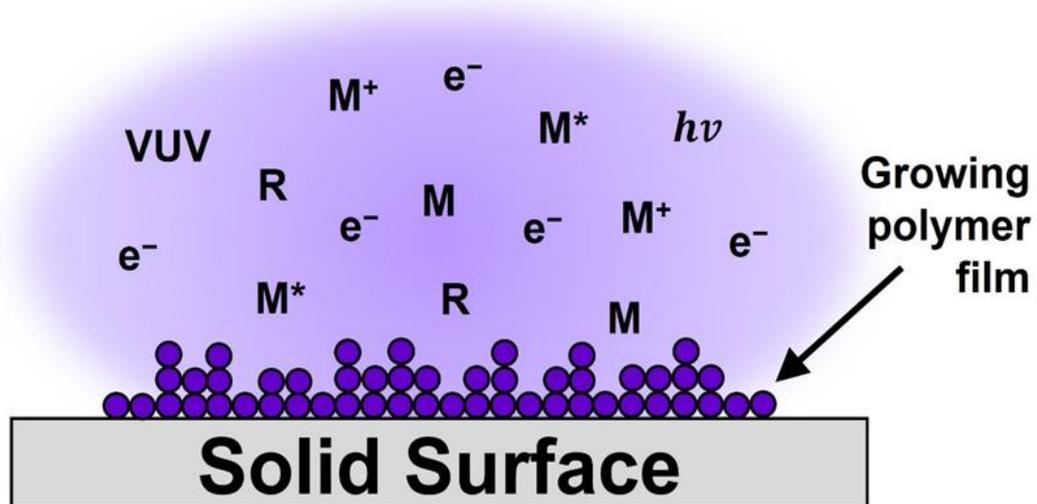
Figure 2. 1: Schematic representation of plasma polymerisation using an electric glow discharge under vacuum conditions (or glow discharge polymerisation), where present species undertake inelastic collisions, leading to the growth of a plasma polymer film. Symbols denote: e⁻, electrons; VUV, vacuum ultraviolet radiation; hv, photons; M, neutral species; M^+, positive ions; M*, excited particles; R, radicals. Schematic adapted from Thiry et al.[15]

Nevertheless, , plasma polymerisation could be performed under continuous wave (CW) or pulsed regime; therefore polymer films grow under different conditions where the polymer chemistry, polymer growth rate, and crosslinking degree varies according to the active species in the plasma bulk, power input, and physicochemical properties of precursor.[13]

2.1.1.5. Continuous Wave Plasma Deposition

Continuous-wave (CW) plasma deposition causes fragmentation of the monomer reducing the availability of the precursor functional groups and leads to the formation of rigid high-crosslinked networks with little or no repeating structure with respect to the original precursor molecule but, at the same time, these networks are stable in aqueous solutions.[16]

Furthermore, processes undertaken under CW regime, are generally associated with high functional retention when used at low input power or deposition downstream, being specifically plasma-phase reactions of the ion–molecule rather than radical–radical or radical–neutral type.[17,18] However, CW polymerisation reaction mechanisms, and functional group retention vary depending on whether the power input is high or low, and the nature of each precursor.[18]

For experimental procedures, plasma is carried out by turning the RF generator on, set at the required power input, while modulating the plasma by changing the capacitance of the matching unit in order to match the impedance of the plasma to that of the RF generator, by minimising the standing wave ratio (SWR) value to 1.

2.1.1.6. Pulsed Plasma Depositions

Pulsed plasma depositions are performed Pulsed plasma depositions are performed by modulating the power on and off in millisecond (ms) or microsecond (µs) lapses in the presence of the gas or precursor to ignite the plasma, where the ratio of the on (t_{ON}) and off (t_{OFF}) times, denotes the effective power delivery in the system (duty cycle), Equation 2. 7.[19]

$$P_a = P_p \left(\frac{t_{ON}}{t_{ON} + t_{OFF}} \right)$$

Equation 2. 7

where P_a is the average power input, and P_p is the delivered power to the glow discharge.[20]

The mechanism process implies that the precursor molecules are activated at the t_{ON} lapse of the pulse, then the deposition due to the polymerisation of longer-lived radicals from the gas phase occurs at the t_{OFF} lapse of the pulse. Nevertheless, t_{ON} and t_{OFF} values should be calculated according to the physicochemical properties of precursors to optimise the functional group retention during the film deposition. Pulsed plasma deposition with long t_{OFF} intervals extending beyond the initial film growth regime, requires a longer time to process materials with no improvement of the surface chemistry or significant film thickness increment. On the other hand, pulsed plasma deposition with long t_{ON} intervals help to achieve desired thickness in a short time; however, it leads to undesired precursor molecule fragmentation, thus, loss of functional group retention.[2,19] Therefore, the main purpose of the pulsed plasma deposition technique is the high functional group retention of the plasma polymer film.[4]

For experimental procedures, the plasma was pulsed using a pulse generator, which is connected to an RF generator and an oscilloscope. The pulse generator works as an external input to the RF generator controlling the duration of the RF pulses supplied to the plasma reactor. Simultaneously, the pulse generator is connected to an oscilloscope to set the pulse generator to produce a square wave pulse with the desired on (t_{ON}) and off (t_{OFF}) times, and to observe the pulse and pulse shape in the plasma.

2.1.1.7. Inductively Coupled Plasmas

For aims of the work presented in this thesis, cold plasmas are used for the surface functionalisation, and synthesis of thin functional polymer coatings, generated by inductively coupled radiofrequency (RF) discharges given that non-equilibrium or quasi-neutral plasmas allow the formation of different chemical species readily activated for surface functionalisation or deposition.[2,4,5]

For the case of RF inductively coupled plasmas, a helical conductive coil surrounds the plasma system, and, at the same time, it is connected to an RF generator, generating magnetic and electric fields within the plasma volume, and providing electrons with energy to sustain the plasma, Figure 2. 2.[2]
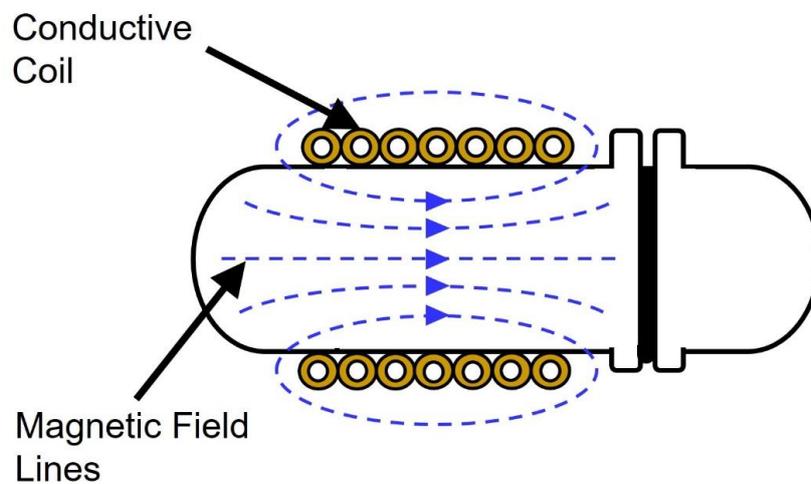
Figure 2. 2: Schematic representation of a magnetic field of an RF inductively coupled plasma.

The plasma current flow generates a magnetic flux or inductance, which is created by the coil and the matching unit device, which is operated to

optimise the power transfer discharge uniformity from the RF generator to the coil and plasma volume, and thus enhancing the plasma process.[2,4]

2.1.2. Experimental Settings for Plasma Deposition

2.1.2.1. Gas-Phase Plasma Deposition

An inductive RF reactor was employed for the plasma deposition experiments (continuous wave and pulsed depositions). It consists of a cylindrical glass reactor, located within a Faraday cage, with a coil wounded around it. The coil is connected to the power supply through a matching unit, Figure 2. 3.
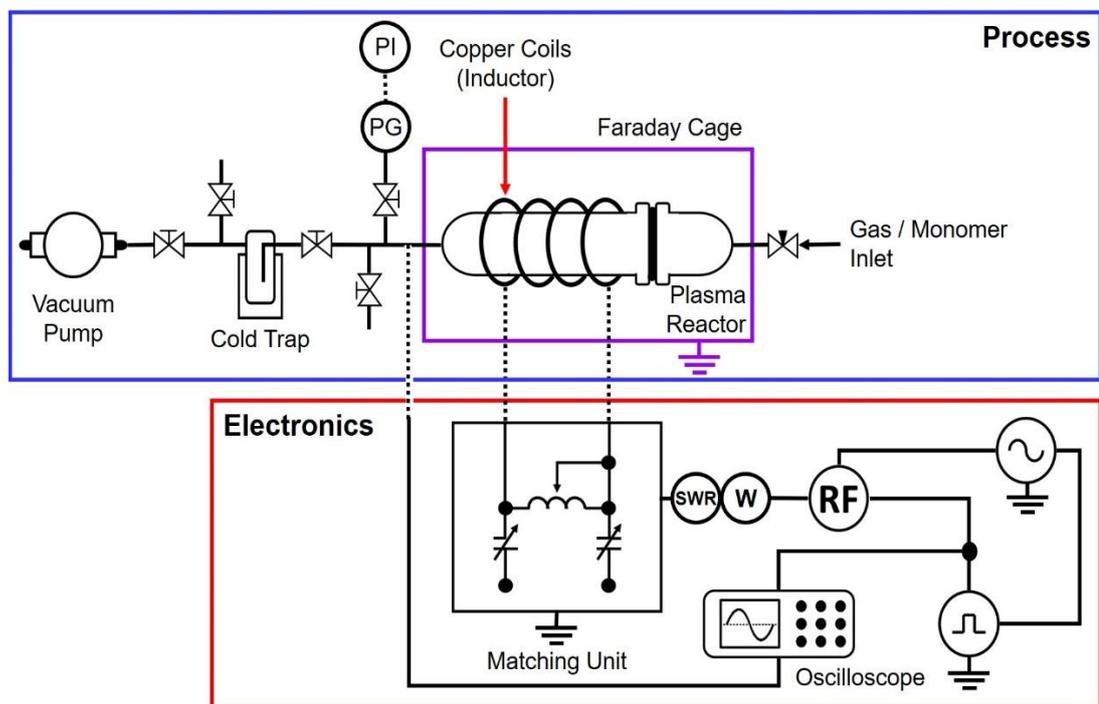
Figure 2. 3: Schematic representation of inductive plasma rig.

Continuous-wave and pulsed plasma deposition of functionalised thin films were undertaken in a cylindrical glass chamber (5 cm diameter, 432 cm^3 volume) enclosed within a Faraday cage.[21] The reactor was connected to a 30 L min^{-1} two-stage rotary pump (E2M2, Edwards Vacuum Ltd.) via a liquid nitrogen cold trap (base pressure less than 2×10^{-3} mbar and air leak rate better than 6×10^{-9} mol s^{-1}).[22] An inductor–capacitor (L–C) impedance matching network was used to minimise the standing wave ratio (SWR) for power transmission from a 13.56 MHz radiofrequency (RF) power generator to a copper coil (4 mm diameter, 11 turns, spanning 10 cm, located 11 cm downstream from the gas inlet) externally wound around the glass chamber. For pulsed plasma deposition, a signal generator (model TG503, Thurlby Thandar Instruments Ltd.) was used to trigger the RF power supply, and the corresponding pulse shape was monitored with an oscilloscope (model V252, Hitachi Ltd.), Figure 2. 3. Prior to each plasma deposition, the reactor was scrubbed with surfactant type detergent, rinsed with propan-2-ol (+99.5%, Fisher Scientific UK Ltd.), and oven dried at 200 °C. Next, a continuous wave air plasma was run at 0.2 mbar pressure and 50 W for 30 min, in order to remove any residual contaminants from the chamber walls. Then, substrates were placed in the middle of the chamber in order to carry out CW or pulsed plasma depositions.

2.1.2.2. Atomised Spray Plasma Deposition

Atomised spray plasma deposition was carried out in an electrodeless, cylindrical T-shape glass reactor volume 1117 cm^3, base pressure below 3×10^{-3} mbar, and a leak rate better than 2×10^{-9} mol s^{-1}) enclosed in a Faraday cage. The chamber was pumped by a 30 L min^{-1} two-stage rotary pump (model E2M2, Edwards Vacuum Ltd.) attached to a liquid nitrogen cold trap, and the system pressure monitored by a thermocouple gauge. An L–C impedance matching network was used to minimise the standing wave ratio for power transmitted from a 13.56 MHz radiofrequency (RF) power supply to a copper coil (4 mm diameter, 7 turns) located downstream from an atomiser

(20 μm diameter median droplet size, model No. 8700-120, Sono-Tek Corp.), which was driven by a broadband ultrasonic generator (120 kHz, model No. 06-05108, Sono-Tek Corp.). Prior to each deposition, the chamber was scrubbed with detergent, rinsed with propan-2-ol and acetone (+99%, Fisher Scientific Ltd.), and oven dried. Next, a continuous wave air plasma was run at 0.2 mbar pressure and 50 W for 30 min, in order to remove any remaining residual contaminants from the chamber walls. Substrates were placed downstream in line-of-sight from the atomiser in order to carry out ambient temperature deposition using continuous-wave plasma at optimal power in conjunction with atomisation of a liquid or a solid-liquid slurry into the reaction chamber, and optimal flow rate conditions for each case, Figure 2. 4.[23,24]
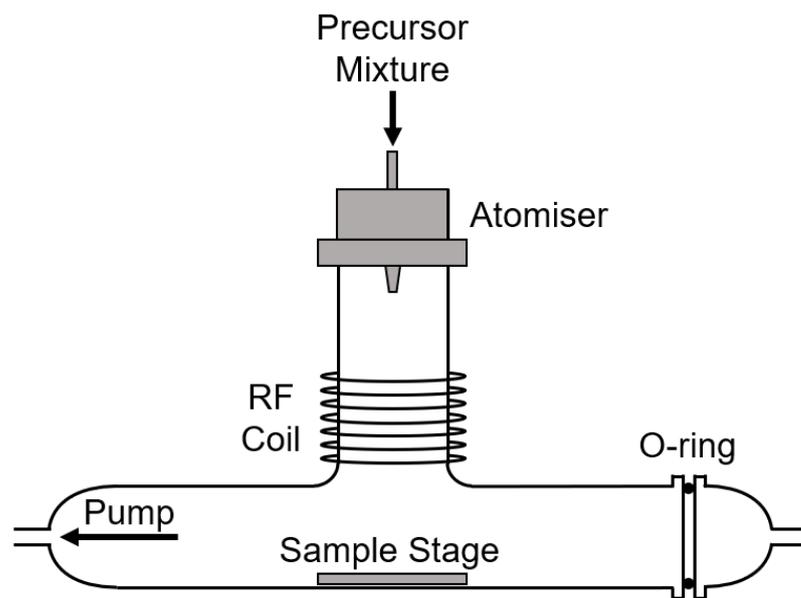
Figure 2. 4: Atomised spray plasma deposition (ASPD) chamber. Figure created by I. Castaneda-Montes.[23]

2.2. Infrared Spectroscopy

2.2.1. Basics of Infrared Spectroscopy

Fourier transform infrared (FTIR) spectroscopy is a non-destructive characterisation technique useful to identify the presence of functional groups of molecules contained in a sample by their definite characteristic absorption frequencies within the infrared spectrum. The infrared spectrum of any given sample is interpreted by using the characteristic frequencies of functional groups to identify the molecular structure of the substance.[25,26]

Infrared radiation is a form of thermal energy capable of inducing molecular vibrations in covalent bonds. When the electromagnetic field interacts with a molecule, whose atoms are distributed at different energy levels or states, a quantum of energy is either emitted or absorbed, due to the energy transference from the field to the molecule, provoking a difference in energy between the two quantised states (ΔE) and to the dipole moment taking place, satisfying Bohr's frequency condition, Equation 2. 8:[27,28]

$$\Delta E = h v \qquad \text{Equation 2. 8}$$

where h = 6.626×10^{-34} J s, and v is the frequency or the electromagnetic field in which the molecule is exposed. In other words, in terms of the infrared spectroscopy technique, infrared radiation passes through a test sample (i.e., it is transmitted), and some other frequencies are absorbed by the sample, leading to molecular vibrations, allowing the instrument to evaluate both, the transmitted and absorbed particular energies.[27,29] Furthermore, in order to get infrared absorptions from a given molecule, it must possess an electric dipole moment which changes as the chemical bond expands and contracts, during the vibration generated when in the presence of infrared electromagnetic field.[26]

The intensity of an infrared absorption band is dependent on the magnitude of the dipole change during the vibration, the larger the change, the stronger the absorption band. Experimentally, the intensity of the absorption band due to a functional group also depends on how many times that group occurs in the sample (concentration), intramolecular/intermolecular bonding, the phase of the sample, the solvent (if any), and on neighbouring atoms/groups; the resulting absorption spectrum then reveals individual peaks corresponding to the frequency of a vibration of a part of a sample molecule.[25] In terms of concentration, the quantification of absorbed infrared photons (A) is related to Beer–Lambert Law, Equation 2. 9:

$$A = \varepsilon lc$$
<div align="right">Equation 2. 9</div>

where **ε** is the absorptivity, **l** is the path length, and **c** is the concentration of molecules in the sample.[30]

Nevertheless, although functional group frequencies occur within narrow limits, interference or perturbation may cause a shift of the characteristic bands due to the electronegativity of neighbouring groups or atoms, or the spatial geometry of the molecule. Often, functional groups have more than one characteristic infrared absorption band associated with them. Two or more functional groups often absorb in the same region and can be distinguished from each other through other characteristic infrared bands which occur in non-overlapping regions. Thus, the presence of a band at a frequency should not be used on its own as an indication of the presence of a functional group; it should be confirmed with other bands or characterisation techniques.[25]

Experimentally, the Michelson interferometer is the standard for use in FTIR spectrometry, Figure 2. 5. The device consists of four arms. The infrared source, two perpendicular plane mirrors (fixed and moving mirrors), and a semi-reflecting beamsplitter which bisects the planes of the two

mirrors. The main function of the beamsplitter is to respectively reflect light and transmit light toward the mirrors, from which they are reflected back to the beamsplitter, where they are recombined into a single light beam (they interfere when both beam waves superpose to form a single wave) that leaves the interferometer, interacts with the sample and strikes the detector. Figure 2. 5.[27,30]
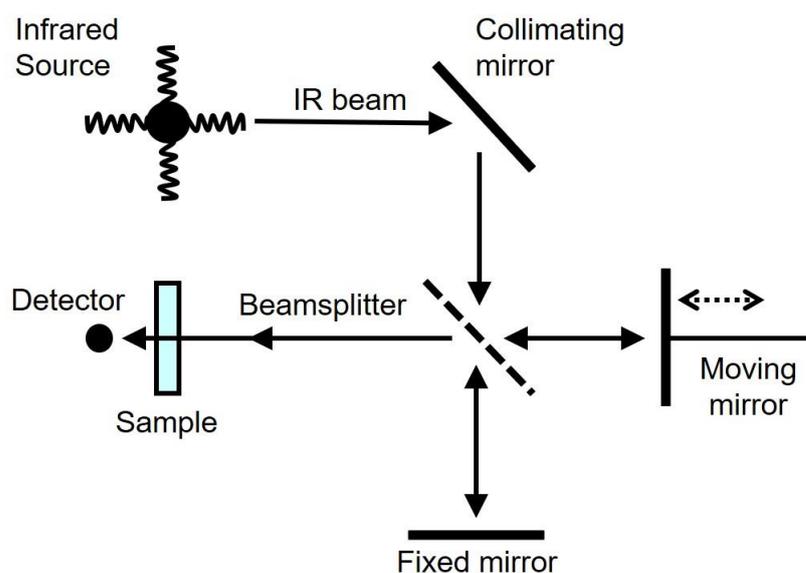
Figure 2. 5: Michaelson interferometer. Based on schematic by Smith.[30]

2.2.1.1. Reflection–Absorption Infrared Spectroscopy (RAIRS)

RAIRS is a useful technique to obtain the spectrum of a coating which is deposited on shiny and smooth surfaces, such as silicon wafers. During the reflectance-absorbance process, the infrared beam reflects from a flat mirror, passes through the coating, reflects from the base substrate to pass the coating again, off a second flat mirror, then it is captured and focused onto the FTIR detector, Figure 2. 6. This technique results advantageous for being

fast and easy to apply, surface-sensitive while non-destructive; however, the applications are limited by the nature of required base substrates.[30]
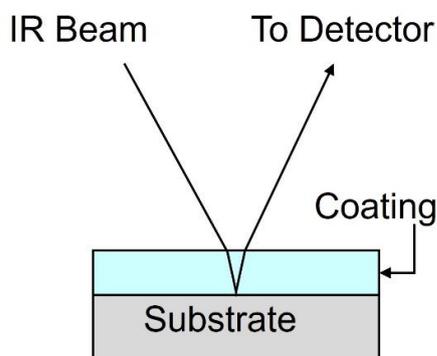
Figure 2. 6: Reflectance-absorbance process. The light beam passes through the sample (coating), reflects from the shiny and smooth base substrate, and passes through the sample for a second time, and then focused onto the FTIR detector. Based on schematic by Smith.[30]

2.2.1.2. Attenuated–Total–Reflectance (ATR) Spectroscopy

ATR spectroscopy is based on the total–internal–reflection phenomenon, which consists of a beam of infrared radiation entering a crystal in order to undergo total–internal–reflection, under condition of the angle of incidence (θ) at the sample–crystal interface being greater than the critical angle (which is function of the refractive indices of the two surfaces). During the ATR process, the beam penetrates a fraction of a wavelength beyond the reflecting surface, so the sample (i.e., coating) selectively absorbs radiation from the infrared beam, the beam loses energy at the wavelength where the material absorbs, and then the resulting beam is captured by the FTIR detector, Figure 2. 7. Different designs of ATR instrument cells allow characterisation of liquid and solid samples, and continuous flow characterisation in order to detect spectral changes in a fluid.[27]
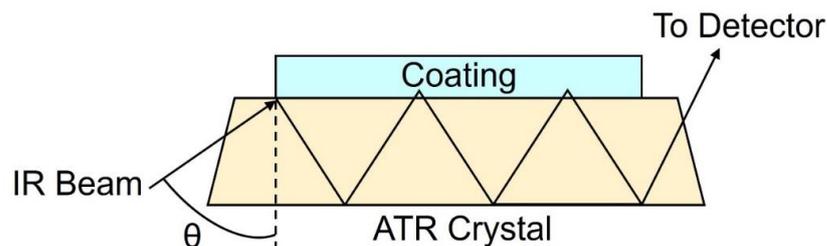
Figure 2. 7: Typical infrared attenuated–total–reflectance spectroscopy process. Based on schematic by Sturart.[27]

2.2.2. Experimental Settings for Infrared Spectroscopy

Fourier transform infrared (FTIR) analysis was performed using an FTIR spectrometer (Spectrum One, Perkin Elmer Inc.) equipped with a liquid nitrogen cooled MCT detector. The spectra were averaged over 285 scans at 4 cm^{-1} resolution across the 500–4000 cm^{-1} wavenumber range.

Reflection–absorption infrared spectroscopy (RAIRS) analysis of plasma deposited films and further functionalised surfaces on silicon wafers, was performed using a variable angle reflection–absorption accessory (Specac Ltd.) set to a grazing angle of 66° to the substrate normal.

Attenuated–total–reflection (ATR) spectra of plasma deposited films and further functionalised surfaces on cloth, liquid monomers, and solid precursors were acquired using a single reflection instrument accessory (model Golden Gate, Specac Ltd.).

2.3. X-Ray Photoelectron Spectroscopy

X-ray photoelectron spectroscopy (XPS) is a surface characterisation technique useful to identify the elemental composition from the top-most

atomic layers of a surface.[31] The XPS analysis is carried out in a vacuum chamber where a solid sample is irradiated with X-ray photons capable of penetrating 1–10 µm into the bulk material. The X-ray photon energy is absorbed by the bulk material atoms and ejects electrons of different kinetic energies. Only the electrons from the top atomic layers (1–5 nm) are capable of being ejected by the X-ray photons without losing kinetic energy which corresponds to the valence or core level of the atoms. Therefore, the kinetic energy of the ejected photoelectrons from the valence or core levels are associated with the elemental composition of the solid surface. The overall process is known as the photoelectric effect, Figure 2. 8. [31,32,33]
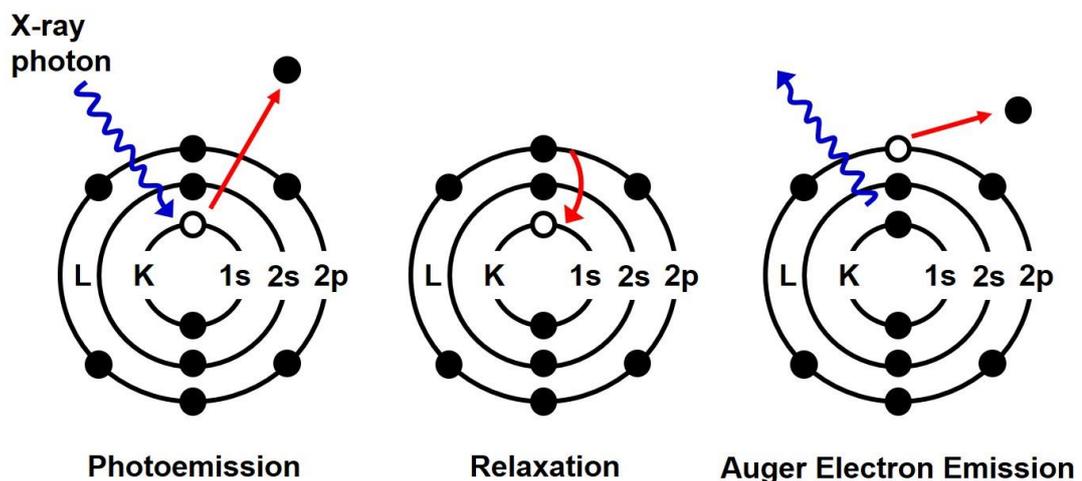
Figure 2. 8: Photoelectric effect, subsequent relaxation, and Auger electron emission: an X-ray photon ejects a photoelectron from the atomic core level, such space is subsequently filled by an electron from a higher valence level at the relaxation step, causing the Auger electron emission which takes up the remaining excess energy as kinetic energy.[34] Based on schematic by Wren et al.[33]

The kinetic energy (E_K) of the emitted photoelectrons is quantified and analysed to produce a spectrum of electron intensity as a function of binding energy (E_B). The kinetic energy is proportional to the X-ray photon energy and the binding energy of the material atoms. Therefore, the kinetic energy

of the ejected photoelectrons can be calculated by the modified Einstein photoelectric equation, Equation 2. 10.[31,32]

$$E_K = hv - E_B - \varphi_S$$

<div style="text-align: right">Equation 2. 10</div>

where hv is the X-ray photon energy, and φ_s is the spectrometer photoelectric work function of the solid. The binding energy may be regarded as the energy difference between the initial and final states after the photoelectron has left the atom, and it is measured with respect to the highest occupied level of the solid and the Fermi level of the spectrometer to which the sample is connected electrically,[26,31,35] as described by Koopmans theorem.[36]

Experimentally, the electron energy distribution can be measured using an electrostatic energy analyser which conventionally consists of two electrically isolated concentric hemispheres with a potential difference between them, Figure 2. 9. The electrostatic field selectively allows electrons with kinetic energy equal to the pass energy through to the detector. Electrons with kinetic energy lower than the pass energy are attracted by the inner positive concentric hemisphere and neutralised, whereas the higher energy electrons are lost when they hit the outer concentric hemisphere. The ejected photoelectron spectrum is obtained from the scan of electron kinetic energies by retarding the electrons to the pass energy using a negatively charged retard plate electrode. The change of negative voltage on the retard plate allows electrons with different kinetic energies go through the analyser to the detector.[26]
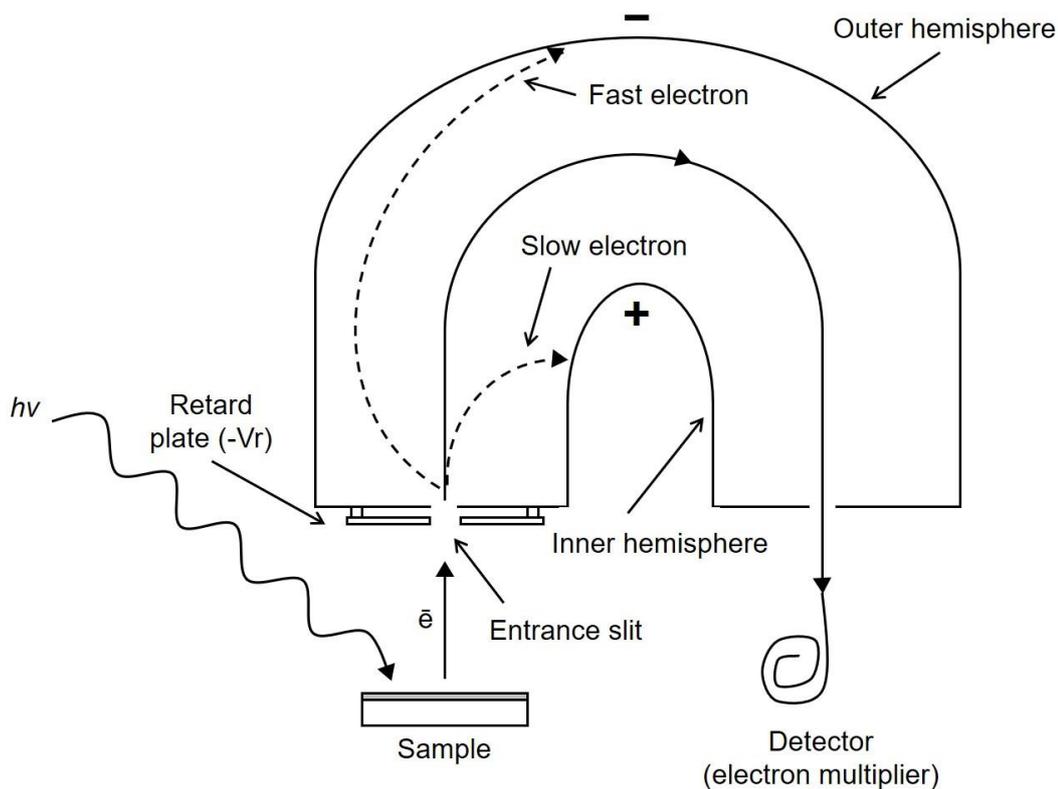
Figure 2. 9: Electrostatic energy analyser used in electron/ion spectroscopic analysis of surfaces. Based on schematic of Hoffman, S.[37]

Two types of X-ray source are in common usage, monochromated and non-monochromated. Non-monochromated sources utilise Kα Al (1486.6 eV) or Mg Kα (1253.6 eV) X-ray source radiation, these materials are bombarded with electrons up to 15 keV in energy. The X-ray output consists of a continuous energy distribution extending up to the incident electron energy (Bremsstrahlung), with much higher intensity at the characteristic Kα energy.[38] The spectrum is obtained as a plot of the number of detected electrons per energy interval versus their kinetic energy.[31]

X-ray induced sample damage is a common problem during the XPS analysis of materials and can cause the spectrum to change with exposure time.[39] Thus, samples cannot be used for other characterisation analysis after being exposed to X-rays. In all experimental chapters of the present

thesis, the XPS technique is employed to obtain surface elemental compositions using a non-monochromated X-ray source.

2.3.1. Experimental Settings for X-Ray Photoelectron Spectroscopy

Surface chemical compositions of the plasma deposited layers and/or further functionalised surfaces were measured by X-ray photoelectron spectroscopy (XPS) using an electron spectrometer (model ESCALAB II, VG Scientific Ltd.) fitted with an unmonochromatised Mg Kα X-ray source (1253.6 eV) and a concentric hemispherical analyser. Photoemitted electrons were collected at a take-off angle of 20° from the substrate normal with electron detection in the constant analyser energy mode (CAE mode pass energy = 20 eV). Experimentally determined instrument sensitivity (multiplication) factors were C(1s):O(1s):N(1s) equals 1.00:0.35:0.70 respectively. A linear background was subtracted from core-level spectra and then fitted using Gaussian peak shapes with a constant full-width-half-maximum (FWHM).[40] All binding energies are referenced to the Mg $K\alpha_{1,2}$ C(1s) hydrocarbon peak $-\underline{C}_xH_y$ at 285.0 eV.[41]

2.4. Scanning Electron Microscopy

Scanning electron microscopy (SEM) is a topographic technique for high-resolution imaging of surfaces, in which a beam of electrons is scanned across a sample (instead of light used in optical light microscopes to form images). The scanning electron microscope generates a beam of incident electrons at the top of an electron column above the sample chamber, this column as well as the sample chamber are at moderate vacuum to allow the

electrons to travel from the electron thermal emission beam source to the sample and then, to the detectors. The electrons are focused into a small beam by a series of electromagnetic lenses in the scanning electron microscope column. Scanning coils near the end of the column direct and position the focused beam onto the sample surface. Electrons in the beam penetrate the bulk surface, interact with its atoms, and the obtained signals are collected and processed to obtain images and chemistry of the sample surface, Figure 2. 10. The SEM image does not form a real image of the sample but a serial data stream, an electronic grayscale image with surface details at the micro- and nanoscale.[42–44]
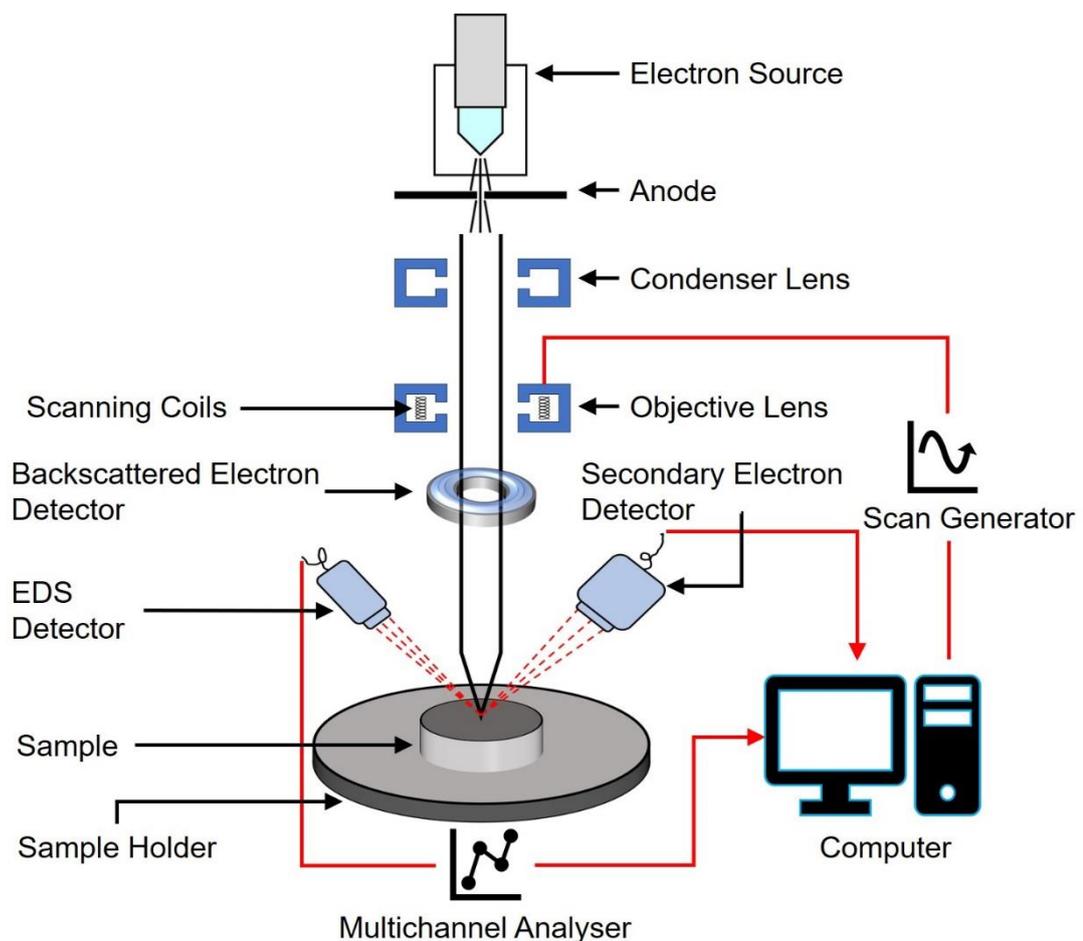
Figure 2. 10: Image formation in the scanning electron microscope. Adapted from schematic by Ul-Hamid.[44]

While obtaining the SEM image from the sample surface, different types of signals are generated. High-energy electrons ejected by an elastic collision of an incident electron, usually with a sample atom's nucleus, are known as backscattered electrons; emitted lower-energy electrons resulting from inelastic scattering are called secondary electrons, which are ejected after collisions with the nucleus where substantial energy loss occurs or by the ejection of loosely bound electrons from the sample atoms; and characteristic x-rays. The backscattered electrons are analysed to provide a three-dimensional high-resolution image of the surface while secondary electron images show topographic illumination and contrast.[42–44]

Commonly, SEM samples are mounted on a stub (sample holder) taken from an aluminium disc (1 cm diameter approximately), with the sample being glued to the stub, Equation 2. 10. To prepare the mounted samples, they must be coated with a conducting layer to overcome charging of the surface by the electron beam.[45] For aims of the present thesis, gold sputter coating was performed on samples in all cases where it applies.

2.4.1. Experimental Settings for Scanning Electron Microscopy

For scanning electron microscopy analysis, samples and substrates were correspondingly mounted onto carbon disks supported by aluminium stubs; for thicknesses, the samples were mounted onto 45°-tilted aluminium stubs in order to measure different cross-sectional points along the deposited coating or further functionalised surface on silicon wafers, and then covered with a 5–10 nm evaporated gold layer (Polaron SEM Coating Unit, Quorum Technologies Ltd.). Electron micrographs were acquired using a scanning electron microscope (model Vega 3LMU, Tescan Orsay Holding, a.s.) operating in secondary electron detection mode at an accelerating voltage of 8 kV, and a working distance of 8–10 mm.

2.5. Water Contact Angle

The contact angle technique is an indirect method to determine the wettability, which is associated to the free surface energy (γ), of a solid surface. The free surface energy of a solid surface corresponds to the difference of internal energy between the surface molecules and the bulk molecules.[46] Surface molecules have disrupted intermolecular forces due to the lack of neighbouring molecules as compared to the bulk molecules. These intermolecular forces of the surface molecules are the sum of the polar forces and non-polar forces (van der Waals forces), and thus, the excess of surface free energy is quantified by the Helmholtz free energy.[47] Hence, the contact angle method is used to determine indirectly the surface free energy of a solid surface (γ_{SG}) by measuring the angle formed between a liquid droplet with known surface tension, and a solid surface—the equilibrium contact angle is the result of the mechanical equilibrium of a liquid droplet on a solid surface. The measurement of the contact angle is carried out at the intersection of a solid–liquid interface by applying a geometric tangent at the solid–liquid–gas system—the equilibrium contact angle value is a function of the surface tension of the liquid and the surface free energy of the solid surface,[48] Figure 2. 11.
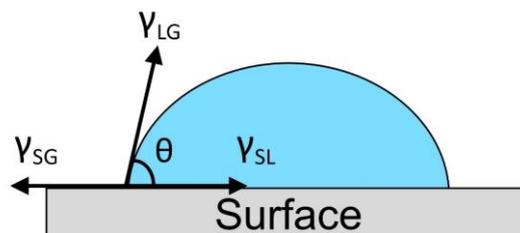
Figure 2. 11: Surface tension forces interacting upon a liquid droplet on a surface, resulting in the corresponding contact angle, θ.

On an ideal flat solid surface, the contact angle (θ) is a relationship of the solid–gas (γ_{LG}), solid–liquid (γ_{SL}), and liquid–gas (γ_{LG}) interface according to the Young equation,[49] Equation 2. 11. Therefore, the wettability of a solid surface can be classified as hydrophilic or hydrophobic, depending on the contact angle values. When the water contact angle is <90°, the surface is hydrophilic; and for water contact angle values >90°, the surface is hydrophobic.[50]

$$\cos\theta = \frac{\gamma_{SG} - \gamma_{SL}}{\gamma_{LG}}$$

Equation 2. 11

2.5.1. Experimental Settings for Water Contact Angle Measurements

Sessile drop static contact angle measurements were carried out at 20 °C using a video capture apparatus in combination with a motorised syringe (model VCA 2500XE, A.S.T. Products Inc.). 1 μL droplet of ultrahigh-purity water (B.S. 3978 grade 1) was employed as probe liquid to determine the wetting properties.

2.6. Film Thickness

Spectrophotometry is a non-destructive technique used to measure the film thickness of a material. The amount of transmitted or reflected light from the material surface is used to approximate the optical constants of the film as a function of the wavelength. The optical constants of a material, refractive index (n) and extinction coefficient (k), are used to describe how the light in air beam travels through a film. The refractive index is the ratio of the speed of light to the speed of light which travels through the material. The extinction coefficient is a measurement of the absorbed light in the film.[51]

When the incident light meets an interface, the light can be reflected or transmitted. The amount of reflected or transmitted light is characteristic of the optical properties and the film thickness of the material. To determine the film thickness, a mathematical model, the Cauchy model, can be used to solve n and k for each wavelength. To minimise the error, the Levenberg–Marquardt algorithm can be used. The obtained transmittance–reflectance curve is then used to calculate the film thickness, Figure 2. 12.[52]
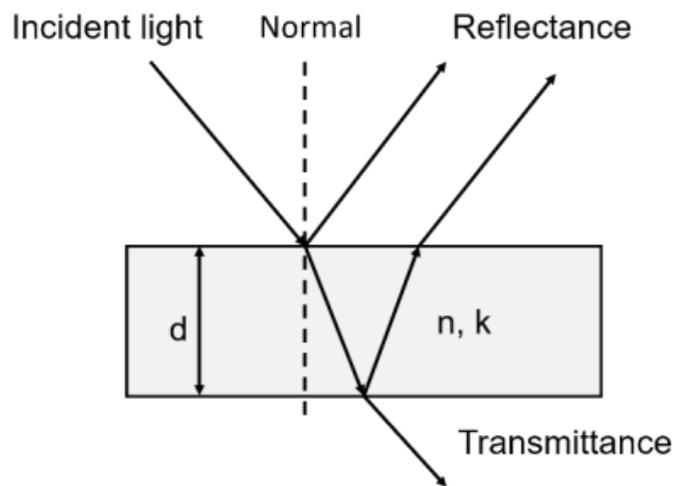
Figure 2. 12: Principle of interference, where the incident light can be both transmitted or reflected when the light travels through a transparent film. The refractive index (n) and extinction coefficient (k) are used to determine the film thickness (d) as a function of the wavelength. Based on schematic by Shimadzu Corporation.[53]

2.6.1. Experimental Settings for Film Thickness Measurements

Film thicknesses of plasma polymer coatings deposited on silicon wafers were measured with a spectrophotometer (model NKD-6000, Aquila Instruments Ltd.). Transmittance–reflectance curves (350–1000 nm wavelength range) were obtained using a parallel (p-)polarised light source at 30° incident angle to the substrate. These were fitted to a Cauchy model

for dielectric materials[54] using a modified Levenberg–Marquardt algorithm (version 2.2 Pro-Optix software, Aquila Instruments Ltd.).[55]

2.7. Antibacterial Activity Test

2.7.1. Bacterial Growth

Bacterial growth refers to the increment of bacterial cells by binary fission. So, when bacteria are inoculated in a nutritious medium for them, the bacterial growth is counted at intervals that represent four phases of growth (growth curve): lag, log, stationary, and death phases, Figure 2. 13.[56,57]
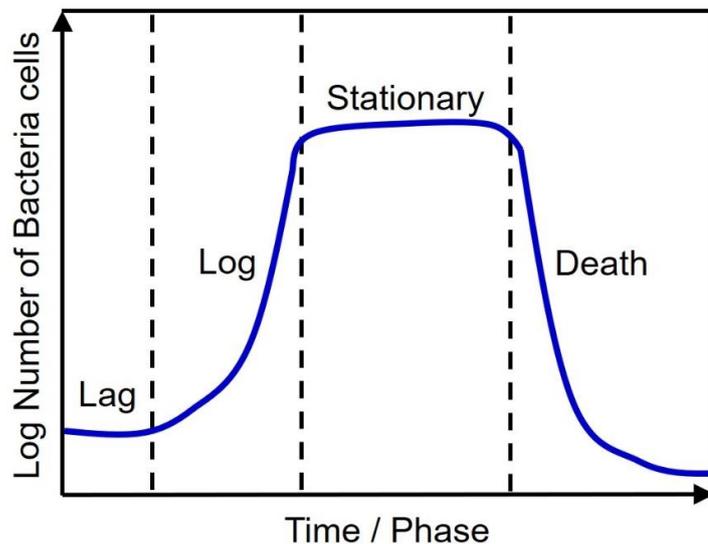
Figure 2. 13: Typical bacterial growth curve, with corresponding growth phases. Based on graphic by Wang et al.[58]

At the lag phase, the bacterial cells adapt to the new media while increasing in size and synthesising enzymes and factors needed for further

bacterial cell division and population growth. Eventually, the cells start their log phase or exponential growth phase, in which bacteria cells reproduce exponentially by means of each generation occurring in the same time interval as the previous ones; this phase continues until nutrients are consumed or toxic products accumulate, at which time the cell growth rate slows, and some cells may begin to die. At the stationary phase, the growth rate slows down, the number of death cells equals the number of new cells, and the population stabilises. Then, at the death phase, the number of death cells overpasses the number of new cells; this often continues until the whole bacterial population dies.[56,57]

2.7.1.1. Measuring Bacterial Growth

Bacterial growth can be measured in different ways. Depending on the method, it is possible to measure cell numbers or population total mass. Population numbers are usually recorded as the number of cells in a millilitre of liquid or, in a gram of solid material.[56] There are different ways to measure microbial growth that should be employed according to the requirements of the research study, however, in the present work, serial dilution for plate counts will be used to quantify the bacterial cell viability after bacteria is in contact with the testing materials after fixed interaction times.

To perform dilutions, Figure 2. 14, first is required to prepare the non-diluted bacterial solution—from which the experimental coating samples in the present thesis will be tested. Since the testing bacteria grow in liquid medium, the bacterial solution displays a turbid appearance due to the increment of cell counts. This turbidity is measured in spectrophotometers, allowing to read optical density values required to identify the optimum point when the prepared non-diluted bacterial solution sample is ready for serial dilutions,[56] that will be used for plate counts.
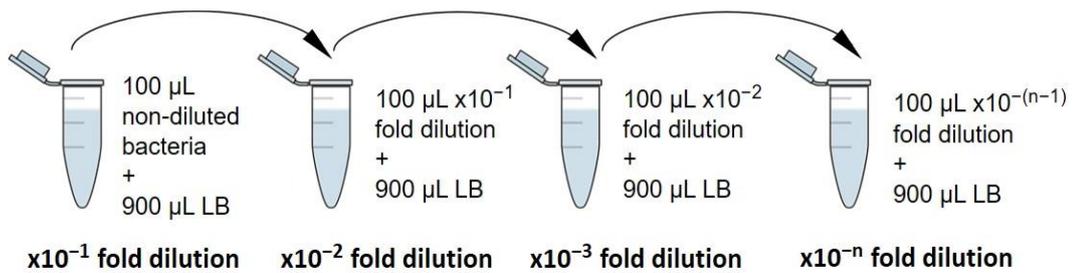
Figure 2. 14: Dilution method. Example of dilution method of 1 mL scale. The 10-fold dilutions are performed as needed for each set of experiments. LB stands for Lysogeny Broth media.

Plate counts method is based on the assumption that each live bacterium divides to produce a single colony, Figure 2. 15. Still, bacteria use to grow linked in chains often forming a colony, not from a single bacterium but from short segments of a chain or from a bacterial clump. Therefore, plate counts are commonly reported as colony-forming units (CFU).[56,59]
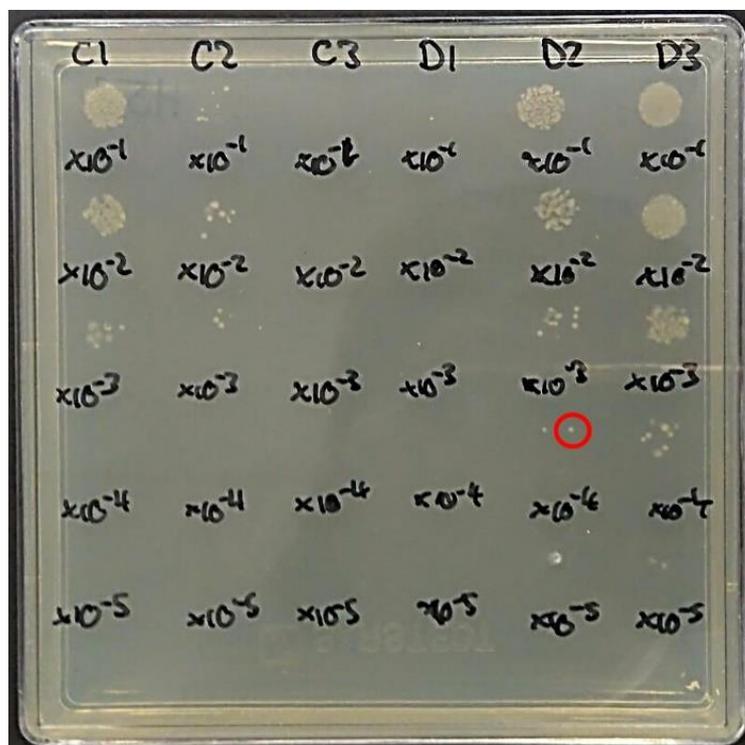
Figure 2. 15: Examples of bacterial growth of bacterial dilutions sequentially plated on an agar plate. Red circle circles a single bacterial colony.

This method requires to be cautious with the numbering of colonies developed in the plate to avoid inaccurate results. The United States Food and Drug Administration convention is to count plates within 25–250 colonies.[60] To accomplish it, the original inoculum is diluted several times as serial dilution. To get the resulting CFU mL^{-1}, the number of colonies counted from the chosen diluted plate is then multiplied with the corresponding dilution factor to figure out how many of those colonies would be if directly representing a 1 mL sample.

2.7.2. Preparation of Bacterial Cultures

Bacterial cultures were prepared using 5 mL of sterile (121 °C for 15 min in an autoclave (model Vario 1528, Dixons Ltd.)) Lysogeny Broth (LB) media (L3022, Sigma-Aldrich Ltd., 2% w/v in Milli-Q$^{®}$ water), starting with a single bacterial colony and grown for 16 h at 37 °C in a shaking incubator (model Stuart Orbital Incubator SI500, Cole-Parmer Instrument Company LLC.) set at 120 rpm. Then, 50 µL of the overnight bacterial culture was used to separately inoculate bacteria in a sterile polystyrene cuvette (10 mm, model 67.742, Sarstedt AG) containing 1 mL of LB. The cuvette was covered with plastic film (Parafilm, Cole-Parmer Instrument Company LLC.) and bacteria were grown as before at 37 °C in a shaking incubator set at 120 rpm. Optical densities of OD_{650nm}=0.400 (spectrometer model BOECO S-30, Boeckel GmbH; for immobilised chitosan coatings in chapter 3) or OD_{600nm}=0.400 (spectrometer model DS-11, DeNovix Inc.; for ASPD poly(acrylic acid) and ASPD metallosurfactant/polymer coatings, in chapters 4 and 5, respectively) were measured to provide bacterial cultures in the mid-log phase of growth.[61]

2.7.3. Antibacterial Test: Dilution Method

This method has been employed in two scales, 1 mL and 100 µL, for experiments developed in Chapter 3 to Chapter 5, correspondingly, followed by colony-forming unit (CFU) plate counting.

- 1 mL scale: For antibacterial testing, sterile microtubes (1.5 mL, Sarstedt AG) were loaded with either control or treated non-woven polypropylene cloth samples (1.4 cm x 1.7 cm pieces loaded to each microtube; 0.41 mm thick, 22.7 ± 4.4 µm fibre diameter, and dimpled structure 0.68 ± 0.16 mm separation, Spunbond, 70 g m^{-2}, Avoca Technical Ltd., UK[21]). Then, 100 µL of the prepared bacterial culture at fixed optical density was dispensed onto each cloth to allow the microorganisms to interact with the surface and left to incubate at 30 °C for 16 h (model Bacterial Incubator 250, LMS Ltd.). Next, 900 µl of sterile LB media was pipetted into each microtube and vortexed (model Vortex-Genie 2, Scientific Industries Inc.), yielding a ten-fold dilution (10^{-1}) of bacteria. Further ten-fold serial dilutions were performed using the same method to give 10^{-2}, 10^{-3}, 10^{-4}, 10^{-5}, and 10^{-6} diluted bacterial concentrations.

- 100 µL scale: For antibacterial testing, sterile 96 well plates (Sarstedt AG) were loaded with either control or treated non-woven polypropylene cloth samples (0.5 cm x 0.5 cm pieces loaded to each well plate; 0.41 mm thick, 22.7 ± 4.4 µm fibre diameter, and dimpled structure 0.68 ± 0.16 mm separation, Spunbond, 70 g m^{-2}, Avoca Technical Ltd., UK[21]). Then, 10 µL of the prepared bacterial culture at fixed optical density was dispensed onto each cloth to allow the microorganisms to interact with the surface for a fixed period (1 min, 2 min, 5 min, and 10 min at room temperature, and 4h and 16 h at 30 °C (model Bacterial Incubator 250, LMS Ltd.) for ASPD (metallosurfactant–polymer) coated samples; tests on chitosan immobilised– and ASPD poly(acrylic acid) coated samples were performed only for 16 h at 30 °C). Next, 90 µL of sterile LB media was

pipetted into each well and mixed with the bacteria on the sample surface, yielding a ten-fold dilution (10^{-1}) of bacteria. Further ten-fold serial dilutions were performed using the same method to give 10^{-2}, 10^{-3}, 10^{-4}, 10^{-5}, 10^{-6} diluted bacteria concentrations.

Colony-forming unit (CFU) plate counting was then carried out by pipetting 10 µL diluted bacterial solution spots from each sample onto sterile semi-solid LB agar plates (EZMix™ powder, dust-free, fast-dissolving fermentation medium, Sigma-Aldrich Ltd.), and incubated at 30 °C for 16 h. Finally, the number of bacterial colonies visible at each dilution were counted where appropriate to calculate the corresponding CFU mL^{-1}. The results presented are the mean and standard deviation of at least 3 independent experiments.

2.7.4. Growth Inhibition Assays

To perform these tests, 0.6% LB agar was prepared (1% w/v tryptone (Melford Laboratories Ltd.), 0.5% w/v yeast extract (Melford Laboratories Ltd.), 1% w/v NaCl (Fisher Scientific UK, Ltd.), 0.2% v/v 1 M NaOH (Sigma-Aldrich, Inc.) (to pH ~7), 0.6% w/v agar), autoclaved at 121 °C for 15 min, then cooled to 65 °C in a water bath (model JB2, Grant Instruments Ltd.), taken out, carefully mixed with 100 µL of bacteria from prepared culture, poured onto sterile semi-solid LB agar plates (EZMix™ powder, dust-free, fast-dissolving fermentation medium, Sigma-Aldrich Ltd.), and finally dried for 15 min to provide an overlay seeded with bacteria. In one set of control experiments 10 µL spots of chitosan solutions (1% w/v, 2% w/v, and 3% w/v chitosan–1% v/v acetic acid aqueous solutions, and 1% w/v, 2% w/v, and 3% w/v chitosan–2% v/v acetic acid aqueous solutions), were pipetted onto the prepared 0.6% overlay LB agar plates, and incubated at 30 °C for 16 h. In another set of control experiments, 10 µL drops of 1% v/v and 2% v/v acetic acid aqueous solutions, 100% acetic acid, and Milli-Q® water, were pipetted

onto the prepared 0.6% overlay LB agar plates, and incubated at 30 °C for 16 h.

2.8. References

(1) Langmuir, I. Oscillations in Ionized Gases. *Proc. Natl. Acad. Sci. USA* **1928**, *14*, 627–637.

(2) Grill, A. *Cold Plasma in Materials Fabrication: From Fundamentals to Applications*, 1ˢᵗ ed.; IEEE Press: New York, 1994.

(3) Merche, D.; Vandencasteele, N.; Reniers, F. Atmospherric Plasmas for Thin Film Deposition: A Critical Review. *Thin Solid Films* **2012**, *520*, 4219–4236.

(4) Friedrich, J. *The Plasma Chemistry of Polymer Surfaces: Advanced Techniques for Surface Design,* 1ˢᵗ ed.; Wiley-VCH Verlag GmbH & Co. KGaA: Weinheim, 2012.

(5) Boulos, M. I.; Fauchais, P.; Pfender, E. *Thermal Plasmas: Fundamentals and Applications*; Plenum Press: New York, 1994; Vol. 1.

(6) Von Kendell, A.; Schulz-Von der Gathen, V. Foundations of Low-Temperature Plasma Physics—An Introduction. *Plasma Sources Sci. Technol.* **2017**, *26*, 113001.

(7) Eliezer, S.; Eliezer, Y. *The Fourth State of Matter: An Introduction to Plasma Science*, 2ⁿᵈ ed.; IOP Publishing: Bristol, England, 2001.

(8) Meichsner, J.; Schmidt, M.; Schneider, R.; Wagner, H.-E. *Nonthermal Plasma Chemistry and Physics*; CRS Press: London, 2013.

(9) Vandencasteele, N.; Reniers, F. Plasma-Modified Polymer Surfaces: Characterization Using XPS. *J. Electron Spectrosc. Relat. Phenom.* **2010**, *178–179*, 394–408.

(10) Michelmore, A.; Whittle, J. D.; Bradley, J. W.; Short, R. D. Where Physics Meets Chemistry: Thin Film Deposition from Reactive Plasmas. *Front. Chem. Sci. Eng.* **2016**, *10*, 441–458.

(11) Yasuda H. *Plasma Polymerization*. Academic Press,Inc.: Orlando, 1985.

(12) Michelmore, A.; Steele, D. A.; Robinson, D. E.; Whittle, J. D.; Short, R. D. The Link Between Mechanisms of Deposition and the Physico-Chemical Properties of Plasma Polymer Films. *Soft Matter* **2013**, *9*, 6167–6175.

(13) Short, R. D.; Goruppa, A. Plasma Polymerisation: Improved Mechanistic Understanding of Deposition, New Materials and Applications. In *Emerging Themes in Polymer Science*; Ryan, A. J., Ed.; Special Publication-Royal Society of Chemistry: Cambridge, England, 2001.

(14) Morosoff, N. An Introduction to Plasma Polymerization. In *Plasma Deposition, Treatment, and Etching of Polymers*; D'Agostino, R.; Academic Press Inc.: San Diego CA, 1990.

(15) Thiry, D.; Konstantinidis, S.; Cornil, J.; Snyders, R. Plasma Diagnostics for the Low-Pressure Plasma Polymerization Process: A Critical Review. *Thin Solid Films* **2016**, *606*, 19–44.

(16) Li, L.; Dai, J. X.; Xu, H. S.; Zhao, J. H.; Yang, P.; Maurdev, G.; Du Plessis, J.; Lamb, P. R.; Fox, B. L.; Michalski, W. P. Combined Continuous Wave and Pulsed Plasma Modes: For More Stable Interfaces with Higher Functionality on Metal and Semiconductor Surfaces. *Plasma Process. Polym.* **2009**, *6*, 615–619

(17) Voronin, S. A.; Zelzer, M.; Fotea, C.; Alexander, M. R.; Bradley, J. W. Pulsed and Continuous Wave Acrylic Acid Radio Frequency Plasma Deposits: Plasma and Surface Chemistry. *J. Phys. Chem. B* **2007**, *111*, 3419–3429.

(18) Haddow, D. B.; France, R. M.; Short, R. D.; Bradley, J. W.; Barton, D. A Mass Spectrometric and Ion Energy Study of the Continuous Wave Plasma Polymerization of Acrylic Acid. *Langmuir* **2000**, *16*, 5654–5660.

(19) Mishra, G.; McArthur, S. L. Plasma Polymerization of Maleic Anhydride: Just What Are the Right Deposition Conditions? *Langmuir* **2010**, *26*, 9645–9658.

(20) Nakajima, K.; Bell, A. T.; Shen, M. Plasma Polymerization of Tetrafluoroethylene. *J. Polym. Sci. Polym. Chem. Ed.* **1979**, *23*, 2627.

(21) Gürsoy, M.; Harris, M. T.; Downing, J. O.; Barrientos-Palomo, S. N.; Carletto, A.; Yaprak, A. E.; Karaman, M.; Badyal, J. P. S. Bioinspired Fog Capture and Channel Mechanism Based on the Arid Climate Plant *Salsola crassa. Colloids Surf. A* **2017**, *529*, 195–202.

(22) Ehrlich, C. D.; Basford, J. A. Recommended Practices for the Calibration and Use of Leaks. *J. Vac. Sci. Technol., A* **1992**, *10*, 1–17.

(23) Castaneda-Montes, I.; Ritchie, A. W.; Badyal, J. P. S. Atomised Spray Plasma Deposition of Hierarchical Superhydrophobic Nanocomposite Surfaces. *Colloids Surf., A* **2018**, *558*, 192–199.

(24) Ward, L. J. Atomisation of a Precursor into an Excitation Medium for Coating A Remote Substrate. U.S. Patent 7,968,154 B2, June 28, 2011.

(25) Socrates, G. *Infrared and Raman Characteristic Group Frequencies: Tables and Charts*. John Wiley and Sons Ltd: England, 2001.

(26) Attard, G.; Barnes, C. Surfaces. Oxford University Press: England, 1998.

(27) Stuart, B. H. In *Infrared Spectroscopy: Fundamentals and Applications*; Ando, D. J., Ed.; Analytical Techniques in the Sciences (AnTS); John Wiley & Sons, Ltd.: Chichester, England, 2004.

(28) Nakamoto, K. *Infrared and Raman Spectra of Inorganic and Coordination Compounds*, 4th ed.; John Wiley & Sons: New York, 1986.

(29) Miller, F. A. Introduction. In *Course Notes on the Interpretation of Infrared and Raman Spectra*; Mayo, D. W., Miller, F. A., Hannah, R. W., Eds.; John Willey & Sons, Inc.: New Jersey, USA, 2003.

(30) Smith, B. C. *Fundamentals of Fourier Transform Infrared Spectroscopy*, 2nd ed.; CRC Press Taylor & Francis Group: Boca Raton, 2011.

(31) Moulder, J. F.; Stickle, W. F.; Sobol, P. E.; Bomben, K. D. *Handbook of X-ray Photoelectron Spectroscopy: A Reference Book of Standard Spectra for Identification and Interpretation of XPS Data*. Chastain, J., Eds.; Perkin-Elmer Corporation, Physical Electronics Division: United States of America, 1992.

(32) Briggs, D. XPS: Basic Principles, Spectral Features and Qualitative Analysis. In *Surface Analysis by Auger and X-ray Photoelectron Spectroscopy*; Briggs, D., Grant, J. T., Eds.; IM Publications and Surface Spectra Limited: England, 2003.

(33) Wren, A. W.; Laffir, F. R.; Mellot, N. P.; Towler, M. R. X-Ray Photoelectron Spectroscopy: Studies from Industrial & Bioactive Glass to Biomaterials. In *X-Ray Photoelectron Spectroscopy*; Wagner, J. M., Ed.; Nova Science Publishers, Inc.: New York, USA, 2011.

(34) Briggs, D. In *Surface Analysis of Polymers by XPS and Static SIMS*; Clarke, D. R., Suresh, S., Ward, I. M., Eds.; Cambridge Solid State Science Series; Cambridge University Press: New York, USA, 1998.

(35) Gross, S.; Arelao, L. XPS as a Powerful Tool to Investigate the Surface Pproperties of Simple, Doped and Mixed Metal Oxides. In *X-Ray Photoelectron Spectroscopy*; Wagner, J. M., Ed.; Nova Science Publishers, Inc.: New York, USA, 2011.

(36) Koopmans, T. Über die Zuordnung von Wellenfunktionen und Eigenwerten zu den Einzelnen Elektronen Eines Atoms. *Phys.* **1934**, *1*, 104–113.

(37) Hofmann, S. In *Auger- and X-Ray Photoelectron Spectroscopy in Materials Science, A User-Oriented Guide*; Ertl, G., Lüth, H., Mills, D. L., Eds.; Springer Series in Surface Sciences; Springer: Heidelberg, Germany, 2013.

(38) Briggs, D. In *Surface Analysis of Polymers by XPS and Static SIMS*; Clarke, D. R., Suresh, S., Ward, I. M., Eds.; Cambridge Solid State Science Series; Cambridge University Press: New York, USA, 1998.

(39) Beamson, G.; Briggs, D. *High Resolution XPS of Organic Polymers: The Scienta ESCA300 Database*; John Wiley and Sons Ltd: England, 1992.

(40) Evans, J. F.; Gibson, J. H.; Moulder, J. F.; Hammond, J. S.; Goretzki, H. Angle Resolved ESCA Analysis of Plasma Modified Polystyrene. *Fresenius' Z. Anal. Chem.* **1984**, *319*, 841–844.

(41) Johansson, G.; Hedman, J.; Berndtsson, A.; Klasson, M.; Nilsson, R. Calibration of Electron Spectra. *J. Electron Spectrosc. Relat. Phenom.* **1973**, *2*, 295−317.

(42) Reimer, L. Scanning Electron Microscopy: Physics of Image Formation and Microanalysis. In *Springer Series in Optical Sciences*; Hawkes, P. W., Eds.; Springer-Verlag Berlin Heidelberg GmbH: Germany, 1998.

(43) Goldstein, J. I.; Newbury, D. E.; Echlin, P.; Joy, D. C.; Roming, A. D. Jr.; Lyman, C. E.; Fiori, C.; Lifshin, E. *Scanning Electron Microscopy and X-Ray Microanalysis: A Text for Biologists, Materials Scientists, and Geologists*, 2nd ed.; Plenum Press: New York, 1992.

(44) Ul-Hamid, A. *A Beginner's Guide to Scanning Electron Microscopy*, 1st ed.; Springer Nature Switzerland AG: Switzerland, 2018.

(45) Reed, S. J. B. *Electron Microprobe Analysis and Scanning Electron Microscopy in Geology*; Cambridge University Press: New York, 2005.

(46) Decker, E. L.; Frank, B.; Suo, Y.; Garoff, S. Physics of Contact Angle Measurement. *Colloid Surf., A* **1999**, *156*, 177–189.

(47) Katoh, K. Contact Angle and Surface Tension Measurement. In *Surface and Interfacial Tension Measurement, Theory, and Applications*; Hartland, S., Ed.; Marcel Dekker, Inc.: USA, 2004.

(48) Yuan, Y.; Lee, T. R. Contact Angle and Wetting Properties. In *Surface Science Techniques*. Bracco, G., Holst, B., Eds.; Springer Series in Surface Sciences 51; Springer: Heidelberg, 2013.

(49) Starostina, I. A.; Stoyanov, O. V.; Deberdeev, R. Y. Thermodynamics of Surface Phenomena in Polymer-Metal Adhesive Joints. In *Polymer Surfaces and Interfaces Acid-Base Interactions and Adhesion in Polymer-Metal Systems*, D'Amore, A., Balkose, D., Guarrotxena, N., Hamrang, A., Jimenez, A., Zaikov, G. E., Eds.; Apple Academic Press: Toronto, 2014.

(50) Zisman, W. A. Relation of the Equilibrium Contact Angle to Liquid and Solid Constitution. In *Contact Angle, Wettability and Adhesion*; Gould, R. F., Ed.; American Chemical Society: Washington, 1964.

(51) Fujiwara, H. *Spectroscopic Ellipsometry Principles and Applications*. John Wiley & Sons Ltd: England, 2007.

(52) Lovering, D. NKD-6000 Technical Manual, Aquila Instruments, Cambridge: U.K., 1998.

(53) Shimadzu Excellence in Science: Film-Thickness Measurement Web Site. http://www.shimadzu.com/an/uv/support/uv/ap/film.html (accessed June 16, 2020).

(54) Dieblod, A. C.; Chism, W. W. Characterisation and Metrology of Medium Dielectric Constant Gate Dielectric Films. In *High Dielectric Constant Materials*: *VSLI MOSFET Applications*; Huff, H. R., Gilmer, D. C., Eds.; Springer-Verlag: Berlin, 2005.

(55) Lovering, D. NKD-6000 Technical Manual; Aquila Instruments: Cambridge, 1999.

(56) Tortora, G. J.; Funke, B. R.; Case, C. L. Microbiology: An Introduction. 11th Ed.; Pearson Education Inc.: USA, 2013.

(57) Encyclopædia Britannica, Inc. Growth of Bacterial Populations. https://www.britannica.com/science/bacteria/Growth-of-bacterial-populations#ref955451, Accessed: May 20, 2020.

(58) Wang, L.; Fan, D.; Chen, W.; Terentjev, E. M. Bacterial Growth, Detachment and Cell Size Control on Polyethylene Terephthalate Surfaces. *Nature* **2015**, *5*, 15159.

(59) Thomas, P.; Sekhar, A. C.; Upreti, R.; Mujawar, M. M.; Pasha, S. S. Optimization of Single Plate-Serial Dilution Spotting (SP-SDS) with Sample Anchoring as an Assured Method for Bacterial and Yeast CFU Enumeration and Single Colony Isolation From Diverse Samples. *Biotechnol. Rep.* **2015**, *8*, 45–55.

(60) Gorsuch, J. P.; Jones, Z.; Le Saint, D.; Kitts, C. L. Ennumeration of Industrial *Bacillus* Assemblages in Comercial Products with Customized Plate-Counting Assays. *J. Microbiol. Methods* **2019**, *164*, 105682.

(61) Bot, C. T.; P, rodan, C. Quantifying the Membrane Potential During *E. coli* Growth Stages. *Biophys. Chem.* **2010**, *146*, 133–137.

3. Surface Immobilisation of Chitosan

3.1. Introduction

Chitosan (poly(D-glucosamine)) is a linear polysaccharide containing 1,4-β-linked D-glucosamine units, Scheme 3. 1. It is synthesised from chitin which is the second most abundant natural polymer (this is a low-cost material, produced in large quantities as a waste product of the crab meat industry).[1,2]
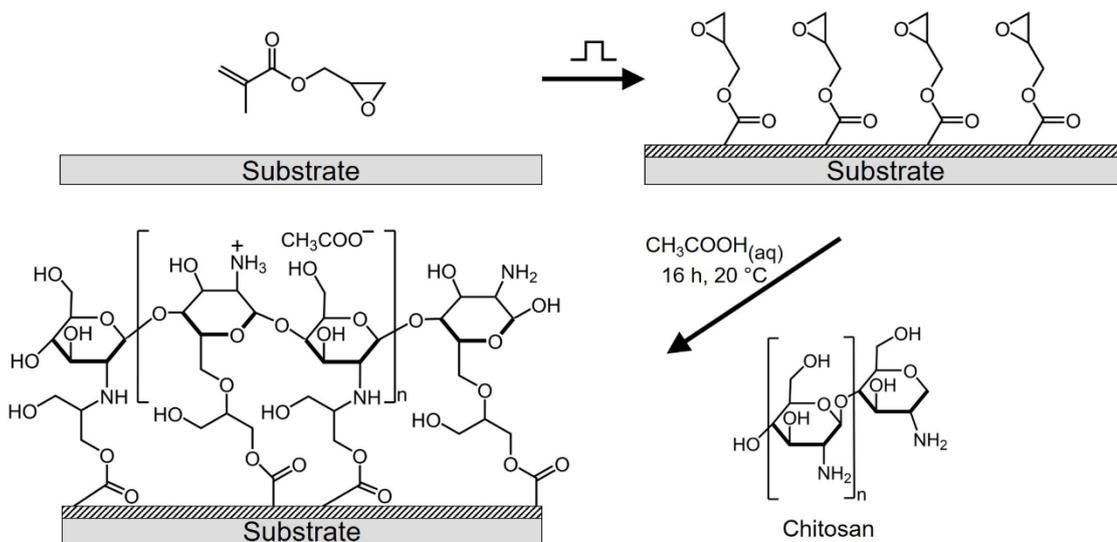
Scheme 3. 1: Pulsed plasma deposition of poly(glycidyl methacrylate) film followed by surface immobilisation of chitosan. The diagram illustrates a variety of potential nucleophilic substitution surface tethering linkages and an example of a protonated amine group accompanied by an acetate counterion.

Chitosan displays antimicrobial activity against a broad spectrum of bacterial species, fungi and viruses.[3] It is non-toxic, biocompatible, and biodegradable.[4–7] Materials functionalised with chitosan therefore have significant potential in a wide range of societal antibacterial applications including the food industry,[8] biomedical devices,[9,10] water sanitation[11] and air filtration.[12] In this context, earlier methodologies targeting the surface immobilisation of chitosan include the pad-dry-cure method,[13] multilayer processing,[14] crosslinking,[15,16] co-condensation,[17] conventional polymerisation reactions,[18–20] surface impregnation,[21] sol-gels,[22] electrospinning[23] and solid-liquid phase separation.[24] However, in all these cases, there is a requirement for a specific substrate material to facilitate

surface tethering and frequently the need for significant quantities of chemicals and elevated temperatures.

As described above, surface immobilisation of chitosan has been performed and studied by several research groups. The main importance of grafting chitosan onto a surface relies on the versatility of chitosan itself. Chitosan, being one of the most studied natural polymers, is a non-toxic, antimicrobial, biocompatible, and bioactive molecule, in which the presence of hydroxyl and amino groups in its molecular structure allows further chemical modifications (e.g., protonation, alkylation, quaternarization, thiolation, graft copolymerisation, etc.) with controlled molecular architecture which are useful for a wide range of industries including pharmaceutical, food, biomedical, agricultural, water treatment, textile, cosmetic, etc.[25–29]

Plasma functionalisation is a substrate and shape independent approach that offers several significant benefits, such as its easily applicability at industrial scale since it is a one-step synthesis and processing for surfaces, obtaining high-quality results, selectivity enhancing surface properties without affecting the bulk material conditions, requiring minimum quantity of the precursor, then producing none or minimal waste. Hence, it was chosen as the base method in this study to produce chitosan functionalised surfaces in combination with a simple surface impregnation post-treatment approach.[30–35,58] Table 3. 1 shows a comparison of reported approaches of surface immobilisation of chitosan onto surfaces assisted with plasma techniques.

Table 3. 1: Comparative table of chitosan immobilisation methods assisted with plasma techniques

Approach	Substrate	Plasma Procedures	Application
Chitosan immobilised on surface-grafted agent.	Polypropylene monofilament[31]	Surface activation with oxygen plasma to create hydroperoxide groups to induce grafting of poly(acrylic acid).	Biomedical
	Poly-L-lactic acid film[36]	Glow discharge parallel plate argon plasma activation At 32 W.	Biomedical

Approach	Substrate	Plasma Procedures	Application
	Polypropylene cloths[37,]	RF low-pressure argon plasma, 30 mTorr, 180 s, for activation, and second treatment at 100 W, 35 mTorr, 200 s after rinsing in acrylic acid for further immobilisation of chitosan.	Wastewater treatment
	Polyurethane[38]	RF low-pressure nitrogen plasma at 0.2 mbar, 60 W, 120 s.	Biomedical
	LDPE[39]	Atmospheric pressure non-thermal DBD plasma assisted copolymerisation	Antifouling surfaces
Direct current (DC) discharge plasma surface modification.	Chitosan films[40,41]	Low-pressure direct current discharge.	Tunning of physical and chemical features.
Plasma activation followed by stepwise process to immobilise chitosan.	Polyurethane films[42]	Surface activation with oxygen plasma at 100 W for 10 min.	Biomedical
Plasma activation followed by pad-dry-cure method to immobilise chitosan.	Wool[43]	Atmospheric DBD plasma activation of wool fabric at 20 kV, 300 W, 7 min.	Textile industry
Low-temperature plasma activation for further immobilisation of chitosan.	Cotton[44]	Geneal gas plasma processes.	Textile industry
Plasma induced deposition of chemically active groups (e.g., epoxide) for further immobilisation of other molecules (e.g., chitosan)	Not specified[45–49]	General gas plasmas processes.	General
Plasma induced deposition of epoxide groups	Polymers used for optical devices and	General gas plasmas processes.	Biomedical

Approach	Substrate	Plasma Procedures	Application
for further immobilisation of carbohydrates.	implants.[50,51]		

A number of methods to plasma-functionalise surfaces and further immobilise molecules of interest have been reported previously.[52,53] For instance, Li et al.,[54] reported functionalisation of non-woven fabrics by a two-step process whereby low temperature dielectric barrier discharge (DBD) plasma is used to functionalise fabrics with active functional groups for later immersion into chitosan-acetum solution; however the DBD approach is restricted in the area it can cover due to the apparatus used for this technique. Furthermore, Chabrecek, et al.,[55,56] and Kamel, et al.,[57] reported the use of plasma-induced polymerisation to fabricate chemically active coatings with a variety of functional groups, including epoxides. Their goal was to modify surfaces with different biocompatible compounds, such as proteins, hirudin and lectins, glycoproteins, carbohydrates, polysaccharides, and amino functionalised polymers and telomers. Other research groups have also utilised epoxide-surface functionalisation to further immobilise molecules of interest. Levi et al.,[58] reported the covalent attachment of biopolymer nanoparticle surfaces to epoxide linking compounds, capable to bind other molecules for drug delivery applications. Similarly, Kunita et al.[59] functionalised polypropylene surfaces with epoxide groups using a supercritical CO_2 approach to further immerse the surface in a bath of ethylenediamine and obtain amine functional groups on the surface. Qiu, et al.,[60] reported surface functionalisation with epoxide reactive groups to make them conventionally react with another moiety by a repetitive layer-by-layer absorption process, while Wu,[61] treated cotton fabric with low temperature plasma, then modified it with 2,3-epoxypropyltimethylammonium chloride, before a final treatment with chitosan. Finally, Ding et al.,[62] reported the provision of functional groups from poly-L-lactic acid as the base to immobilise chitosan on a surface by plasma graft polymerisation.

In this present study, chitosan was tethered onto plasmachemical epoxy-functionalised non-woven polypropylene cloth and then evaluated for antibacterial activity against representative bacterial species, Scheme 3. 1. The approach involved amine and hydroxyl groups of chitosan undergoing S_N1 nucleophilic substitution reactions with surface epoxide centres of pulsed plasma deposited poly(glycidyl methacrylate) thin films under acidic conditions.[63–65] The amine group in chitosan is expected to be the most active nucleophilic site in chitosan.[66] Strong covalent attachment of the plasmachemical deposited functional layer to the underlying substrate occurs via free radical sites created at the interface during the onset of plasma exposure.[67] Further advantages include speed (single-step), solventless processing, energy efficiency, and the reactive gaseous nature of the electrical discharge which provides with a free pinhole coating while maintaining the integrity of the substrate material. Taking advantage of the fact the plasmachemical method is not material specific, non-woven polypropylene cloth was selected as the substrate. This provides additional benefits, including being less prone to fungal growth compared to natural materials such as cotton,[68–70] and is mechanically more robust relative to resins,[71] hydrogel,[72] or electrospun chitosan materials.[12] Hence, the proposed methodology for surface tethering of chitosan can be adapted through the use of other techniques or precursors for surface functionalisation, carbohydrate polymers, chitosan derivatives, molecules or polymers containing amine groups, pH or solvents. Potential applications include filtration, food packaging, agriculture, adhesion and healthcare.

3.2. Experimental

3.2.1. Chitosan Functionalised Surfaces

Pulsed plasma deposition of epoxide functionalised thin films was undertaken as described in Chapter 2 Section 2.1.2.1 Gas-Phase Plasma Deposition. Silicon (100) wafer (14–24 mΩ cm resistivity, Silicon Valley

Microelectronics Inc.) and glass microscope slide (Academy Science Ltd.) substrates were ultrasonicated in a 1:1 v/v mixture of propan-2-ol / cyclohexane (+99.99 wt%, Acros Organics™) for 15 min, air dried, followed by air plasma cleaning (0.2 mbar pressure and 50 W) for 20 min prior to film deposition. Non-woven polypropylene (hierarchical, 0.4 mm thick, 22.7 ± 4.4 µm fibre diameter, with dimpled structure separation of 0.7 ± 0.2 mm, Spunbond, 70 g m^{-2}, Avoca Technical Ltd., UK) was used for antibacterial testing.[73] Each 2.38 cm^2 piece of non-woven cloth was rinsed in ethanol and excess ethanol removed with absorbent paper tissue wipes (Kimtech Science, Kimberly-Clark Europe Ltd.) prior to placement inside the plasma reactor. Following evacuation to the system base pressure, glycidyl methacrylate precursor (+97%, Sigma-Aldrich Ltd., further purified using freeze–pump–thaw cycles) vapour was admitted into the chamber at 0.2 mbar pressure, and the electrical discharge ignited using a pulse duty cycle on-period (t_{on}) of 20 µs and an off-period (t_{off}) of 20 ms, in conjunction with 40 W peak power (P_{on}) for a duration of 30 min to deposit a film thickness of 436 ± 14 nm (as measured on the silicon wafer substrate). For the present work, these experimental parameters for plasma processing have been reproduced as studied and compared by Tarducci et al.,[64] where the epoxide group retention is being affected by the power input per molecule (i.e., Yasuda parameter) when comparing plasma depositions in continuous wave and pulsed modes, respectively.

Upon extinction of the plasma, the precursor vapour was allowed to continue purging through the chamber for 15 min. Finally, the system was evacuated to base pressure and vented to the atmosphere.

Given that chitosan (poly(D-glucosamine)) is water-insoluble, it was dissolved in an aqueous acidic solution leading to polyelectrolyte formation through the protonation of chitosan amine groups, Scheme 3. 1. Acetic acid (+99%, Fisher Scientific UK Ltd.) at dilute concentrations was employed for this purpose.[74] The pulsed plasma poly(glycidyl methacrylate) functionalised substrates were immersed into an aqueous solution of chitosan (medium molecular weight 190,000–310,000 Da, 75–85% deacetylation grade, Sigma-Aldrich, Ltd. at 1% w/v, 2% w/v, or 3% w/v)–acetic acid (at 1% or 2% v/v). Following reaction with these solutions for 16 h at 20 °C, each sample was

thoroughly rinsed with the respective acetic acid aqueous solution and then with autoclaved Milli-Q® water (Milli-Q® Integral 15 Water Purification System, Millipore Corp.) in order to remove any unbound physisorbed chitosan. Finally, the chitosan tethered surfaces were dried at room temperature in preparation for characterisation and antibacterial testing.

3.2.2. Film Characterisation

Film thickness spectrophotometry (for pulsed plasma poly(glycidyl methacrylate) film), infrared spectroscopy, X-ray spectroscopy, and antibacterial test, were employed as characterisation techniques to determine the physicochemical features and antibacterial properties of the poly(glycidyl) methacrylate and immobilised chitosan surfaces. The corresponding characterisation procedures were carried out as described in Chapter 2 Experimental Techniques.

3.2.3. Antibacterial Testing

For antibacterial testing, chitosan-treated cloth samples were cut into pieces of 1.4 cm x 1.7 cm. Antibacterial testing was carried out against Gram-positive *Staphylococcus aureus* FDA 209P (an MSSA strain; ATCC 6538P) and Gram-negative *Escherichia coli* K12 BW25113 (CGSC 7636; *Δ lacZ4787* (::*rrnB3*) *hsdR514 Δ*(*araD-araB*)568 *Δ*(*rhaD-rhaB*)568 *rph-1*). Bacterial cultures were prepared as described in Chapter 2 Section 2.7 Antibacterial Activity Test. Optical densities OD_{650nm} = 0.4 (0.4 ± 0.0 for *S. aureus*, and 0.4 ± 0.0 for *E. coli*) were measured using a spectrophotometer (model BOECO S-30, Boeckel GmbH) to provide bacterial cultures in the mid-log phase of growth.[75] Antibacterial tests were performed by the dilution method at 1 mL scale, followed by colony-forming unit (CFU) plate counting,

as described in Chapter 2 Section 2.7 Antibacterial Activity Test. For reference, *S. aureus* and *E. coli* bacterial growth inhibition assays were also undertaken in order to visualise the effectiveness of the respective chitosan—acetic acid aqueous solutions employed for chitosan tethering to pulsed plasma poly(glycidyl methacrylate) functionalised cloths, as described in Chapter 2 Section 2.7 Antibacterial Activity Test.

3.3. Results

3.3.1. Pulsed Plasma Deposited Poly(Glycidyl Methacrylate)

The infrared spectrum of liquid glycidyl methacrylate precursor includes the following absorbances: C–H stretching vibration modes at 3002 cm^{-1} and 2947 cm^{-1}, a strong acrylate ester carbonyl (C=O) stretch at 1721 cm^{-1}, acrylate carbon–carbon double bond stretch at 1638 cm^{-1}, C–H bending at 1446 cm^{-1}, epoxide ring breathing at 1258 cm^{-1}, epoxide ring antisymmetric deformation at 902 cm^{-1}, epoxide ring symmetric deformation at 840 cm^{-1}, and an epoxide group absorbance at 757 cm^{-1}, Figure 3. 1.[64,76–80]

For pulsed plasma deposited poly(glycidyl methacrylate) film, characteristic infrared absorbances include: C–H stretches at 3002 cm^{-1} and 2953 cm^{-1}, ester carbonyl stretching at 1732 cm^{-1}, a C–H bending mode doublet at 1480 cm^{-1} and 1453 cm^{-1}, epoxide ring breathing at 1260 cm^{-1}, epoxide ring antisymmetric deformation at 916 cm^{-1}, epoxide ring symmetric deformation at 854 cm^{-1}, and an epoxide group absorbance at 751 cm^{-1}, Figure 3. 1.[71] Disappearance of the glycidyl methacrylate precursor carbon–carbon double bond stretch at 1638 cm^{-1} can be attributed to step-wise polymer chain growth during pulsed plasma deposition.[64,78–82]
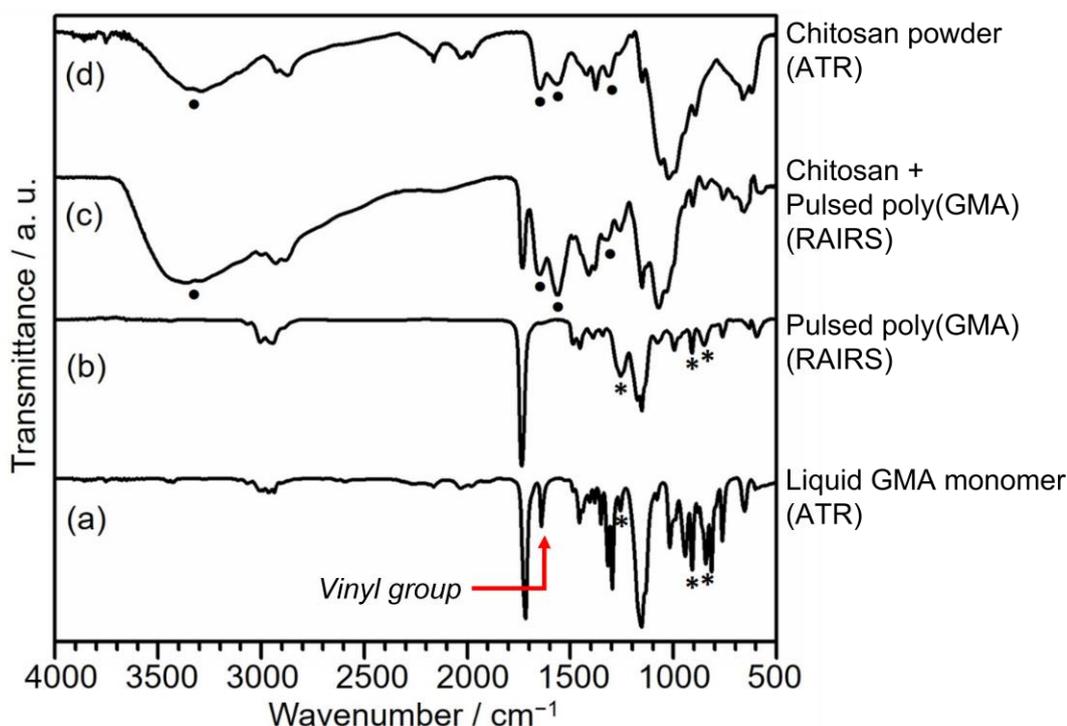
Figure 3. 1: Infrared spectra of: (a) liquid glycidyl methacrylate precursor (Attenuated–total–reflection, ATR); (b) pulsed plasma deposited poly(glycidyl methacrylate) film (Reflection–absorption infrared spectroscopy, RAIRS); (c) chitosan surface immobilised onto pulsed plasma deposited poly(glycidyl methacrylate) film (RAIRS) (optimum 3% w/v chitosan – 2% v/v acetic acid); and (d) chitosan powder (ATR). ✱ and ● denote characteristic infrared absorbances for epoxide group and chitosan, respectively.

For the pulsed plasma deposited poly(glycidyl methacrylate) films, X-ray photoelectron spectroscopy (XPS) analysis detected the presence of only carbon and oxygen with no Si(2p) signal from the underlying silicon wafer substrate, thereby confirming a pin-hole free layer, Table 3. 2. The measured elemental composition is consistent with the theoretical value expected for step-wise growth of poly(glycidyl methacrylate) chains during pulsed plasma deposition.[64,81] The C(1s) envelope could be fitted to the following Gaussian Mg K$\alpha_{1,2}$ components: $-\underline{C}_xH_y$ (285.0 eV), $\geqslant\underline{C}(C=O)O$ (285.6 eV), $O-\underline{C}H_2-CO$ (286.7 eV), epoxide carbon (287.1 eV) and $\geqslant C(\underline{C}=O)O$ (289.1 eV) groups, Figure 3. 2 and Table 3. 3. This is in good agreement with the monomer repeat unit of poly(glycidyl methacrylate).[64,80,83] Wide scans (Supporting research data published in Durham University Research Data

Repository. DOI: http://doi.org/10.15128/r2v405s940b) did not show other components suggesting contamination.

Table 3. 2: XPS compositions for: glycidyl methacrylate (GMA) and chitosan precursors (theoretical); pulsed plasma deposited poly(glycidyl methacrylate); and surface immobilised chitosan (optimum 3% w/v chitosan – 2% v/v acetic acid). Figure 3. 3 and Figure 3. 4.

System	Composition / at. %		
	C	O	N
GMA (Theoretical)	70.0	30.0	0
Pulsed poly(GMA)	72.0 ± 0.9	28.0 ± 0.9	0
Chitosan (Theoretical)	54.5	36.4	9.1[†]
Pulsed poly(GMA)–Chitosan	64.7 ± 0.5	28.4 ± 0.6	6.9 ± 0.7

[†] In practice, this value is expected to be lower due to the presence of acetylated chitin units contained within the polysaccharide structure of chitosan.[6]

Table 3. 3: XPS C(1s) compositions for: glycidyl methacrylate (GMA), and pulsed plasma deposited poly(glycidyl methacrylate), Figure 3. 2. A theoretical C(1s) fitting of the spectrum for surface immobilised chitosan (optimum 3% w/v chitosan – 2% v/v acetic acid) and corresponding experimental raw data are shown in Figure 3. 3.

System	C(1s) Carbon Component / %				
	$-\underline{C}_xH_y$	$\geqslant\underline{C}(C=O)O$	$O-\underline{C}H_2-CO$	Epoxide	$\geqslant C(\underline{C}=O)O$
GMA (Theoretical)	28.6	14.3	14.3	28.6	14.3
Pulsed poly(GMA)	24.2 ± 0.3	18.8 ± 0.4	15.5 ± 0.2	27.2 ± 0.9	14.2 ± 0.3
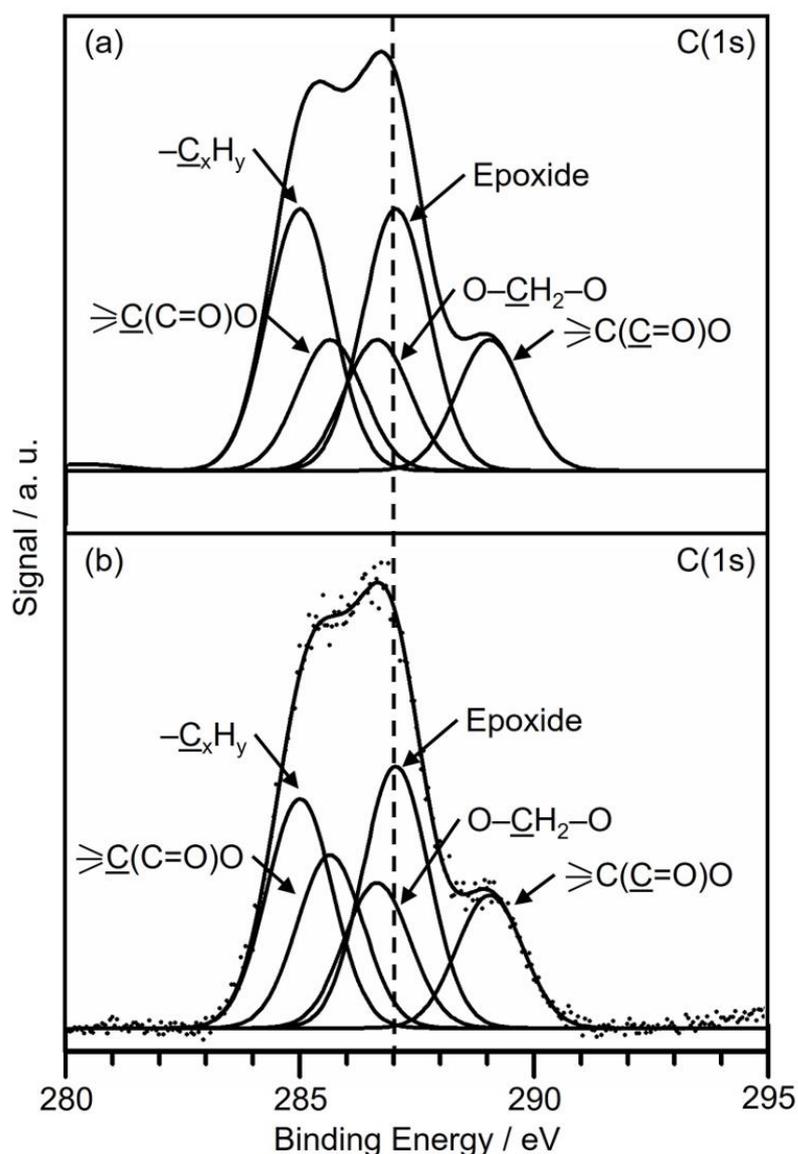
Figure 3. 2: XPS C(1s) spectrum of (a) theoretical glycidyl methacrylate and, (b) pulsed plasma poly(glycidyl methacrylate) deposited onto silicon wafer. Table 3. 2 and Table 3. 3.

3.3.2. Chitosan Surface Tethering

Pure chitosan shows the following infrared absorbances: polysaccharide structure N–H and O–H stretches in the 3600–3200 cm^{-1} region; C–H antisymmetric and symmetric stretches at 2926 cm^{-1} and 2877 cm^{-1} respectively; NH2 group N–H bending mode and amide (I) –C=O stretch at 1646 cm^{-1} (from acetylated chitin units[2,84]); amide (II) N–H bending at 1556 cm^{-1} (from acetylated chitin units[2]); –CH2– and –CH3 bending deformations

at 1425 cm^{-1} and 1377 cm^{-1} respectively; amide (III) vibration mode at 1315 cm^{-1} (from remaining N-acetylglucosamine chitin units[85]); chitosan amine (II) –C–N stretch at 1252 cm^{-1}; C–O–C bridge antisymmetric stretch at 1150 cm^{-1}; C–O stretches at 1067 cm^{-1} and 1028 cm^{-1}; and out of plane ring C–H bending at 896 cm^{-1}, Figure 3. 1.[86–91]

Following chitosan immobilisation onto the pulsed plasma deposited poly(glycidyl methacrylate) film, the following characteristic chitosan features were visible: polysaccharide structure N–H and O–H stretches between 3600–3200 cm^{-1}; polysaccharide C–H antisymmetric and symmetric stretches at 2928 cm^{-1} and 2885 cm^{-1} respectively; NH$_2$ group N–H bending mode and amide (I) –C=O stretch at 1646 cm^{-1} (from acetylated chitin units[2,84]); amide (II) N–H bending at 1556 cm^{-1} (from acetylated chitin units[2] and overlap with the acetate ion band at 1600 cm^{-1} associated with acid–base interactions between chitosan amine groups and acetic acid solution[84,87]); –CH$_2$– and –CH$_3$ bending deformations at 1412 cm^{-1} and 1377 cm^{-1} respectively; amide (III) vibration mode at 1324 cm^{-1} (from N-acetylglucosamine chitin units[2]); chitosan amine (II) –C–N stretch at 1263 cm^{-1}; C–O–C bridge antisymmetric stretch at 1151 cm^{-1}; C–O stretch at 1029 cm^{-1}; as well as polysaccharide bands in the 1110–840 cm^{-1} region, Figure 3. 1.[86,87,92] The ester carbonyl (C=O) stretch at 1733 cm^{-1} from the underlying poly(glycidyl methacrylate) film was also observed—which is consistent with the RAIRS technique sub-surface sampling depth (0.5–5 μm).[93]

XPS analysis provided further evidence for the surface immobilisation of chitosan onto the pulsed plasma deposited poly(glycidyl methacrylate) film—detecting only carbon, oxygen, and nitrogen, Table 3. 2. The slightly higher carbon (hence lower oxygen and nitrogen) content measured relative to the theoretical chitosan composition may be due to the presence of remaining acetylated chitin units contained within the polysaccharide structure of chitosan or some adventitious hydrocarbon, Figure 3. 3.[6] The XPS N(1s) amine (–$\underline{N}$H$_2$ at 399.6 eV) and protonated amine (–$\underline{N}$H$_3$$^+$ at 401.1 eV) environments confirmed chitosan surface tethering as well as support for the rationale of charged centres for antibacterial activity,[94] Figure 3. 4 and Figure 3. 5. A solution concentration of 3% w/v chitosan–2% v/v acetic acid

was found to give rise to a high level of chitosan immobilisation (total %N) and amine group protonation (%–$\underline{N}H_3^+$), Figure 3. 5. Approximately 16% of the chitosan amine groups are positively charged, Table 3. 4.
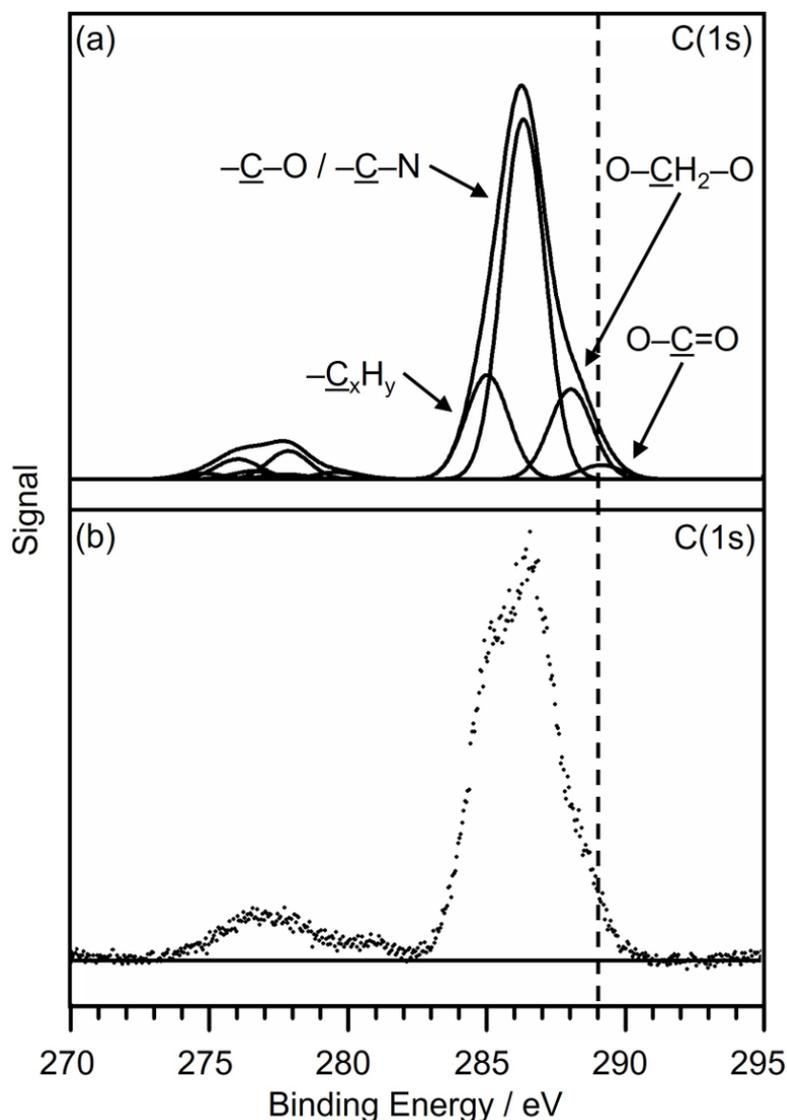
Figure 3. 3: XPS C(1s) of: (a) theoretical fit for chitosan functionalised cloths employing a ratio of 5.81 at. % –$\underline{N}H_2$ (unprotonated chitosan amine) : 1.09 at. % –$\underline{N}H_3^+$ (protonated amine and therefore CH_3COO^- counterion; for cloths made using 3% w/v chitosan–2% v/v acetic acid aqueous solution ($CH_3COOH_{(aq)}$)), and assuming no acetylation of chitosan; and (b) experimental raw data for the corresponding chitosan film on polyethylene cloths (optimum 3% w/v chitosan–2% v/v acetic acid aqueous solution ($CH_3COOH_{(aq)}$)). The latter was not fitted due to the overlapping carbon environments present in the real sample (e.g., acetylated units, natural chitosan impurities and adventitious carbon). Peaks at the 275–280 eV region are dismissed since they are likely to be satellites.
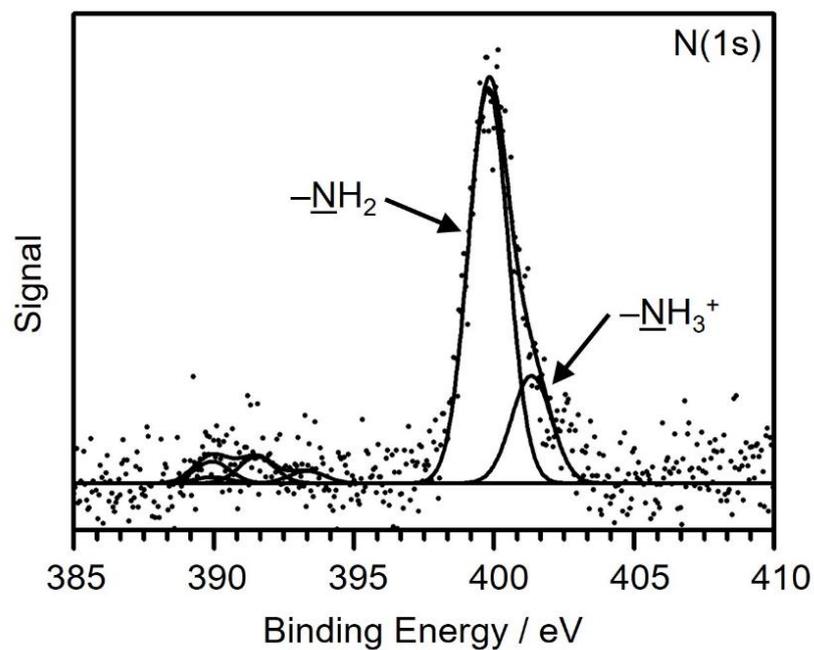
Figure 3. 4: XPS N(1s) amine and protonated amine environments present on chitosan functionalised (optimum 3% w/v chitosan–2% v/v acetic acid aqueous solution) cloths. Peaks at the 390–395 eV region are dismissed since they are likely to be satellites.
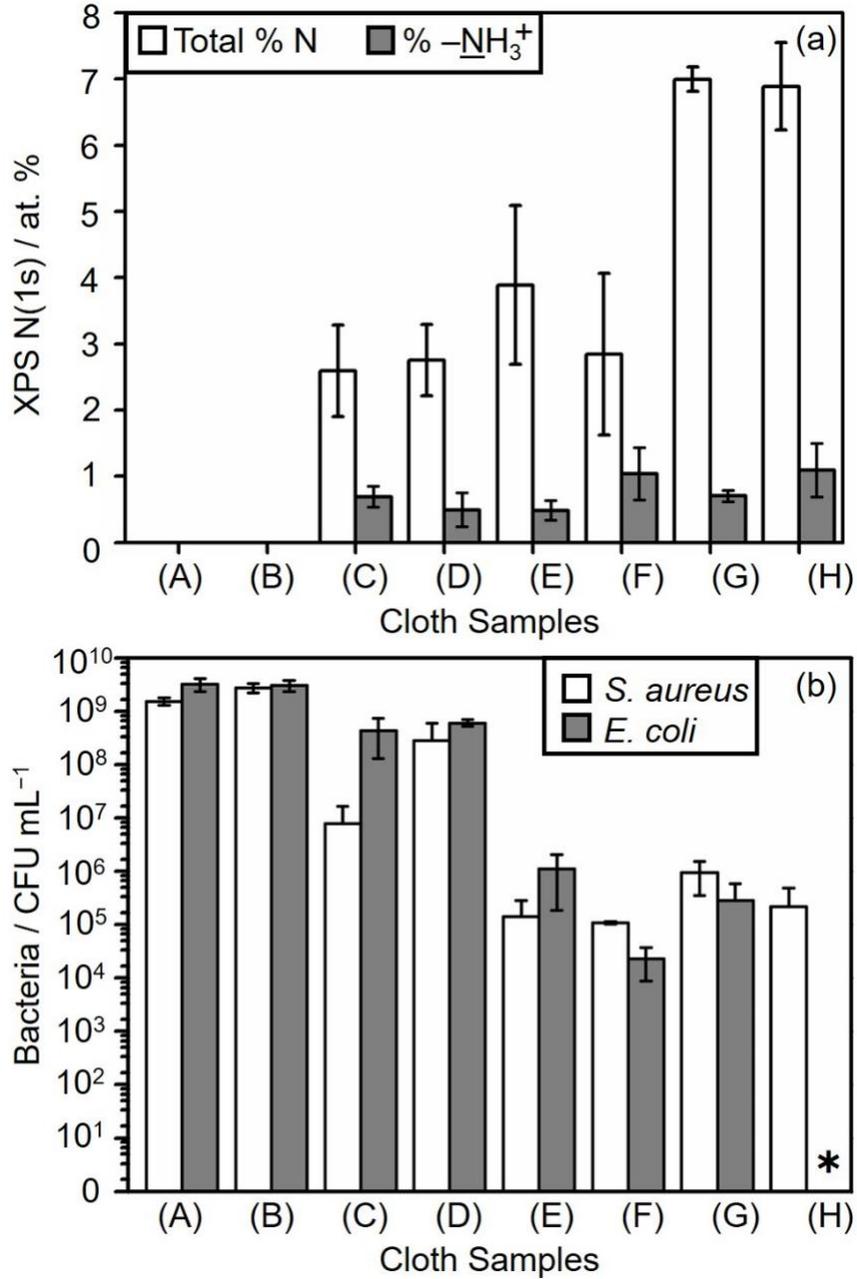
Figure 3. 5: (a) XPS N(1s) content and (b) antibacterial activities of cloths against Gram-positive *S. aureus* and Gram-negative *E. coli* bacterial strains: (A) untreated control; (B) pulsed plasma deposited poly(glycidyl methacrylate) coating control; surface immobilised chitosan using chitosan–acetic acid aqueous solutions: (C) 1% w/v chitosan–1% v/v acetic acid; (D) 1% w/v chitosan–2% v/v acetic acid; (E) 2% w/v chitosan–1% v/v acetic acid; (F) 2% w/v chitosan–2% v/v acetic acid; (G) 3% w/v chitosan–1% v/v acetic acid; and (H) 3% w/v chitosan–2% v/v acetic acid, where ✱ indicates 100% antibacterial efficacy against *E. coli*. Error bars indicate standard deviation for at least 3 sample repeats.

Table 3. 4: XPS N(1s) protonated amine content for non-woven polypropylene cloth samples.

Description	XPS
	N(1s) –$\underline{N}H_3^+$ / at. %
Untreated	0 ± 0
Pulsed plasma poly(glycidyl methacrylate)	0 ± 0
1 % w/v Chitosan– 1% v/v $CH_3COOH_{(aq)}$	0.7 ± 0.2
1 % w/v Chitosan– 2% v/v $CH_3COOH_{(aq)}$	0.5 ± 0.3
2 % w/v Chitosan– 1% v/v $CH_3COOH_{(aq)}$	0.5 ± 0.1
2 % w/v Chitosan– 2% v/v $CH_3COOH_{(aq)}$	1.0 ± 0.4
3 % w/v Chitosan– 1% v/v $CH_3COOH_{(aq)}$	0.7 ± 0.1
3 % w/v Chitosan– 2% v/v $CH_3COOH_{(aq)}$	1.1 ± 0.4

3.3.3. Antibacterial Testing

Chitosan immobilised onto pulsed plasma deposited poly(glycidyl methacrylate) coated cloths displayed significant antibacterial activity by contact killing, against both *S. aureus* and *E. coli* bacterial species. The highest antibacterial activity (a log reduction = 9) was achieved by employing 3% w/v chitosan–2% v/v acetic acid aqueous solution for chitosan surface tethering against *E. coli*, Figure 3. 5. The level of antibacterial activity correlates with the surface concentration of N(1s) –$\underline{N}H_3^+$ groups measured by XPS (approximately 16% of the chitosan amine groups are protonated), Figure 3. 5 and Figure 3. 6. Compared to Gram-positive *S. aureus*, Gram-

negative *E. coli* displayed a greater sensitivity towards surface immobilised chitosan for the highest surface concentration of–$\underline{N}H_3^+$ groups.
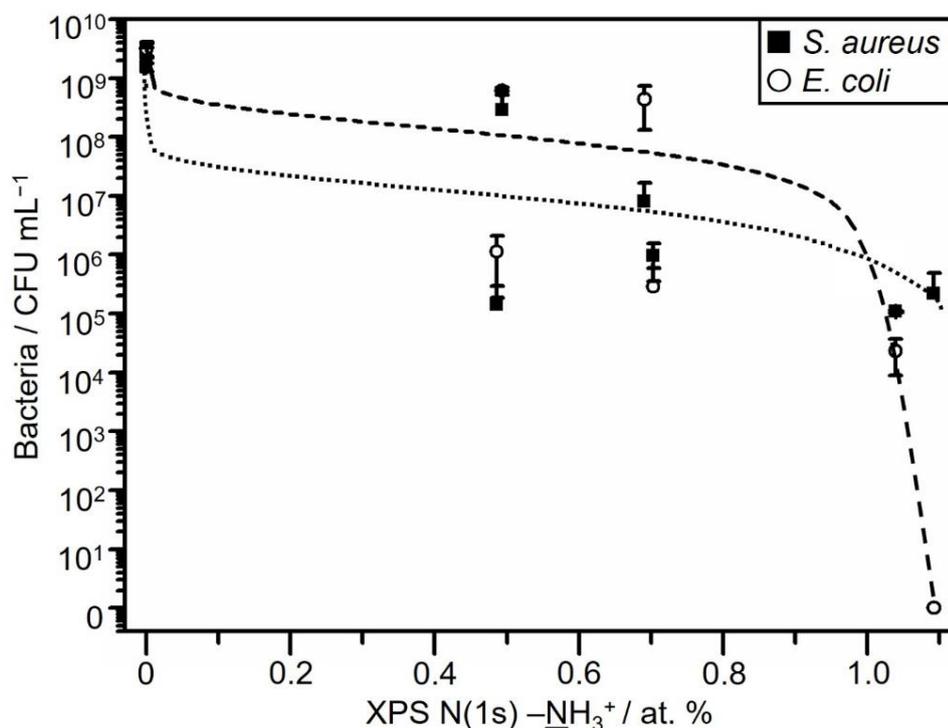
Figure 3. 6: Correlation between antibacterial activity and XPS protonated nitrogen content for chitosan functionalised cloths. 0 at. % –$\underline{N}H_3^+$ corresponds to untreated and pulsed plasma poly(glycidyl methacrylate) coated cloth controls, Table 3. 4. The lower line corresponds to Gram-positive *S. aureus* and the upper to Gram-negative *E. coli*.

Control antibacterial tests on untreated and pulsed plasma poly(glycidyl methacrylate) coated non-woven polypropylene cloths displayed no antibacterial activity against *S. aureus* and *E. coli*, Figure 3. 6. Additional control experiments were carried out using the solutions employed for surface tethering of chitosan: dilute chitosan–acetic acid aqueous solutions inhibited growth of both *E. coli* and *S. aureus*, whereas dilute aqueous acetic acid solutions alone (1% v/v and 2% v/v) did not, Figure 3. 7 and Figure 3. 8. Although the literature indicates acetic acid and acetic acid aqueous solutions themselves display antibacterial activity at very low concentrations,[95] it should be noted that the results among research works will vary depending on the initial bacterial concentration reported in each study. The zone of growth inhibition did not extend beyond the area exposed

to each chitosan-acetic acid solution, which is in keeping with a contact mode of action with little or no diffusion into the surrounding media. Acetic acid aqueous solutions were only found to become effective as antibacterial agents at much higher concentrations, where pH becomes an important factor.[96,97]
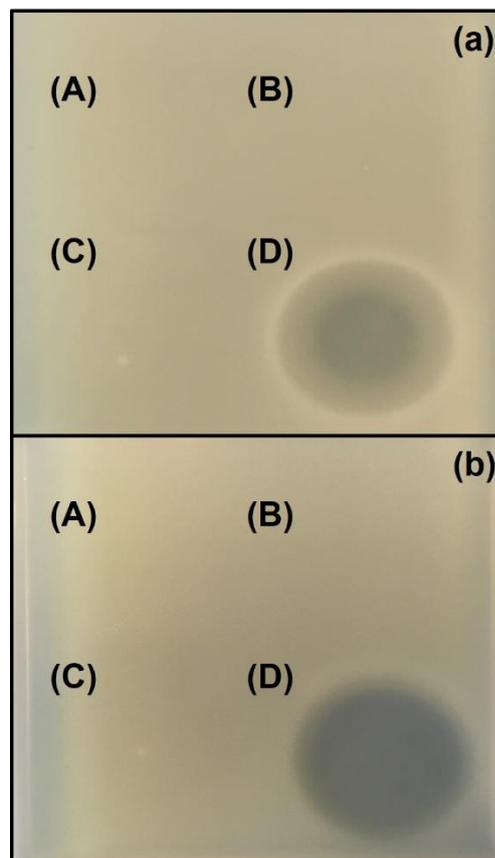
Figure 3. 7: Bacterial growth inhibition assay using 0.6% LB overlay agar plates containing (a) *E. coli* and (b) *S. aureus*: (A) water, (B) 1% v/v acetic acid aqueous solution, (C) 2% v/v acetic acid aqueous solution, and (D) 100% acetic acid. The dark circles represent zones of bacterial growth inhibition.
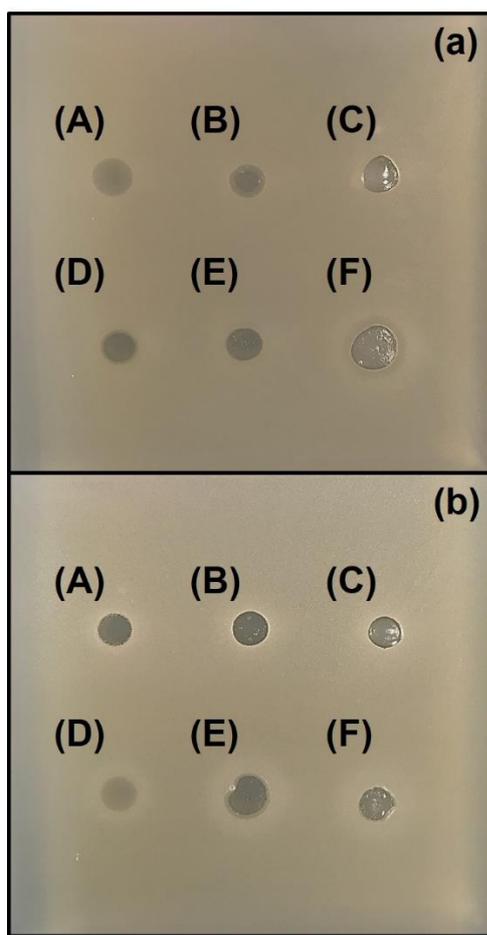
Figure 3. 8: Bacterial growth inhibition assay for chitosan–acetic acid aqueous solutions, using 0.6% LB overlay agar plates containing (a) *E. coli* and (b) *S. aureus*: (A) 1% w/v chitosan–1% v/v acetic acid, (B) 2% w/v chitosan–1% v/v acetic acid, (C) 3% w/v chitosan–1% v/v acetic acid, (D) 1% w/v chitosan–2% v/v acetic acid, (E) 2% w/v chitosan–2% v/v acetic acid, (F) 3% w/v chitosan–2% v/v acetic acid. The dark circles represent zones of bacterial growth inhibition.

Any variability noted in our experiments most likely reflects the fact that natural polymers (such as chitosan) tend not to have well-defined physicochemical properties.[98,99] An additional contributing factor may be the consistency of bacterial cell exposure to the cloth pieces.

3.4. Discussion

The antibacterial activity of chitosan is known to be governed by molecular weight, degree of deacetylation, amine group concentration along the

polysaccharide chain, positive charge density and physical appearance (particle size, shape and surface area, Figure 3. 9).[6,7,12,100–105] It is also influenced by the medium through which chitosan is deployed (e.g. solution, hydrogel, coating etc.),[6,7] the methodologies used to evaluate their antibacterial effect in the given conditions,[100] the natural source of obtention and production methods that all play a role defining the physicochemical properties of the final product.[106–108]

Figure 3. 9: Physical appearance comparison among Sigma-Aldrich chitosan powders from different batches and country of origin.

The chitosan functionalised cloths in the present study display high levels of antibacterial activity against *S. aureus* and *E. coli*, Figure 3. 5. It

might have been expected that coatings prepared with 2% w/v chitosan–2% v/v acetic acid aqueous solutions would offer improved antibacterial activity and higher percentage of protonated chitosan glucosamine units due to the lower amount of chitosan dissolved with 2% v/v acetic acid aqueous solution. However, the optimum 3% w/v chitosan–2% v/v acetic acid solution utilised for surface tethering proved the most effective, yielding a log reduction of > 9 against *E. coli*, which substantially exceeds the minimal clinical standard (a log reduction in survival of > 3).[109,110] This may be attributed to a higher retention of both, protonated and non-protonated chitosan glucosamine units on the surface, which is in good agreement with the results presented in Figure 3. 5 and Table 3. 4, where the XPS measured concentration of N(1s) –$\underline{N}H_3^+$ groups for coatings made with 3% w/v– and 2% w/v chitosan–2% v/v acetic acid aqueous solutions are ~16% and ~29% of the chitosan amine groups, respectively. However, these percentages correspond to their respective XPS measured nitrogen content totals of ~6.9% at. and ~2.8% at., providing further evidence that amine groups in chitosan are more readily protonated in 2% w/v chitosan–2% v/v acetic acid aqueous solution, but the higher concentration of non-protonated glucosamine species in 3% w/v chitosan–2% v/v acetic acid solution is likely to enhance their antibacterial activity, compared to coatings prepared with other proposed chitosan–acetic acid aqueous solution concentrations, Table 3. 4, and Figure 3. 5. Although less active against *S. aureus*, 2–3% w/v chitosan treated pulsed plasma poly(glycidyl methacrylate) functionalised cloths produced 3–4 log reductions in bacterial survival. For 3% w/v chitosan concentration, the comparison between 1% v/v versus 2% v/v acetic acid aqueous solution concentrations suggests that the latter promotes greater tethering of chitosan to epoxide groups on the surface in combination with higher levels of polysaccharide amine centre protonation (approximately 16% of the chitosan amine groups are positively charged), Figure 3. 5. It is the surface concentration of protonated amine groups which appears to govern the level of antibacterial activity, Figure 3. 6.

At least four possible mechanisms exist for the antibacterial interaction between chitosan and microorganisms. First, the positively charged amine groups of the chitosan glucosamine units are attracted towards negatively

charged components in microbial cell surfaces and membranes, thereby damaging or destroying the cell wall structure through interactions with cell membrane lipids or proteins, which in turn perturbs the entry of nutrients or causes leakage of the intracellular contents.[100,103,111] A second possibility is that following interaction with the cell wall, chitosan penetrates the bacterial cell, leading to electrostatic binding to DNA (this will interfere with the synthesis of nucleic acids as well as metabolic activities).[104] A third mechanism involves protonated chitosan polymer chain amine groups competing with divalent chelation of metal ions required for microorganism growth and survival (concurrently, chitosan primary and secondary hydroxyl groups can bind to biologically-relevant metal ions).[3,6] The fourth reported explanation entails chitosan acting as a thick polymer barrier layer which damages the metabolic activity of microorganisms by blocking the cells from receiving essential nutrients or preventing the transportation of metabolite excretion.[105] In agreement with results for the coatings in the present study, it is most likely that the protonated glucosamine groups in chitosan readily interact with the negatively charged cell surface through electrostatic interactions causing physical membrane disruption,[104,112,113] given the fact that the samples with higher content of protonated chemical species displayed higher antibacterial efficiency, Figure 3. 6.

Furthermore, bacteria species display different levels of sensitivity towards chitosan, due to their cell wall properties, metabolism, and age (e.g., exponential growth versus stationary phase).[101,113,114] Previous studies reported contradictory results regarding the differential sensitivity of Gram-positive and Gram-negative bacteria towards chitosan.[115,116] The susceptibility of Gram-positive bacteria is explained on the basis of electrostatic interactions occurring between chitosan and the peptidoglycan cell wall,[100] which contains teichoic acids (consisting mainly of an alcohol and negatively charged phosphate), playing a role in binding and regulating the movement of cations (e.g., interaction with chitosan polycation) into and out of the cell wall. [117] However, in contrast, in the present investigation, it was observed that Gram-negative *E. coli* is more susceptible to killing by chitosan functionalised cloth surfaces, Figure 3. 6. Such higher antibacterial activity towards Gram-negative bacterium could be attributed to a thinner cell wall

thickness (e.g., 7–8 nm for *E. coli*) compared to Gram-positive bacterium (e.g., 20–80 nm for *S. aureus*).[118] The comparatively thicker and more rigid peptidoglycan layer (which helps preserve the integrity of the cell) for Gram-positive bacterial strains is expected to be less susceptible to membrane damage during electrostatic attraction towards positively charged substrates.[119] Therefore, despite the coatings with higher content of protonated chitosan glucosamine groups appearing to readily react with the cell membrane, there may still be physical limitations from the bacterial cell that show that the amount of protonated species may not be enough to kill bacteria by means of electrostatic or chemical interactions (contact killing) between the coating and the bacterial cell surface; there is the possibility that the antibacterial activity of the coatings presented in this study is a synergy between several or all of the four possible mechanisms outlined above, where the physical barrier from chitosan still acts when the chemical features of the coating are not sufficient to kill the bacteria by direct contact.

3.5. Conclusions

Chitosan immobilised onto pulsed plasma poly(glycidyl methacrylate) functionalised cloths displays antibacterial activity against Gram-positive *S. aureus* (log reduction = 4) and Gram-negative *E. coli* (log reduction = 9) bacteria. A correlation was found between the concentration of protonated chitosan amine groups and the measured level of antibacterial activity. However, the physical and chemical features of different batches of chitosan may potentially interfere with the performance of the final product; solutions made with chitosan from different batches may vary in their content of protonated chitosan glucosamine units and may consequently affect their antibacterial efficacy, which is in agreement with the discrepancies mentioned above regarding the variability of results displayed from different chitosan antibacterial applications. Furthermore, as chitosan is a natural and readily biodegradable molecule, the regeneration of the coated material does not guarantee long-term or repeated use. Nevertheless, compared with other

approaches, the coating made with 3% w/v chitosan–2% v/v acetic acid aqueous solution offers a simple eco-friendly process, that requires low amounts of precursor in the plasma functionalisation step, with no requirements of further treatment at high temperatures that could damage delicate bulk materials such as non-woven polypropylene cloths and other sensitive polymers. In the same way proposed in this work, plasma assisted functionalisation of surfaces to immobilise chitosan is being studied and appears to perform well for different industrial and biomedical applications; it could be concluded that plasma process parameters can be set to obtain a functionalised surface that allows to immobilise chitosan with any proposed deposition method, as compared above. In addition, the use of a non-toxic biodegradable chitosan–acetic acid aqueous solution provides high efficiency in generating the desired final product. The simplicity of this two-step, substrate-independent approach makes it amenable for a wide range of biomedical and antifouling applications.

3.6. References

(1) Owlad, M.; Aroua, M. K.; Daud, W. A. W.; Baroutian, S. Removal of Hexavalent Chromium-Contaminated Water and Wastewater: A Review. Water, Air, Soil Pollut. 2009, 200, 59–77.

(2) Rinaudo, M. Chitin and Chitosan: Properties and Applications. *Prog. Polym. Sci.* **2006**, *31*, 603–632.

(3) Xing, K.; Zhu, X.; Peng, X.; Qin, S. Chitosan Antimicrobial and Eliciting Properties for Pest Control in Agriculture: A Review. Agron. Sustainable Dev. 2015, 35, 569–588.

(4) Gouda, I.; Larm, O. Solid Substrate Coated with an Aminopolysaccharide. U.S. Patent 5,668,193, September 16, 1997.

(5) Dutta, P. K.; Tripathi, S.; Mehrotra, G. K.; Dutta, J. Perspectives for Chitosan Based Antimicrobial Films in Food Applications. *Food Chem.* **2009**, *114*, 1173–1182.

(6) Jennings, J. A.; Bumgardner, J. D. Chitosan Based Biomaterials Volume 1: Fundamentals. In *Woodhead Publishing Series in Biomaterials*; Woodhead Publishing; Elsevier: Duxford, 2017; Vol. 122; pp 3–6, 31–34, 84.

(7) Jennings, J. A.; Bumgardner, J. D. Chitosan Based Biomaterials Volume 2: Fundamentals. In *Woodhead Publishing Series in Biomaterials*; Woodhead Publishing; Elsevier: Duxford, 2017; Vol. 123; pp 12, 36–37, 74,147,150,177, 245–247.

(8) Roller, S. Chitosan: New Food Preservative or Laboratory Curiosity? In *Natural Antimicrobials for the Minimal Processing of Foods*; Roller, S., Ed.; Woodhead Publishing Limited and CRC Press LLC: Cornwall, 2004; pp 158–165.

(9) Zhang, L.; Huang, X.; Yang, Q.-L.; Yang, Y.; Shen, C.-Y. Biomedical Application of Chitosan-Based Polyelectrolyte Hydrogels. *Zhongguo Zuzhi Gongcheng Yanjiu* **2012**, *16*, 8127–8132.

(10) Khor, E.; Lim, L. Y. Implantable Applications of Chitin and Chitosan. *Biomaterials* **2003**, *24*, 2339–2349.

(11) Elwakeel, K. Z.; Guibal, E. Selective Removal of Hg(II) from Aqueous Solution by Functionalized Magnetic-Macromolecular Hybrid Material. *Chem. Eng. J.* **2015**, *281*, 345–359.

(12) Ferrero, F.; Tonetti, C.; Periolatto, M. Adsorption of Chromate and Cupric Ions onto Chitosan-Coated Cotton Gauze. *Carbohydr. Polym.* **2014**, *110*, 367–373.

(13) Lim, S.-H.; Hudson, S. M. Application of a Fiber-Reactive Chitosan Derivative to Cotton Fabric as an Antimicrobial Textile Finish. *Carbohydr. Polym.* **2004**, 56, 227–234.

(14) Luckachan, G. E.; Mittal, V. Anti-Corrosion Behavior of Layer by Layer Coatings of Cross-Linked Chitosan and Poly(Vinyl Butyral) on Carbon Steel. *Cellulose* **2015**, *22*, 3275–3290.

(15) Zhang, Y.; Ji, C. Electro-Induced Covalent Cross-Linking of Chitosan and Formation of Chitosan Hydrogel Films: Its Application as an Enzyme Immobilization Matrix for Use in a Phenol Sensor. *Anal. Chem.* **2010**, *82*, 5275–5281.

(16) El-Dib, F.I.; Hussein, M. H. M.; Hefni, H. H. H.; Eshaq, G.; ElMetwally, A. E. Synthesis and Characterization of Crosslinked Chitosan Immobilized on Bentonite and its Grafted Products with Polyaniline. *J. Appl. Polym. Sci.* **2014**, *131*, 41078

(17) Torres, J. D.; Faria, E. A.; SouzaDe, J. R.; Prado, A. G. S. Preparation of Photoactive Chitosan–Niobium (V) Oxide Composites for Dye Degradation. *J. Photochem. Photobiol., A* **2006**, *182*, 202–206.

(18) Chen, Y.; Shi, T.; Qi, S.; Yang, M.; Meng, N.; Gong, Z.-N.; Huang, B. Alkylpolyglycoside Inducing Poly(Butylene Terephthalate) Non-Woven Graft Copolymerization of Chitosan. *J. Southeast Univ. (Engl. Ed.).* **2012**, *28*, 474–479.

(19) Ashassi-Sorkhabi, H.; Bagheri, R.; Rezaei-Moghadam, B. Sonoelectrochemical Synthesis of PPy-MWCNTs-Chitosan Nanocomposite Coatings: Characterization and Corrosion Behavior. *J. Mater. Eng. Perform.* **2015**, *24*, 385–392.

(20) Liu, S. X.; Kim, J. T. Characterization of Surface Modification of Polyethersulfone Membrane. *J. Adhes. Sci. Technol.* **2011***, 25*, 193–212.

(21) Carlson, R. P.; Taffs, R.; Davison, W. M.; Stewart, P. S. Anti-Biofilm Properties of Chitosan-Coated Surfaces. *J. Biomater. Sci., Polym. Ed.* **2008**, *19*, 1035–1046.

(22) Chen, X.; Jia, J.; Dong. S. Organically Modified Sol-Gel/Chitosan Composite Based Glucose Biosensor. *Electroanalysis* **2003**, *15*, 608–612.

(23) Matsuda, A.; Kagata, G.; Kino, R.; Tanaka, J. Preparation of Chitosan Nanofiber Tube by Electrospinning. *J. Nanosci. Nanotechnol.* **2007**, *7*, 852–855.

(24) Zhao, J.; Han, W.; Tang, M.; Tu, M.; Zeng, R. Structure, Morphology and Cell Affinity of Poly(L-lactide) Films Surface-Functionalized with Chitosan Nanofibers via a Solid-Liquid Phase Separation Technique. *Mater. Sci. Eng., C* **2013**, *33*, 1546–1553.

(25) Pokhrel, S.; Yadav, P. N. Functionalization of Chitosan Polymer and Their Applications. *J. Macromol. Sci., A* **2019**, *56*, 450–475.

(26) Merk. Chitosan: A Versatile Platform for Pharmaceutical Applications. https://www.sigmaaldrich.com/MX/es/technical-documents/technical-article/materials-science-and-engineering/drug-delivery/chitosan-a-versatile-platform (accessed May 12, 2022).

(27) Jayakumar, R.; Prabaharan, M.; Reis, R. L.; Mano, J. F. Graft Copolymerized Chitosan—Present Status and Applications. *Carbohydr. Polym.* **2005**, *62*, 142–158.

(28) Thakur, V. K.; Thakur, M. K. Recent Advances in Graft Copolymerization and Applications of Chitosan: A Review. *ACS Sustainable Chem. Eng.* **2014**, *2*, 2637–2652.

(29) Argüelles-Monal, W. M.; Lizardi-Mendoza, J.; Fernández-Quiroz, D.; Recillas-Mota, M. T.; Montiel-Herrera, M. Chitosan Derivatives: Introducing New Functionalities with a Controlled Molecular Architecture for Innovative Materials. *Polymers* **2018**, *10*, 342.

(30) Lu, T.; Qiao, Y.; Liu, X. Surface Modification of Biomaterials Using Plasma Immersion Ion Implantation and Deposition. *Interface Focus.* **2012**, *2*, 325–336.

(31) Saxena, S.; Ray, A. R.; Gupta, B. Chitosan Immobilization on Polyacrylic Acid Grafted Polypropylene Monofilament. *Carbohydr. Polym.* **2010**, *82*, 1315–1322.

(32) Grill, A. *Cold Plasma in Materials Fabrication: From Fundamentals to Applications*, 1st ed.; IEEE Press: New York, 1994, pp 3–20, 31–38, 65, 93–100, 152–153.

(33) Erra, P.; Molina, R.; Cuesta, A.; Tascon, J. M. D.; Julia, R. R. Chitosan Treatment on Wool Pretreated with Cold Plasma. *Adv. Chitin Sci.* **1997**, *2*, 791–796.

(34) Cernakova, L.; St'ahel, P.; Kovacik, D.; Johansson, K.; Cernak, M. Low-Cost High-Speed Plasma Treatment of Paper Surfaces. *TAPPI Advanced Coating Fundamentals Symposium, Turku, Finland, Feb. 8–10, 2006.* **2006**, 1–11.

(35) Wang, C.-X.; Lu, J.-C; Xia, T.-P.; Cong, M.-Y.; Shi, S.-J. Study on Wool Fabric Treated with H_2O_2/ Plasma/ Chitosan. *Yinran Zhuji.* **2013**, *30*, 39–42.

(36) Ding, Z.; Chen, J. N.; Gao, S. Y.; Chang, J. B.; Zhang, J. F.; Kang, E. T. Immobilization of Chitosan onto Poly-L-lactic Acid Film Surface by Plasma Graft Polymerization to Control the Morphology of Fibroblast and Liver Cells. Biomaterials 2004, 25, 1059–1067.

(37) Vandenbossche, M.; Jimenez, M.; Casetta, M.; Bellayer, S.; Beaurain, A.; Bourbigot, S.; Traisnel, M. Chitosan-Grafted Nonwoven Geotextile for Heavy Metals Sorption in Sediments. *React. Funct. Polym.* **2013***, 73*, 53–59.

(38) Bahrami, N., Khorasani, S. N.; Mahdavi, H.; Ghiaci, M.; Mokhtari, R. Low-Pressure Plasma Surface Modification of Polyurethane Films with Chitosan and Collagen Molecules. *J. Appl. Polym. Sci.* **2019**, *136*, 47567.

(39) Pandiyaraj, K. N.; Ramkumar, M. C.; Kumar, A. A.; Padmanabhan, P. V. A.; Pichumani, M.; Bendavid, A.; Cools, P.; De Geyter, N.; Morent, R.; Kumar, V.; Gopinath, P.; Su, P.-G.; Deshmukh, R. R. Evaluation of Surface Properties of Low

Density Polyethylene (LDPE) Films Tailored by Atmospheric Pressure Non-Thermal Plasma (APNTP) Assisted Co-Polymerization and Immobilization of Chitosan for Improvement of Antifouling Properties. *Mater. Sci. Eng. C* **2019**, *94*, 150–160.

(40) Demina, T. S.; Drozdova, M. G.; Yablokov, M. Y.; Gaidar, A. I.; Gilman, A. B.; Zaytseva-Zotova, D. S.; Markvicheva, E. A.; Akopova, T. A.; Zelenetskii, A. N. DC Discharge Plasma Modification of Chitosan Films: An Effect of Chitosan Chemical Structure. *Plasma Process. Polym.* **2015**, *12*, 710–718.

(41) Demina, T. S.; Bikmulina, P. Y.; Birdibekova, A. V.; Kuryanova, A. S.; Frolova, A. A.; Koteneva, P. I.; Aksenova, N. A.; Kosheleva, N. V.; Khlebnikova, T. M.; Akopova, T. A.; Timashev, P. S. Modification of the Chemical Structure, Morpholgy, and Cytocompatibility of Chitosan Films via Low Frequency Plasma Treatment. *Appl. Biochem. Microbiol.* **2022**, *58*, 118–125.

(42) Kara, F.; Aksoy, E. A.; Yuksekdag, Z.; Aksoy, S.; Hasirci, N. Enhancement of Antibacterial Properties of Polyurethanes by Chitosan and Heparin Immobilization. *Appl. Surf. Sci.* **2015**, *357*, 1692–1702.

(43) Shahidi, S.; Mahmood, G.; Sanaz, D. Preparation of Multifunctional Wood Fabric using Chitosan after Plasma Treatment. *J. Text. I.* **2015**, *106*, 1127–1134.

(44) Wu, X. High-Efficiency Dyeing and Finishing Process of Cotton Fabric. CN 104988713. July 28, 2015.

(45) Chabrecek, P.; Lohmann, D. Method of Producing a Reactive Coating by After-Glow Plasma Polymerization. U. S. Patent 6,436,481 B1, Aug 20, 2002.

(46) Chabrecek, P.; Lohmann, D. Reactive Coatings. WO 98/28026, July 2, 1998.

(47) Kamel, I.; Soll, D. B. Method of Making Biocompatible Surface Modified Materials. US 5080924, Jan 14, 1992.

(48) Morra, M.; Cassinelli, C.; Cahalan, L. L.; Cahalan, P. T. Methods for Surface Modification. US 6632470 B2, Oct 14, 2003.

(49) Levi, R. J.; Labhasetwar, V. D.; Song, C. S. Surface-Modified Nanoparticles and Method of Making and Using Same. EU 0805678 B1, October 29, 2003.

(50) Chatelier, R. C.; Dai, L.; Griesser, H. J.; Li, S.; Zientek, P.; Lohmann, D.; Chabrecek, P. Multi-layer material. JP 3650394 B2, Feb 25, 2005.

(51) Qiu, Y.; Winterton, C.; Lally, J. M. Process for Surface Modifying Substrates and Modified Substrates Resulting Therefrom. US 6852352 B2, Feb 8, 2005.

(52) Lei, J.; Yang, L.; Zhan, Y.; Wang, Y.; Ye, T.; Li, Y.; Deng, H.; Li, B. Plasma Treated Polyethylene Terephthalate/Polypropylene Films Assembled with Chitosan and Various Preservatives for Antimicrobial Food Packaging. *Colloids Surf., B* **2014**, *114*, 60–66.

(53) Xu, L.; Huang, Y.-A.; Zhu, Q.-J., Ye, C. Chitosan in Molecularly-Imprinted Polymers: Current and Future Prospects. *Int. J. Mol. Sci.* **2015**, *16*, 18328–18347.

(54) Li, D.; Zhang, D. Preparation Method of Antibacterial Non-Woven Fabric. CN Patent 102,978,898 A, March 20, 2013.

(55) Chabrecek, P.; Lohmann, D. Method of Producing a Reacctive Coating by After-Glow Plasma Polymerization. U. S. Patent 6,436,481 B1, August 20, 2002.

(56) Chabrecek, P.; Lohmann, D. Reactive Coatings W. O. Patent 98/28026, July 2, 1998.

(57) Kamel, I.; Soll, D. B. Method of Making Biocompatible Surface Modified Materials. U. S. Patent 5,080,924, January 14, 1992.

(58) Levi, R. J.; Labhasetwar, V. D.; Song, C. S. Surface-Modified Nanoparticles and Method of Making and Using Same. E. U. Patent 0,805,678 B1, January 04, 1996.

(59) Kunita, M. H.; Girotto, E. M.; Muniz, E. C.; Rubira, A. F. Polypropylene Grafted with Glycidyl Methacrylate Using Supercritical CO_2 Medium. *Braz. J. Chem. Eng.* **2006**, *23*, 267–271.

(60) Qiu, Y.; Winterton, C.; Lally, J. M. Process for Surface Modifying Substrates and Modified Substrates Resulting Therefrom. U. S. Patent 6,852,353 B2, February 8, 2005.

(61) Wu, X. High-Efficiency Dyeing and finishing Process of Cotton Fabric. CN Patent 104,988,713, July 28, 2015.

(62) Ding, Z.; Chen, J.; Gao, S.; Chang, J.; Zhang, J.; Kang. E. T. Immobilization of Chitosan onto Poly-L-Lactic Acid Film Surface by Plasma Graft Polymerization to Control the Morphology of Fibroblast and Live Cells. *Biomater.* **2004**, *25*, 1059–1067.

(63) Amsden, B. G.; Sukarto, A.; Knight, D. K.; Shapka, S. N. Methacrylated Glycol Chitosan as a Photopolymerizable Biomaterial. *Biomacromolecules* **2007**, *8*, 3758–3766.

(64) Tarducci, C.; Kinmond, E. J.; Badyal, J. P. S.; Brewer, S. A.; Willis, C. Epoxide-Functionalized Solid Surfaces. *Chem. Mater.* **2000**, *12*, 1884–1889.

(65) Bruice, P. Y. *Organic Chemistry*, 7th ed.; Pearson Education Inc.: Upper Saddle River: 2014; pp 502–517, 527, 672.

(66) Mu, X.; Yang, X.; Zhang, D.; Liu, C. Theoretical Study of the Reaction of Chitosan Monomer with 2,3-Epoxypropyl-Trimethyl Quaternary Ammonium Chloride Catalyzed by an Imidazolium-Based Ionic Liquid. *Carbohydr. Polym.* **2016**, *146*, 46–51.

(67) Yasuda, H. *Plasma Polymerization;* Academic Press: New York, 1985.

(68) Bright, T. B.; Morris, L. E.; Summers, F. Mildew in Cotton Goods. *J. Text. Inst., Trans.* **1924**, *15,* T547–558.

(69) Galloway, L. D. 19—The Fungi Causing Mildew in Cotton Goods. *J. Text. Inst., Trans.* **1930**, *21,* T277–286.

(70) Behera, B. K.; Sardana, A. Studies on Polypropylene-Cotton Spun Yarns and their Fabrics. *Indian J. Fibre Text. Res.* **2001**, *26*, 280–286.

(71) Elwakeel, K. Z. Removal of Cr(VI) from Alkaline Aqueous Solutions Using Chemically Modified Magnetic Chitosan Resins. *Desalination* **2010**, *250*, 105–112.

(72) Yu, Z.; Zhang, X.; Huang, Y. Magnetic Chitosan – Iron(III) Hydrogel as a Fast and Reusable Adsorbent for Chromium(VI) Removal. *Ind. Eng. Chem. Res.* **2013**, *52*, 11956–11966.

(73) Gürsoy, M.; Harris, M. T.; Downing, J. O.; Barrientos-Palomo, S. N.; Carletto, A.; Yaprak, A. E.; Karaman, M.; Badyal, J. P. S. Bioinspired Fog Capture and Channel Mechanism Based on the Arid Climate Plant *Salsola crassa*. *Colloids Surf., A* **2017**, *529*, 195–202.

(74) Rinaudo, M.; Pavlov, G.; Desbrières, J. Influence of Acetic Acid Concentration on the Solubilization of Chitosan. *Polymer* **1999**, *40*, 7029–7032.

(75) Bot, C. T.; Prodan, C. Quantifying the Membrane Potential During *E. coli* Growth Stages. *Biophys. Chem.* **2010**, *146*, 133–137.

(76) Boscher, N. D.; Hilt, F.; Duday, D.; Frache, G.; Fouquet, T.; Choquet, P. Atmospheric Pressure Plasma Initiated Chemical Vapor Deposition Using Ultra-Short Square Pulse Dielectric Barrier Discharge. *Plasma Process. Polym.* **2015**, *12*, 66–74.

(77) Kunita, M. H.; Girotto, E. M.; Muniz, E. C.; Rubira, A. F. Polypropylene Grafted with Glycidyl Methacrylate Using Supercritical CO_2 Medium. *Braz. J. Chem. Eng.* **2006**, 23, 267–271.

(78) Bellamy, L. J. *The Infra-Red Spectra of Complex Molecules*. 3rd ed.; Chapman and Hall Ltd.: London, 1975; pp 38–39, 204–205.

(79) Lin-Vien, D.; Colthup, N. B.; Fateley, W. G.; Grasselli, J. G. *The Handbook of Infrared and Raman Characteristic Frequencies of Organic Molecules*, 1st ed.; Academic Press; San Diego: 1991; pp 62, 155–158, 163.

(80) Brown, P. S.; Wood, T. J.; Schofield, W. C. E.; Badyal, J. P. S. A Substrate-Independent Lift-Off Approach for Pattering Functional Surfaces. *ACS Appl. Mater. Interfaces* **2011**, *3*, 1204–1209.

(81) Oehr, C.; Müller, M.; Elkin, B.; Hegemann, D.; Vohrer, U. Plasma Grafting — A Method to Obtain Monofunctional Surfaces. *Surf. Coat. Technol.* **1999**, *116–119*, 23–25.

(82) Zhang, C.; Wang, Y.; Guo, J.; Liu, Y.; Zhou, Y. Chitosan Nanoparticle Carrier Based on Surface Molecularly Imprinted Polymers for the Recognition and Separation of Proteins. *RSC Adv.* **2015**, *5*, 106197–106205.

(83) Beamson, G.; Briggs, D. *High Resolution XPS of Organic Polymers: The Scienta ESCA300 Database*; John Wiley & Sons Ltd.: England, 1992; pp 130–131.

(84) Kasaai, M. R. A Review of Several Reported Procedures to Determine the Degree of N-Acetylation for Chitin and Chitosan Using Infrared Spectroscopy. *Carbohydr. Polym.* **2008**, *71*, 497–508.

(85) Brugnerotto, J.; Lizardi, J.; Goycoolea, F. M.; Argüelles-Monal, W.; Desbrieres, J.; Rinaudo, M. An Infrared Investigation in Relation with Chitin and Chitosan Characterization. *Polymer* **2001**, *42*, 3569–3580.

(86) Fernandes-Queiroz, M.; Teodosio-Melo, K. R.; Araujo-Sabry, D.; Lanzi-Sassaki, G.; Oliveira-Rocha, H. A. Does the Use of Chitosan Contribute to Oxalate Kidney Stone Formation? *Mar. Drugs* **2015**, *13*, 141–158.

(87) Mansur, H. S.; Mansur, A. A. P.; Curti, E.; De Almeida, M. V. Functionalized-Chitosan/Quantum Dot Nano-Hybrids for Nanomedicine Applications: Towards Biolabeling and Biosorbing Phosphate Metabolites. *J. Mater. Chem. B* **2013**, *1*, 1696–1711.

(88) Negrea, P.; Caunii, A.; Sarac, I.; Butnariu, M. The Study of Infrared Spectrum of Chitin and Chitosan Extract as Potential Sources of Biomass. *Dig. J. Nanomater. Biostruct.* **2015**, *10*, 1129–1138.

(89) Qiao, C.; Ma, X.; Zhang, J.; Yao, J. Molecular Interactions in Gelatin/Chitosan Composite Films. *Food Chem.* **2017**, *235*, 45–50.

(90) Song, C.; Yu, H.; Zhang, M.; Yang, Y.; Zhang, G. Physicochemical Properties and Antioxidant Activity of Chitosan from the Blowfly *Chrysomya megacephala* Larvae. *Int. J. Biol. Macromol.* **2013**, *60*, 347–354.

(91) Vino, A. B.; Ramasamy, P.; Shanmugam, V.; Shanmugam, A. Extraction, Characterization and *In vitro* Antioxidative Potential of Chitosan and Sulfated Chitosan from Cuttlebone of *Sepia aculeata* Orbigny, 1848. *Asian Pac. J. Trop. Biomed.* **2012**, S334-S341.

(92) Lawrie, G.; Keen, I.; Drew, B.; Chandler-Temple, A.; Rintoul, L.; Fredericks, P.; Grondahl, L. Interactions Between Alignate and Chitosan Biopolymers Characterized Using FTIR and XPS. *Biomacromolecules* **2007**, *8*, 2533–2541.

(93) Chakrabarti, C. L.; Akh, G.; Hutton, J. C. ATR and Reflectance IR Spectroscopy, Applications. *Spectrochim. Acta, Part B* **1999**, *33*, 153–193.

(94) van der Mei, H. C.; Engels, E.; de Vries, J.; Dijkstra, R. J. B.; Busscher, H. J. Chitosan Adsorption to Salivary Pellicles. *Eur. J. Oral Sci.* **2007**, *115*, 303–307.

(95) Halstead, F. D.; Rauf, M.; Moiemen, N. S.; Bamford, A.; Wearn, C. M.; Fraise, A. P.; Lund, P. A.; Oppenheim, B. A.; Webber, M. A. The Antibacterial Activity of Acetic Acid against Biofilm-Producing Pathogens of Relevance to Burns Patients. *Plos One* **2015**, *10*, e0136190.

(96) Ryssel, H.; Kloeters, O.; Germann, G.; Schäfer, Th.; Wiedemann, G.; Oehlbauer, M. The Antimicrobial Effect of Acetic Acid—An Alternative to Common Local Antiseptics? *Burns* **2009**, *35*, 695–700.

(97) Matsuda, T.; Yano, T.; Maruyama, A.; Kumagai, H. Antimicrobial Activities of Organic Acids Determined by Minimum Inhibitory Concentrations at Different pH Ranged from 4.0 to 7.0. *Nippon Shokuhin Kogyo Gakkaishi* **1994**, *41*, 687–702.

(98) Schoen, F. J. Applications of Biomaterials in Functional Tissue Engineering. In *Biomaterials Science: An Introduction to Materials in Medicine*; Ratner, B. D.; Hoffman, A. S.; Schoen, F. J.; Lemons, J. E., Eds.; Elsevier: Oxford, 2013; p 1294.

(99) No, H. K.; Park, N. Y.; Lee, S. H.; Meyers, S. P. Antibacterial Activity of Chitosans and Chitosan Oligomers with Different Molecular Weights. *Int. J. Food Microbiol.* **2002**, *74*, 65–72.

(100) Fernandez-Saiz, P. Chitosan and Chitosan Blends as Antimicrobials. In Antimicrobial Polymers; Lagarón, J. M.; Ocio, M. J., Eds.; John Wiley and Sons, Inc.: Hoboken, 2012; pp 72, 81, 84–85.

(101) Kong, M.; Chen, X. G.; Xing, K.; Park, H. J. Antimicrobial Properties of Chitosan and Mode of Action: A State of the Art Review. *Int. J. Food Microbiol.* **2010**, 144, 51–63.

(102) Xing, K.; Chen, X. G.; Liu, C. S.; Cha, D. S.; Park, H. J. Oleoyl-Chitosan Nanoparticles Inhibits *Escherichia coli* and *Staphylococcus aureus* by Damaging the Cell Membrane and Putative Binding to Extracellular or Intracellular Targets. *Int. J. Food Microbiol.* **2009**, *132*, 127–133.

(103) Liu, H.; Du, Y.; Wang, X.; Sun, L. Chitosan Kills Bacterial Through Cell Membrane Damage. *Int. J. Food Microbiol.* **2004**, *95*,147–155.

(104) Li, X.-F.; Feng, X.-Q.; Yang, S.; Fu, G.-Q.; Wang, T.-P.; Su, Z.-X. Chitosan Kills *Escherichia coli* Through Damage to Be of Cell Membrane Mechanism. *Carbohydr. Polym.* **2010**, *79*, 493–499.

(105) Vishu, K. A. B.; Varadaraj, M. C.; Gowda, L. R.; Tharanathan, R. N. Characterization of Chito-Oligosaccharides Prepared by Chitosanolysis with the Aid of Papain and Pronase, and Their Bactericidal Action Against *Bacillus cereus* and *Escherichia coli*. *Biochem. J.* **2005**, *391*, 167–175.

(106) Schoen, F. J. Applications of Biomaterials in Functional Tissue Engineering. In *Biomaterials Science: An Introduction to Materials in Medicine*; Ratner, B. D.; Hoffman, A. S.; Schoen, F. J.; Lemons, J. E., Eds.; Elsevier: Oxford, 2013; p 1294.

(107) No, H. K.; Park, N. Y.; Lee, S. H.; Meyers, S. P. Antibacterial Activity of Chitosans and Chitosan Oligomers with Different Molecular Weights. *Int. J. Food Microbiol.* **2002**, *74*, 65–72.

(108) Eaton, P.; Fernandes, J. C.; Pereira, E.; Pintado, M. E.; Malcata, F. X. Atomic Force Microscopy Study of The Antibacterial Effects of Chitosans on *Escherichia coli* and *Staphylococcus aureus*. *Ultramicroscopy* **2008**, *108*, 1128–1134.

(109) FTTS-AA-001 *Specified Requirements of Antibacterial Textiles for General Use*. The Committee for Conformity Assessment of Accreditation and Certification on Functional and Technical Textiles: Taiwan, 2005.

(110) Harrison, J. J.; Turner, R. J.; Ceri, H. Persister Cells, The Biofilm Matrix and Tolerance to Metal Cations in Biofilm and Planktonic *Pseudomonas aeruginosa*. *Environ. Microbiol.* **2005**, *7*, 981–994.

(111) Chung, Y. C.; Chen, C. Y. Antibacterial Characteristics and Activity of Acid-Soluble Chitosan. *Bioresour. Technol.* **2008**, *99*, 2806–2814.

(112) Muzzarelli, R.; Tarsi, R.; Filippini, O.; Giovanetti, E.; Biagini, G.; Varaldo, P. E. Antimicrobial Properties of N-Carboxylbutyl Chitosan. *Antimicrob. Agents Chemother.* **1990**, *34*, 2019–2023.

(113) Chung, Y.-C.; Su, Y.-P.; Chen, C.-C.; Jia, G.; Wang, H.-I.; Wu, J. C. G.; Lin, J.-G. Relationship between Antibacterial Activity of Chitosan and Surface Characteristics of Cell Wall. *Acta Pharmacol. Sin.* **2004**, *25*, 932–936.

(114) Sonohara, R.; Muramatsu, N.; Ohshima, H.; Kondo, T. Difference in Surface Properties between *Escherichia coli* and *Staphylococcus aureus* as Revealed by Electrophoretic Mobility Measurements. *Biophys. Chem.* **1995**, *55*, 273–277.

(115) Guney, A.; Kara, F.; Ozgen, O.; Aksoy, E. A.; Hasirci, V.; Hasirci, N. Surface Modification of Polymer Biomaterials. In *Biomaterial Surface Science*; Taubert, A.; Mano, J. F.; Rodríguez-Cabello, J. C., Eds.; Wiley-VCH Verlag GmbH & Co.: Weinheim, 2013; pp 140–141.

(116) Mellegård, H.; Strand, S. P.; Christensen, B. E.; Granum, P. E.; Hardy, S. P. Antibacterial Activity of Chemically Defined Chitosans: Influence of Molecular Weight, Degree of Deacetylation and Test Organism. *Int. J. Food Microbiol.* **2011**, *148*, 48–54.

(117) Tortora, G. J.; Funke, B. R; Case, C. L. *Microbiology An Introduction*, 12th ed.; Pearson Education, Inc.: New York, 2016; p 81.

(118) Goy, R. C.; Morais, S. T. B.; Assis, O. B. G. Evaluation of the Antimicrobial Activity of Chitosan and its Quaternized Derivative on *E. coli* and *S. aureus* Growth. *Rev. Bras. Farmacogn*. **2016**, *26*, 122–127.

(119) Gottenbos, B. Antimicrobial Effects of Positively Charged Surfaces on Adhering Gram-positive and Gram-negative Bacteria. *J. Antimicrob.* Chemother*. **2001**, *48*, 7–13.

4. Antibacterial Atomised Spray Plasma Deposited Poly(Acrylic Acid) Coatings

4.1. Introduction

Acrylic acid is a biodegradable organic compound, which consists of vinyl and carboxylic acid functional groups connected to each other, Scheme 4. 1.[1] Acrylic acid naturally occurs in marine algae, and its broad-spectrum antibacterial activity is related to its acidic potentiation.[2–4] Nevertheless, acrylic acid can be obtained by different synthesis routes, with the two-step oxidation of polypropylene being the main industrial production method. However, economic and environmental reasons have led researchers to develop alternative approaches to its synthesis.[5,6]
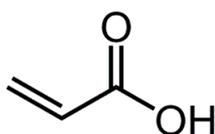
Scheme 4. 1: Acrylic acid.

Among other uses, acrylic acid is employed to develop poly(acrylic acid) materials for different applications, including biomedicine.[7–9] The physical features and antibacterial properties of poly(acrylic acid) makes it an attractive choice to modify surfaces without altering the bulk properties of materials.[10–12] There have been different approaches to coat a variety of substrates with poly(acrylic acid), including graft polymerisation reaction,[13–15] hydrolysis followed by drop casting deposition,[8] electrospun,[9,16] a variety of plasma polymerisation methods[10,11,17–19] and hydrogels.[20] However, the different setup for these techniques may require high power rate and temperature, and multiple steps, that at the end, produce coatings with poor chemical and mechanical stabilities, i.e., unstable coatings in aqueous media that wash off or with low carboxyl functional group retention.[10,11] For plasma coatings, there have been a range of studies looking at ways to overcome the drawbacks mentioned, however, the poor stability of the coatings obtained not only relates to solubility issues but also the demanding process conditions themselves.[11,21–23] Given the limitations reported by these previous reports, in this study, atomised spray plasma deposition (ASPD) of

poly(acrylic acid) was chosen as an attractive approach to overcome problems related to the stability and functionality of the coating. Stable ASPD poly(acrylic acid) coatings are possible to develop by optimising the deposition parameters when the poly(acrylic acid) deposition rate varies with the acrylic acid flow-rate whilst maintaining the power input constant during the ASPD process. This is because lower precursor flow-rates are associated with higher molecule fragmentation due to an excess of energy per surface molecule; on the contrary, higher precursor flow-rates are associated with energy deficiency leading to incomplete polymerisation. So, the optimal deposition-rate will be achieved when the power input allows enough energy to properly polymerise the coating without excessive molecule fragmentation (i.e., optimisation to control the energy-per-molecule described by the Yasuda parameter to avoid excessive molecular fragmentation of the precursor molecule within the plasma).[24,25]

Short chain carboxylic acids are known to be toxic to *Escherichia coli* by inducing bacterial cell membrane damage,[26] due to the deprotonated carboxyl group ($-COO^-$) present in aqueous media, and consequently allowing strong electrostatic interactions with essential metal ions for bacterial metabolism.[27,28] The antibacterial activity of poly(acrylic acid) has been studied in both, solution[29] and immobilised onto a surface.[30,31] For example, Gratzl et al.[8] investigated the antibacterial activity in both solution and surface against *E. coli* and *S. aureus*, and observed that poly(acrylic acid) displays higher antibacterial efficacy when immobilised onto a surface. Therefore, the antibacterial activity of the coating could be attributed to the deprotonated carboxyl groups on the ASPD poly(acrylic acid) surface, disrupting bacterial cell metabolic functionalities by undertaking electrostatic interactions with the bacterial cell membrane, rather than provision of a diluted concentration of the deprotonated poly(acrylic acid) material in solution (which requires to reach an equilibrium of charges across the membrane[32]), since the interaction between bacteria and poly(acrylic acid) changes in each of these conditions.[33]

The atomised spray plasma deposition (ASPD) is a substrate-independent technique, which allows high functional group retention of the precursor while it is atomised into the electrical discharges, and thus

decreases the energy-per-molecule at optimum conditions. The ASPD technique involves the atomisation of precursor into an excited medium created by electrical discharges. The excited plasma species (electrons, ions, vacuum ultraviolet (VUV) photons and radicals) activate the carbon–carbon double bond of the acrylic acid in the plasma phase which then undertakes the conventional radical polymerisation and polymer growth on the substrate surface, producing crosslinked polymer coatings covalently attached to the surface.[34–36] Furthermore, low-pressure ASPD offers the advantage of being adaptable to treat considerable size areas of different substrates (settings for the present work allowed the uniform coatings of substrates ~10 cm lenght) without the size and narrow amplitude limitations for the substrate seen when the plasma treatment is performed at atmospheric pressure, where a tiny distance between electrodes is required, and the treated section to be analysed represents a proof-of-concept study rather than a potentially scalable approach.[18,19,34,37] In this study, the ASPD technique was employed to fabricate ASPD poly (acrylic acid) coatings deposited onto polypropylene cloth, Scheme 4.2, whose antibacterial activity was tested against *E. coli* and displayed 100% efficacy.
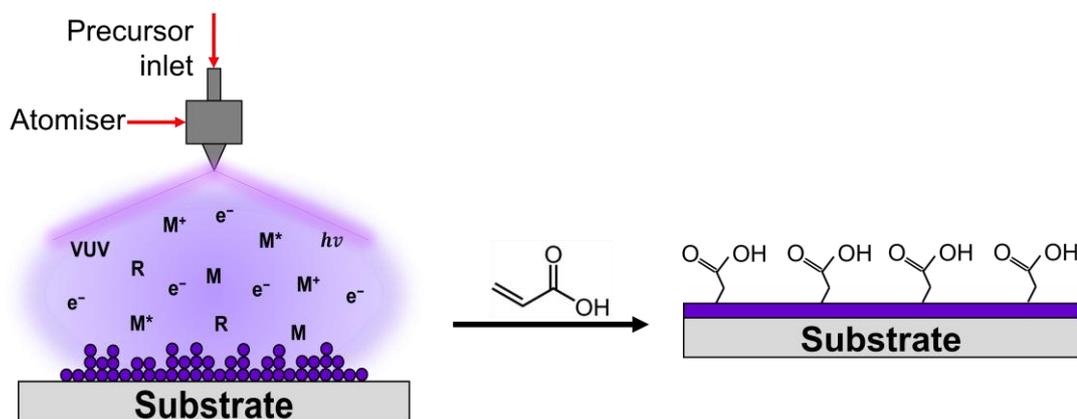
Scheme 4. 2: Atomised spray plasma deposition of poly(acrylic acid) coatings on surfaces.

The fabrication of ASPD poly(acrylic acid) coatings was carried out on polypropylene cloth, given its suitability for antibacterial activity testing. This approach is expected to produce a polymeric crosslinked film on the surface,

which is covalently attached onto the substrate surface due to the free radical sites created at the plasma–surface interface during the onset of plasma exposure. The ASPD experimental parameters for this study were carefully chosen to obtain a coating which is stable in aqueous media while retaining a considerable carboxy group content.[34,38]

4.2. Experimental

4.2.1. Atomised Spray Plasma Deposited (ASPD) Poly(Acrylic Acid) Coatings

The precursor material used was acrylic acid (99%, Sigma-Aldrich Ltd.), Scheme 4. 1. Acrylic acid precursor was loaded into a sealable glass delivery tube and degassed using multiple freeze–pump–thaw cycles. Substrates for coating were silicon (100) wafer (14–24 mΩ cm resistivity, Silicon Valley Microelectronics Inc.), ultrasonicated in a 1:1 v/v mixture of propan-2-ol / cyclohexane (+99.99% wt%, Acros Organics™) for 15 min, air dried, followed by air plasma cleaning (0.2 mbar pressure and 50 W) for 20 min prior to ASPD treatment; and hierarchical-coarse non-woven polypropylene cloth sample sets of 0.25 cm^2 and 2.38 cm^2 area respectively (0.4 mm thick, 22.7 ± 4.4 µm fibre diameter, and dimpled structure 0.7 ± 0.2 mm separation, Spunbond, 70 g m^{-2}, Avoca Technical Ltd., UK[39]). The hierarchical-coarse non-woven polypropylene cloth substrates were washed with ethanol (+99.8%, Fisher Scientific Ltd., UK) for 20 min, and any excess ethanol removed with absorbent paper tissue wipes (Kimtech Science, Kimberly-Clark Europe Ltd.) and vacuum dried. Substrates were placed downstream in line-of-sight from the atomiser prior to surface treatment.

Atomised spray plasma deposition was carried out as described in Chapter 2 Section 2.1.2.2 Atomised Spray Plasma Deposition. Ambient temperature ASPD was carried out using 10 W continuous wave plasma in conjunction with atomisation of acrylic acid precursor slurry into the reaction

chamber employing an optimised flow rate of $25 \pm 4 \times 10^{-4}$ mL s^{-1} (higher flow rates produce unstable films due to incomplete polymerisation). Upon plasma extinction, the atomiser was switched off and the system evacuated to base pressure, followed by venting to the atmosphere.[34]

4.2.2. Film Characterisation

Infrared spectroscopy was employed to characterise the ASPD poly(acrylic acid) coatings on polypropylene cloth, and acrylic acid precursor; X-ray spectra were obtained from ASPD poly(acrylic acid) coatings on silicon wafer; and antibacterial test were carried out to determine the antibacterial activity of the ASPD poly(acrylic acid) coatings on polypropylene cloth. The corresponding characterisation procedures were carried out as described in Chapter 2 Experimental Techniques.

4.2.3. Antibacterial Testing

For antibacterial testing, the cloth samples were cut into two separate sets of 5 mm × 5 mm and 1.4 cm × 1.7 cm size, respectively. The *E. coli* wild-type strain BW25113 (CGSC 7636; *rrnB3 ΔlacZ4787 hsdR514 Δ(araBAD)567 Δ(rhaBAD)568 rph-1*) was used for sensitivity testing. Bacterial cultures were prepared as described in Chapter 2 Section 2.7 Antibacterial Activity Test. Optical density OD$_{600nm}$ = 0.4 (0.4 ± 0.0) was measured using a spectrophotometer (model DS-11, DeNovix Inc.) to give bacteria in the mid-log phase of growth.[40] Antibacterial tests were performed by the dilution method at 1 mL and 100 µL scale, correspondingly, followed by colony-forming unit (CFU) plate counting, as described in Chapter 2 Experimental Techniques.

4.3. Results

4.3.1. Pulsed Plasma Deposited Poly(Acrylic Acid)

The infrared spectrum of liquid acrylic acid precursor includes the following absorbances: acid –OH stretch in the 3000–2800 cm^{-1} region; acid –OH group absorption in the 2500–2600 cm^{-1} region; acid carboxyl group –C=O stretch at 1698 cm^{-1}; C=C stretch at 1628 cm^{-1}; acid –C–O stretch and acid –OH bend of dimers at 1404 cm^{-1}; acid C–O stretch at 1294 cm^{-1}; acid –C–O–C symmetric and antisymmetric stretches at 1180 cm^{-1} and 1070 cm^{-1} respectively; =CH$_2$ stretch at 982 cm^{-1}, and acid –OH out-of-plane at 921 cm^{-1}, both from the liquid monomer, Figure 4. 1.[41–44]
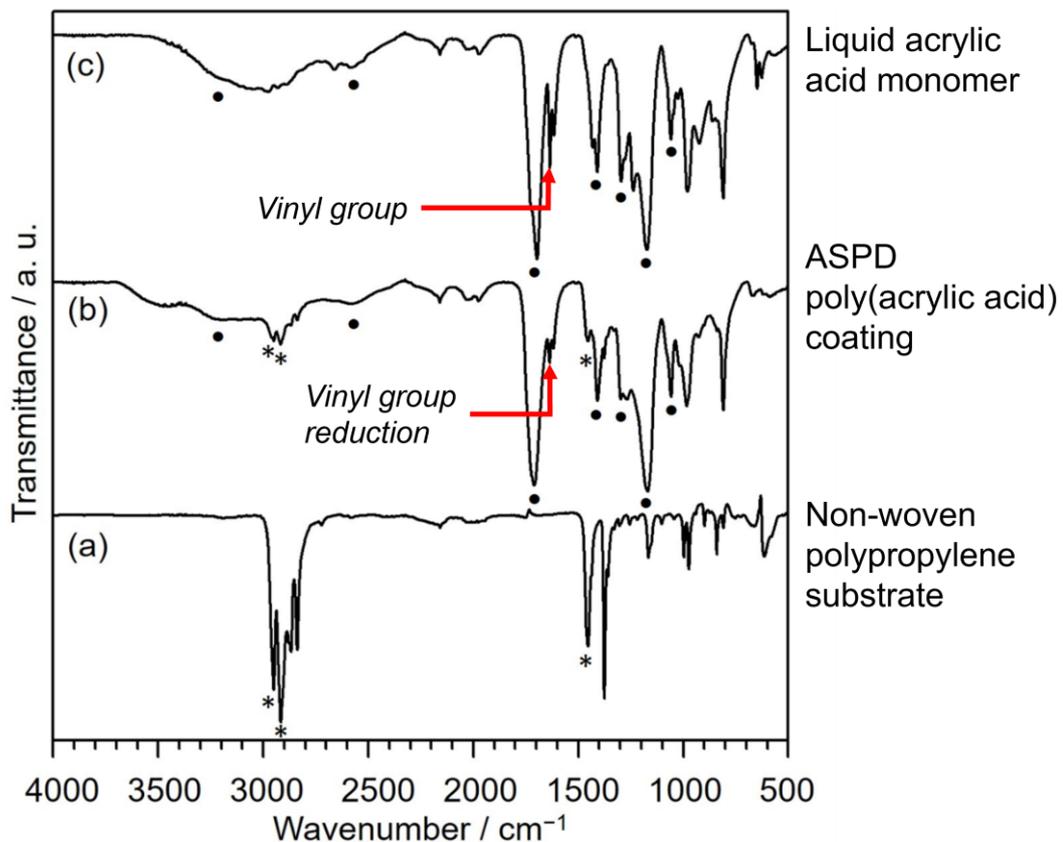
Figure 4. 1: Attenuated–total–reflection (ATR) infrared spectra of: (a) polypropylene cloth substrate; (b) ASPD poly(acrylic acid) coating on polypropylene; (c) liquid acrylic acid monomer. ● and ✱ denote characteristic infrared absorbances for carboxyl group from acrylic acid and underlaying polypropylene, respectively.

The ASPD poly(acrylic acid) coated polypropylene cloth showed the following characteristic poly(acrylic acid) absorption features: acid –OH stretch in the 3000–2800 cm^{-1} region; acid –OH group absorption between 2500–2600 cm^{-1}; acid –C=O stretch at 1705 cm^{-1}; acid –C–O stretch and acid –OH bend of dimers at 1404 cm^{-1}; acid C–O stretch at 1294 cm^{-1}; acid –C–O–C symmetric and antisymmetric stretches at 1180 cm^{-1} and 1070 cm^{-1} respectively; and retention of =CH_2 stretch at 982 cm^{-1} from acrylic acid monomer, Figure 4. 1. Significant reduction of C=C stretch due to acrylic acid polymerisation is observed at 1628 cm^{-1}. [19,41–44] Absorption bands from the underlying polypropylene cloth substrate were also observed in the ASPD poly(acrylic acid) coating, due to the ATR technique sampling depth (0.5–5 μm):[45,46] antisymmetric –CH_3 and CH_2 stretches at 2956 cm^{-1} and 2914 cm^{-1}, respectively; and CH_2 vibration at 1460 cm^{-1}.[47–49] In general, there is observed highly structural retention of the acrylic acid precursor and reduction of the oxygen functionalities corresponding to the carboxyl group after the ASPD process.

For the ASPD poly(acrylic acid) coatings, X-ray photoelectron spectroscopy (XPS) analysis detected the presence of only carbon and oxygen with no Si(2p) signal from the underlying silicon wafer substrate, thereby confirming a pin-hole free layer, Table 4. 1; using a different substrate does not affect the chemistry on the top-most layer of the coating since ASPD is a surface-independent approach.[35] The C(1s) envelope was fitted to three Gaussian Mg $K\alpha_{1,2}$ components: –$\underline{C}_xH_y$ (285.0 eV); –$\underline{C}$–O (287.0 eV), representing oxygen-containing functional groups which are present due to the fragmentation of acrylic acid monomer occurring at the plasma environment;[50] and O–$\underline{C}$=O (289.3 eV),[18] consistent with retention of the carboxy functional group, including the characteristic carboxyl functional group of the poly(acrylic acid),[18,50,51] Figure 4. 2. The XPS spectrum of the theoretical poly(acrylic acid) displayed three C(1s) components: $\underline{C}_xH_y$ (285.0 eV), –$\underline{C}$–COOH (285.4 eV), and O–$\underline{C}$=O (289 eV) that were obtained from a monochromatic XPS instrument which allows the differentiation of carbon components with an energy resolution of ~0.3 eV between them.[52,53] However, a nonmonochromatic XPS instrument was used in this work having a resolution energy of ~1 eV, and thus was unable to identify the –$\underline{C}$–COOH

carbon component with a binding energy shift of 0.4 eV from $\underline{C}_xH_y$.[54,55] However, the corresponding O(1s) Mg Kα$_{1,2}$ components were fitted for: –C=$\underline{O}$ (532.5 eV), and –C–$\underline{O}$ (533.9 eV);[55] the decrease of the atomic oxygen composition also suggests the fragmentation and loss of oxygen containing functionalities, Figure 4. 3.

Table 4. 1: XPS elemental and C(1s) compositions for: theoretical poly(acrylic acid), and ASPD poly(acrylic acid) coating, Figure 4. 2.

System	Composition / at. %		O/C	C(1s) Carbon Component / %			Normalised O–$\underline{C}$=O Retention
	Carbon	Oxygen		$\underline{C}_xH_y$	$\underline{C}$–O	O–$\underline{C}$=O	
Theoretical	60	40	0.67	66.7	0	33.3	100
Experimental	73 ± 0.2	27 ± 0.2	0.37	74.3 ± 2.9	7.7 ± 2.6	18.0 ± 0.3	70
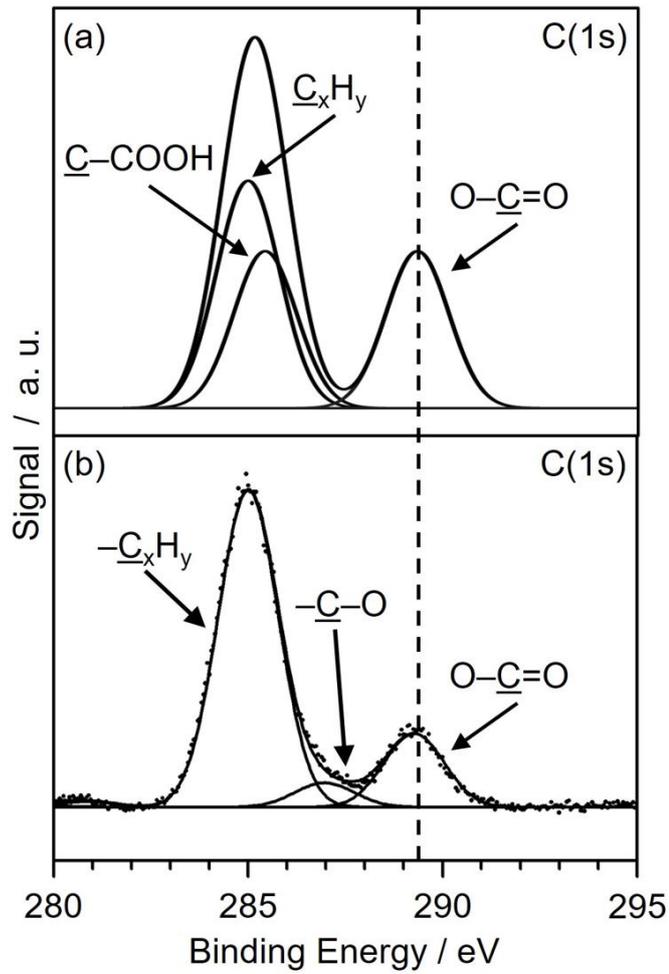
Figure 4. 2: XPS C(1s) spectra of: (a) theoretical poly(acrylic acid), and (b) experimental ASPD poly(acrylic acid) coating on silicon wafer.
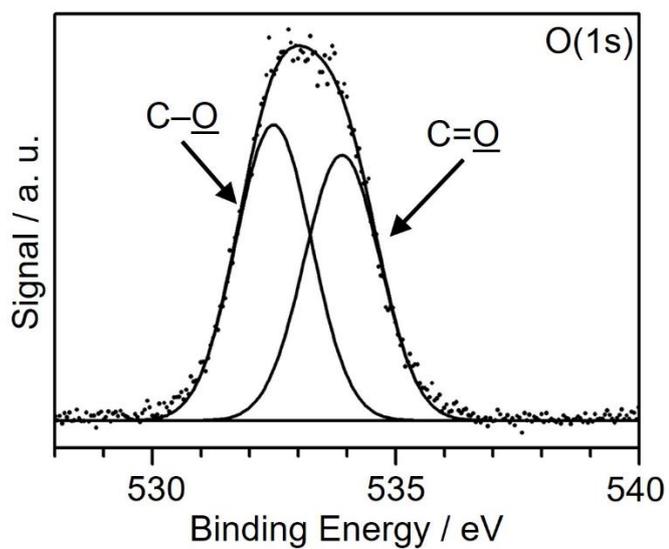
Figure 4. 3: XPS O(1s) spectrum of ASPD poly(acrylic acid) coating on silicon wafer.

Antibacterial testing of the ASPD poly(acrylic acid) coated cloths was performed with *E. coli* wild-type at two different scales (i.e., sets of: 1.4 cm × 1.7 cm, and 5 mm × 5 mm, respectively). The cloths displayed robust antibacterial activity by contact resulting in 100% killing of the bacteria during the 16 h interaction time, Figure 4.4. These results represented a log reduction of 9.8 ± 0.1, exceeding the minimum antibacterial clinical standard criterion (log reduction > 3),[56,57] compared to the untreated polypropylene cloth as reference sample. The ASPD poly(acrylic acid) coating did not wash off or dissolved after 16 h exposure to the liquid environment during the antibacterial tests.
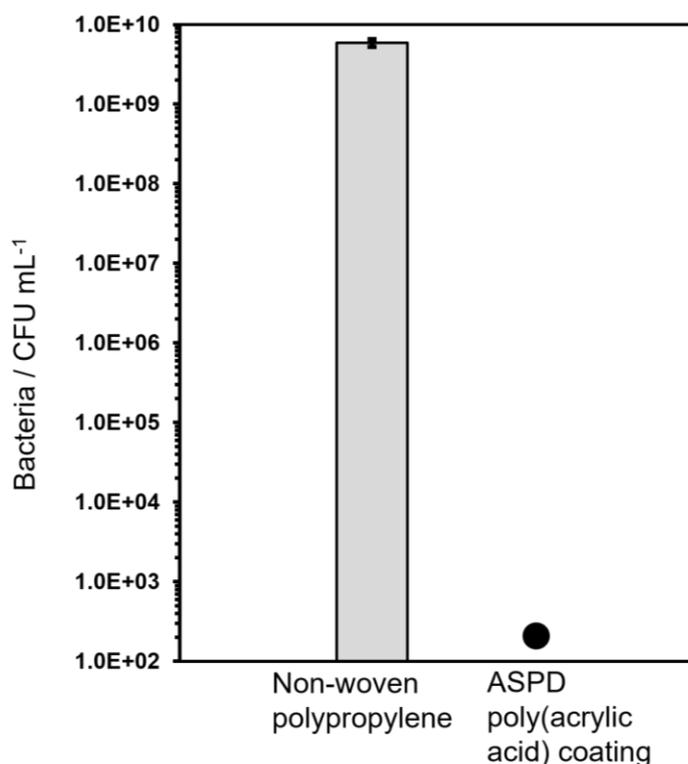
Figure 4. 4: Antibacterial activity of untreated non-woven polypropylene and ASPD poly(acrylic acid) coating on non-woven polypropylene cloth against *E. coli* strain. ● indicates 100% antibacterial efficacy against *E. coli*. Error bars indicate standard deviation for at least 3 sample repeats.

4.4. Discussion

The fabrication of ASPD poly(acrylic acid) coatings yielded excellent antibacterial activity against *E. coli*. The ASPD technique is a reliable process for the challenging industrial scale up of these materials. ASPD process parameters can be tuned for the necessities of the final consumer (e.g., for some applications, high retention of carboxyl groups in the poly(acrylic acid) coatings is not needed[10,58]), by setting plasma operation conditions so the energy input per surface molecule produce a coating with the desired physicochemical features (i.e., Yasuda parameter).[24] In comparison with the aforementioned studies, ASPD poly(acrylic acid) coatings provide high retention of the carboxyl group in equilibrium with the desired physical features of a stable coating in a single step process, without the need of limiting or demanding process requirements, nor further damage effects from overexposure to the plasma environment.[8–23,37] This is also in good agreement with studies of other variants of plasma deposition of poly(acrylic acid), where the carboxyl group retention and stability under aqueous media were investigated.[59–61] Nevertheless, Chen et al.[62] obtained similar carboxylic group retention to what is reported in this work, by performing low pressure plasma-enhanced chemical vapour deposition (PECVD) of acetic acid films which displayed stable wettability due to better functional group retention compared to their atmospheric pressure plasma deposition approach.

Infrared analysis of the ASPD poly(acrylic acid) coating suggested a good structural retention of the acrylic acid precursor after plasma polymerisation. Furthermore, XPS analysis indicated that ASPD poly(acrylic acid) coatings achieved ~70% retention on the surface of the O–C=O groups which include carboxy and carboxylic acid species. This may be due to the incidence of the reactive plasma species at the plasma phase or plasma–surface interface,[63] and the photochemical decarboxylation via C–C (3.61 eV[24]) bond of the precursor molecule caused by vacuum UV radiation,[64,65] as well as the reincorporation of oxygen containing fragments into the polymer coatings.[24,65]

The antibacterial properties of the ASPD poly(acrylic acid) coating are attributed to the chemical deprotonation of the carboxylic acid group in the aqueous testing environment, which is readily able to disturb the metabolic activity taking place at the bacterial cell membrane by changing the overall charge on its surface. This would interfere with electron transport required for the absorption of essential nutrients to generate adenosine triphosphate (essential for producing energy for multiple metabolic processes in the bacterial cell), and eventually causing cell membrane disruption and death.[27,66,67] Separate studies of the antibacterial activity of poly(acrylic acid) material against Gram-negative *E. coli*, and Gram-positive *Staphylococcus aureus*, implicated different possible mechanisms. First, a decrease in pH due to the deprotonation of carboxylic groups impairing pH homeostasis of bacterial cells, leading to subsequent damage of proteins, membranes, and DNA.[12] Second, the acidic conditions promoted by the deprotonation of carboxylic groups could be responsible for the antibacterial activity on the treated surface, due to an ion-exchange effect whereby the high negative charge density of deprotonated carboxylic groups, on the ASPD poly(acrylic acid) coating material, have strong affinity for cations at the cell membrane surface.[8,68,69] Furthermore, the acidic nature of the ASPD poly(acrylic acid) coating surface could make conditions adverse for the growth and proliferation of certain bacteria by maintaining an acidic pH, thus potentially preventing biofilm formation.[8,27]

The ASPD poly(acrylic acid) coatings, therefore, act as antibacterial contact killing coatings, showed good mechanical stability towards aqueous solvents and excellent antibacterial properties. The ASPD poly(acrylic acid) coatings did not wash off during antibacterial testing. Given the physical features of the polymeric matrix, the ASPD poly(acrylic acid) coating appeared stable after 16 h of interaction in aqueous media for the antibacterial test, potentially allowing *ad hoc* long-term usage with biological material.

4.5. Conclusion

The ASPD poly(acrylic acid) coatings on polypropylene cloth display antibacterial activity against Gram-positive *E. coli* (log reduction > 9) bacteria; a correlation is found between the high retention of carboxyl group within the polymeric matrix of the coating surface (as per XPS and FTIR results) and the measured level of antibacterial activity.

The simplicity of the ASPD solventless single step approach makes it amenable for a wide range of biomedical and commercial applications where polymeric antimicrobial surfaces are required. ASPD of poly(acrylic acid) coatings allows the synthesis of   crosslinked surfaces with good physicochemical properties, overcoming oiliness and tendency to wash off or dissolve as reported by other approaches whilst keeping a functionalised coating with the characteristic carboxyl groups from the precursor, due to the optimisation of ASPD settings to apply the adequate amount of energy per surface molecule of acrylic acid precursor atomised at certain flow-rate, to obtain a coating with the desired features and functionalities.

Further antibacterial test against different Gram-negative species, Gram-positives and scanning electron microscopy (SEM) analysis are suggested for deeper surface analysis.

4.6. References

(1) National Library of Medicine, National Center for Biotechnology Information. Acrylic Acid. https://pubchem.ncbi.nlm.nih.gov/compound/Acrylic-acid (accessed April 28, 2020).

(2) Mtolera, M. S. P.; Semesi, A. K. Antimicrobial Activity of Extracts from Six Green Algae from Tanzania. *Curr. Trends Mar. Bot. Res. East Afr. Reg.* **1996**, 211–217.

(3) Sieburth, J. M. Acrylic Acid, an "Antibiotic" Principle in Phaeocystis Blooms in Antarctic Waters. *Sci.* **1960**, *132*, 676–677.

(4) Sieburth, J. M. Antibiotic Properties of Acrylic Acid, a Factor in The Gastroinstestinal Antibiosis of Polar Marine Animals. *J. Bacteriol.* **1961**, *82*, 72–79.

(5) Liu, J.; Wang, P.; Xu, P.; Xu, Z.; Feng, X.; Ji, W.; Arandiyan, H.; Au, C.-T. How to Achieve a Highly Selective Yet Simply Available Vanadium Phosphorus Oxide-Based Catalyst for Sustainable Acrylic Acid Production *via* Acetic Acid-Formaldehyde Condensation. *Chem. Commun.* **2020**, *56*, 1022–1025.

(6) Ramos-Braga, E.; De Souza-Mustafa, G.; De Aguiar-Pontes, D.; Magalhaes-Pontes, L. A. Economic Analysis and Technicalities of Acrylic Acid Production from Crude Glycerol. *Chem. Ind. Chem. Eng. Q.* **2020**, *26*, 59–69.

(7) Australian Government, Department of Agriculture, Water and the Environment, National Pollutant Inventory. Acrylic Acid. http://www.npi.gov.au/resource/acrylic-acid (accessed: April 28, 2020).

(8) Gratzl, G.; Walkner, S.; Hild, S.; Hassel, A. W.; Weber, H. K.; Paulik, C. Mechanistic Approaches on The Antibacterial Activity of Poly(Acrylic Acid) Copolymers. *Colloids Surf., B* **2015**, *126*, 98–105.

(9) Santiago-Morales, J.; Amariei, G.; Letón, P.; Rosal, R. Antimicrobial Activity of Poly(Vinyl Alcohol)-Poly(Acrylic Acid) Electrospun Nanofibers. *Colloids Surf., B* **2016**, *146*, 144–151.

(10) López, L. C., Gristina, R.; Ceccone, G.; Rossi, F.; Favia, P.; D'Agostino, R. Immobilization of RGD Peptides on Stable Plasma-Deposited Acrylic Acid Coatings for Biomedical Devices. *Surf. Coat. Technol.* **2005**, 1000–1004.

(11) Jafari, R.; Tatoulian, M.; Arefi-Khonsari, F. Improvement of the Stability of Plasma Polymerized Acrylic Acid Coating Deposited on PS Beads in a Fluidized Bed Reactor. *React. Funct. Polym.* **2011**, *71*, 520–524.

(12) Gratzl, G.; Paulik, C.; Hild, S.; Guggenbichler, J. P.; Lackner, M. Antimicrobial Activity of Poly(Acrylic Acid) Block Copolymers. *Mater. Sci. Eng., C* **2014**, *38*, 94–100.

(13) Popelka, A.; Novák, I.; Lehocký, M.; Chodák, I.; Sedliacik, J.; Gajtanska, M.; Sedliacikova, M.; Vesel, A.; Junkar, I.; Kleinová, A.; Spírkova, M.; Bílek, F. Antibacterial Treatment of Polyethylene by Cold Plasma for Medical Purposes. *Molecules* **2012**, *17*, 762–785.

(14) Chen, X.; Huang, G.; An, C.; Feng, R.; Yao, Y.; Zhao, S.; Huang, C.; Wu, Y. Plasma-Induced Poly(Acrylic Acid)-TiO$_2$ Coated Polyvinylidene Fluoride Membrane for Produced Water Treatment: Synchrotron X-Ray, Optimization, and Insight Studies. *J. Cleaner Prod.* **2019**, *227*, 772–783.

(15) Ren, Y.; Zhao, J.; Wang, X. Hydrophilic and Antimicrobial Properties of Acrylic Acid and Chitosan Bigrafted Polypropylene Melt-Blown Nonwoven Membrane Immobilized with Silven Nanoparticles. *Text. Res. J.* **2018**, *88*, 182–190.

(16) De Giglio, E.; Cometa, S.; Cioffi, N.; Torsi, L.; Sabbatini, L. Analytical Investigations of Poly(Acrylic Acid) Coatings Electrodeposited on Titanium-Based Implants: A Versatile Approach to Biocompatibility Enhancement. *Anal. Bioanal. Chem.* **2007**, *389*, 2055–2063.

(17) Navarro-Rosales, M.; Ávila-Orta, C. A.; Neira-Velázquez, M. G.; Ortega-Ortiz, H.; Hernánddez-Hernández, E.; Solís-Rosales, S. G.; España-Sánchez, B. L.; González-Morones, P.; Jiménez-Barrera, R. M.; Sánchez-Valdes, S.; Bartólo-Pérez, P. Effect of Plasma Modification of Copper Nanoparticles on their Antibacterial Properties. *Plasma Process. Polym.* **2014**, *11*, 685–693.

(18) Cools, P.; Declercq, H.; De Geyter, N.; Morent, R. A Stability Study of Plasma Polymerized Acrylic Acid Films. *Appl. Surf. Sci.* **2018**, *432*, 214–223.

(19) Ward, L. J.; Schofield, W. C. E.; Badyal, J. P. S. Atmospheric Pressure *Plasma* Deposition of Structurally Well-Defined Polyacrylic Acid Films. *Chem. Mater.* **2003**, *15*, 1466–1469.

(20) Lu, Y.; Wang, D.; Li, T.; Zhao, X.; Cao, Y.; Yang, H.; Duan, Y. Y. Poly(Vinyl Alcohol)/Poly(Acrylic Acid) Hydrogel Coatings for Improving Electrode-Neutral Tissue Interface. *Biomater.* **2009**, *30*, 4143–4151.

(21) Jafari, R.; Arefi-Khonsari, F.; Tatoulian, M.; Le Clerre, D.; Talini, L.; Richard, F. Development of Oligonucleotide Microarray Involving Plasma Polymerized Acrylic Acid. *Thin Solid Films* **2009**, *517*, 5763–5768.

(22) Finke, B.; Schröder, K.; Ohl, A. Structure Retention and Water Stability of Microwave Plasma Polymerized Films from Allylamine and Acrylic Acid. *Plasma Process. Polym.* **2009**, *6*, 570–574.

(23) He, T.; Yang, Z.; Chen, R.; Wang, J.; Leng, Y.; Sun, H.; Huang, N. Enhanced Endothelialization Guided by Fribronectin Functionalized Plasma Polymerized Acrylic Acid Film. *Mater. Sci. Eng., C* **2012**, *32*, 1025–1031.

(24) Yasuda, H. *Plasma Polimerization*; Academic Press: New York, 1985.

(25) Gilliam, M. A.; Yu, Q.; Yasuda, H. Plasma Polymerization Behaviour of Fluorocarbon Monomers in Low-Pressure AF and RF Discharges. *Plasma Process Polym.* **2007**, *4*, 165–172.

(26) Royce, L. A.; Liu, P.; Stebbins, M. J.; Hanson, B. C.; Jarboe, L. R. The Damaging Effects of Short Chain Fatty Acids on *Escherichia coli*. *Appl. Microbiol. Biotechnol.* **2013**, *97*, 8317–8327.

(27) Desbois, A. P.; Smith, V. J. Antibacterial Free Fatty Acids: Activities, Mechanisms of Action and Biotechnological Potential. *Appl. Microbiol. Biotechnol.* **2010**, *85*, 1629–1642.

(28) Ping, X.; Wang, M.; Ge, X. Surface Modification of Poly(Ethylene Terephthalate) (PET) Film by Gamma-Ray Induced Grafting of Poly(Acrylic Acid) and Its Application in Antibacterial Hybrid Film. *Radiat. Phys. Chem.* **2011**, *80*, 567–572.

(29) Vyhnalkova, R.; Eisenberg, A.; Van de Ven, T. Bactericidal Block Copolymer Micelles. *Macromol. Biosci.* **2011**, *11*, 639–651.

(30) Akkilic, N.; De Vos, M. W. Responsive Polymer Brushes for Biomedical Applications. In *Switchable and Responsive Surfaces and Materials for Biomedical Applications*; Zhang, Z., Ed.; Elsevier, Ltd.: Enschede, The Netherlands, 2015; pp 119–146.

(31) Traba, C.; Liang, J. F. Bacteria Responsive Antibacterial Surfaces for Indwelling Device Infections. *J. Control Release*, **2015**, *28*, 18–25.

(32) Brul, S.; Coote, P. Preservative Agents in Foods Mode of Action and Microbial Resistance Mechanisms. *Int. J. Food Microbiol.* **1999**, *50*, 1–17.

(33) Rieger, K. A.; Porter, M.; Schiffman, J. D. Polyelectrolyte-Functionalized Nanofiber Mats Control the Collection and Inactivation of *Escherichia coli*. *Mater.* **2016**, *9*, 297.

(34) Affinito, J. D. Plasma Enhanced Chemical Deposition with Low Vapor Pressure Compounds. U. S. Patent 6,224,948 B1, May 1, 2001.

(35) Castaneda-Montes, I.; Ritchie, A. W.; Badyal, J. P. S. Atomised Spray Plasma Deposition of Hierarchichal Superhydrophobic Nanocomposite Surfaces. *Colloids Surf., A* **2018**, *558*, 192–199.

(36) Affinito, J. D. Plasma Enhanced Chemical Deposition with Low Vapor Pressure Compound. US Patent US6224948 B1, May 1, 2001.

(37) Morent, R.; De Geyter, N.; Trentesaux, M.; Gengembre, L.; Dubruel, P.; Leys, C.; Payen, E. Stability Study of Polyacrylic Acid Films Plasma-Polymerized on Polypropylene Substrates at Medium Pressure. *Appl Surf. Sci.* **2010**, *257*, 372–380.

(38) Ward, L. Application of a Coating Forming Material onto at Least One Substrate. US Patent WO 2003101621 A2, Dec 11, 2003.

(39) Gürsoy, M.; Harris, M. T.; Downing, J. O.; *Barrientos*-Palomo, S. N.; Carletto, A.; Yaprak, A. E.; Karaman, M.; Badyal, J. P. S. Bioinspired Fog Capture and Channel Mechanism Based on the Arid Climate Plant *Salsola crassa. Colloids Surf., A* **2017**, *529*, 195–202.

(40) Bot, C. T.; Prodan, C. Quantifying the Membrane Potential During *E. coli* Growth Stages. *Biophys. Chem.* **2010**, *146*, 133–137.

(41) Bellamy, L. J. *The Infra-Red Spectra of Complex Molecules*. 3rd ed.; Chapman and Hall Ltd.: London, 1975; pp 183–200.

(42) Umemura, J.; Hayashi, S. Infrared Spectra and Molecular Configurations of Liquid and Crystalline Acrylic Acids. *Bull. Inst. Chem. Res., Kyoto Univ.* **1974**, 52, 585–595.

(43) Dong, J.; Ozaki, Y.; Nakashima, K. FTIR Studies of Conformational Energies of Poly(Acrylic Acid) in Cast Films. *J. Polym. Sci. B* **1997**, *35*, 507–515.

(44) Kulbida, A.; Ramos, M. N.; Rasanen, M.; Nieminen, J.; Schrems, O.; Fausto, R. Rotational Isomerism in Acrylic Acid. *J. Chem. Soc. Farady Trans.* **1995**, *91*, 1571–1585.

(45) PerkinElmer Inc. FTIR Spectroscopy Attenuated Total Reflectance (ATR). *Technical Note FTIR Spectroscopy*. PerkinElmer Life and Analytical Sciences: Shelton, U.S.A., 2005.

(46) Shimadzu Corporation. FTIR Analysis Q&A: How Deep Does the Infrared Light Penetrate at the Position of Contact Between the Prism and Sample During ATR Measurements? https://www.shimadzu.com/an/ftir/support/faq/2.html (accessed April 21, 2020).

(47) Lin-Vien, D.; Colthup, N. B.; Fateley, W. G.; Grasselli, J. G. *The Handbook of Infrared and Raman Characteristic Frequencies of Organic Molecules*; Academic Press: San Diego, 1991; pp 9–17.

(48) Jung, M. R.; Horgen, F. D.: Orski, S. V.; Rodríguez-C., V.; Beers, K. L.; Balazs, G. H.; Jones, T. T.; Work, T. M.; Brignac, K. C.; Royer, S.-J.; Hyrenbach, K. D.; Jensen, B. A.; Lynch, J. M. Validation of ATR FT-IR to Identify Polymers of Plastic Marine Debris, Including Those Ingested by Marine Organisms. *Mar. Pollut. Bull.* **2018**, *127*, 704–716.

(49) Morent, R.; De Geyter, N.; Leys, C.; Gengembre, L.; Payen, E. Comparison Between XPS- and FTIR-Analysis of Plasma-Treated Polypropylene Film Surfaces. *Surf. Interface Anal.* **2008**, *40*, 597–600.

(50) Cools, P.; Sainz-García, E.; De Geyter, N.; Nikiforov, A.; Blajan, M.; Shimizu, K.; Alba-Elías, F.; Leys, C.; Morent, R. Influence of DBD Inlet Geometry on the Homogeneity of Plasma-Polymerized Acrylic Acid Films: The Use of a Microplasma–Electrode Inlet Configuration. *Plasma Process. Polym.* **2015**, *12*, 1153–1163.

(51) Dhayal, M.; Cho, S.-I. Leukemia Cells Interaction with Plasma-Polymerized Acrylic Acid Coatings. *Vac.* **2006**, *80*, 636–642.

(52) Crist, B. V. A Review of XPS Data-Banks. *XPS Rep.*, **2007**, *1*, 1–52.

(53) Van de Heide, P. In *XPS Photoelectron Spectroscopy: An Introduction to Principles and Practices*, John Wiley & Sons, Inc.: Canada, 2012; pp 101–138.

(54) Cardona, M., Ley, L., Eds. Photoemission in Solids I: General Principles; Springer-Verlag: Berlin, 1978, pp 52–60.

(55) Wagner, C. D.; Riggs, W. M.; Davis, L. E.; Moulder, J. F.; Muilenberg, G. E. *Handbook of X-Ray Photoelectron Spectroscopy A Reference Book of Standard Data for Use in X-Ray Photoelectron Spectroscopy*; Muilenberg, G. E., Ed.; Perkin-Elmer Corporation, Physical Electronics Division: Minnesota, U.S.A., 1979; pp 110–111.

(56) FTTS-AA-001 *Specified Requirements of Antibacterial Textiles for General Use.* The Committee for Conformity Assessment of Accreditation and Certification on Functional and Technical Textiles: Taiwan, 2005.

(57) Harrison, J. J.; Turner, R. J.; Ceri, H. Persister Cells, The Biofilm Matrix and Tolerance to Metal Cations in Biofilm and Planktonic *Pseudomonas aeruginosa*. *Environ. Microbiol.* **2005**, *7*, 981–994.

(58) Detomaso, L.; Gristina, R.; D'Agostino, R.; Senesi, G. S.; Favia, P. Plasma Deposited Acrylic Acid Coatings: Surface Characterization and Attachment of 3T3 Murine Fibroblast Cell Lines. *Surf. Coat. Technol.* **2005**, *200*, 1022–1025.

(59) Hegemann, D.; Körner, E.; Guimond, S. Plasma Polymerization of Acrylic Acid Revisited. *Plasma Process. Polym.* **2009**, *6*, 246–254.

(60) Voronin, S. A.; Zelzer, M.; Fotea, C.; Alexander, M. R.; Bradley, J. W. Pulsed and Continuous Wave Acrylic Acid Radio Frequency Plasma Deposits: Plasma and Surface Chemistry. *J. Phys. Chem., B* **2007**, *111*, 3419–3429.

(61) Candan, S.; Beck, A. J.; O'Toole, L.; Short, R. D.; Goodyear, A.; Braithwaite, N. St J. The Role of Ions in The Continuous-Wave Plasma Polymerisation of Acrylic Acid. *Phys. Chem. Chem. Phys.* **1999**, *1*, 3117–3121.

(62) Chen, W.-Y.; Matthews, A.; Jones, F. R.; Chen, K.-S. Immobilization of Carboxylic Acid Groups on Polymeric Substrates by Plasma-Enhanced Chemical Vapor or Atmospheric Pressure Plasma Deposition of Acetic Acid. *Thin Solid Films* **2018**, 666, 54–60.

(63) O'Toole, L.; Beck, A. J.; Short, R. D. Characterization of Plasma Polymers of Acrylic Acid and Propanoic Acid. *Macromol.* **1996**, *29*, 5172–5177.

(64) Terlingen, J. G. A.; Takens, G. A. J.; Van der Gaag, F. J.; Hoffman, A. S.; Feijen, J. On the Effect of Treating Poly(Acrylic Acid) with Argon and Tetrafluoromethane Plasmas: Kinetics and Degradation Mechanism. *J. Appl. Polym. Sci.* **1994**, *52*, 39–53.

(65) Friedrich, J. *The Plasma Chemistry of Polymer Surfaces: Advanced Techniques for Surface Design*, 1st ed., Wiley-VCH Verlag GmbH & Co. KGaA: Weinheim, Germany, 2012; pp 160–162.

(66) Rivas, B. L.; Pereira, E. D.; Moreno-Villoslada, I. Water-Soluble Polymer–Metal Ion Interactions. *Prog. Polym. Sci.* **2003**, *28*, 173–208.

(67) Rivas, B. L.; Pereira, E. D.; Palencia, M.; Sánchez, J. Water-Soluble Functional Polymers in Conjuction with Membranes to Remove Pollutant ions from aqueous solutions. *Prog. Polym. Sci.* **2011**, *36*, 294–322.

(68) Qi, X.; Wang, Z.; Ma, S.; Wu, L.; Yang, S.; Xu, J. Complexation Behavior of Poly(Acrylic Acid) and Lanthanide Ions. *Polym.* **2014**, *55*, 1183–1189.

(69) Montavon, G.; Hennig, C.; Janvier, P.; Grambow, B. Comparison of Complexed Species of Eu in Alumina-Bound and Free Polyacrylic Acid: A Spectroscopic Study. *J. Colloid Interface Sci*. **2006**, *300*, 482–490.

5. Antibacterial Atomised Spray Plasma Deposited (Metallosurfactant/ Polymer) Coatings

5.1. Introduction

Metallosurfactants are amphiphilic compounds composed of a surfactant molecule in which the surfactant head group is coordinated with a metal ion.[1,2] Metallosurfactants have the characteristic that the alkyl tail is hydrophobic while the head group, coordinated with the metal ion, is hydrophilic.[1,2] This duality or amphiphilic nature makes metallosurfactants attractive candidates for the assembly of nanoscale, metal-containing colloids, the headgroup ligand can impart a rich metal-coordination chemistry that can be used to tune the nature of the self-assembled structures.[3] Synergistic effects of metal species and surfactant components are expected from metallosurfactants for antibactibacterial activity purposes.

Different metal species exhibit antibacterial activity through different mechanisms. These depend on various factors such as the type of bacteria they interact with—bacterial membranes contain polymers with highly electronegative chemical groups where metal cations are adsorbed by a coordinated bond; concentration and oxidation state of the metal; and the antibacterial test method employed, which depends on the material condition of the metal (e.g., nanoparticle solution, complex, or surfaces); these interactions could induce oxidative stress, protein dysfunction, membrane damage, interference with nutrient assimilation and/or genotoxicity.[4–6] For example, copper and iron metal species are reported to particularly increase intracellular oxidative stress *in vivo* and *in vitro* experiments, against Gram-positive and Gram-negative bacteria, through processes driven by the Fenton reaction.[4,7] Furthermore, copper is known to possess antibacterial activity under dry and wet environments,[6] whereas other metal species such as silver, gold, molybdenum, zinc, magnesium, and titanium only display antibacterial activity under certain conditions.[6,8] However, metals themselves can be toxic for humans; therefore, doses and routes of administration are tuned as needed, or the metal-containing agent is confined to surfaces, such as textiles, polymers, or medical devices.[7]

On the other hand, surfactants themselves are capable of antibacterial activity due to their physicochemical features, such as having an ionic, non-

ionic or zwitterionic headgroup.[9,10] Depending on the chemical synthesis route, attributes such as surfactant alkyl chain length, geometry, spacer groups, and charges (for charged surfactants) can be modified to fulfil different application requirements, including antibacterial activity.[11–15] For instance, Zhang et al.,[16] tested and discussed differences between the antibacterial activity of cationic and anionic surfactants, and found that despite the cationic surfactant being more efficient at disrupting bacterial cell membrane permeability by electrostatic interactions, the use of anionic surfactant afterwards provides even higher antibacterial activity because it readily reacts with membrane proteins after bacterial cell membrane neutralisation with the cationic component. Morsi & El-Salamony[17] compared the antibacterial activity of three different cationic, anionic, and non-ionic surfactants which displayed antimicrobial activity depending on the interaction of each type of surfactant with microbes (i.e., Gram-positive and Gram-negative bacteria, fungi, or yeast). Furthermore, surfactants can also be combined with other antibacterial compounds for biomedical purposes.[18]

Given the advantages that different types of surfactant and metal species offer on their own for antibacterial applications, there have been reports of either functionalisation of metal nanoparticles with surfactants[19] or coordination of surfactants with metal species to form metallosurfactant complexes, in order to improve them for antimicrobial and biomedical applications, due to the synergistic effect offered by metal ion and surfactant molecule combinations.[20–34] In addition, metallosurfactants are of great use for other applications such as surface functionalisation pretreatment for anticorrosion purposes,[35] catalysis,[36–42] preparation of porous[43] and mesoporous materials,[44,45] magnetic resonance imaging,[46–49] CO-release for biological systems,[50] fluid property modifier for CO_2,[51,52] thin-film optoelectronics,[53] thin-film devices,[54] molecular design of metallomesogens,[55] radiolabeling of liposomes,[56] preparation of metal nanoparticles,[57] water remediation,[58,59] and so on.

Copper and iron based metallosurfactants are attractive for surfactant complexation for antimicrobial purposes,[60,61] because they have redox activity which is possible because those metal atoms can accommodate different number of valence electrons in their outermost atomic orbitals,

instead of a single number of valence as redox-inactive metal atoms; nevertheless, such oxidation states of metal atoms are affected by the environment they are in, and the metabolism and subcellular compartments of microorganisms they interact with, Table 5. 1.

Table 5. 1: Iron- and copper-based antibacterial metallosurfactants.

Metal ion	Surfactant/ chelating ligand	Organism tested	Ref.
Fe	Lauric acid Palmitic acid Myristic acid Steric acid Morpholine	*Aspergillus niger* *Candida albicans* *Escherichia coli* *Bacillus subtilis*	62
	Bis-hexadecyl pyridium chloride	*Bacillus cereus* *Bacillus polymyxa* *Klebsiella pneumoniae* *Pseudomonas aeruginosa*	63
	Dodecyl amine Cationic hexadecyl pyridinium chloride	*E. coli* *P. aeruginosa* *Streptococcus faecalis* *Staphylococcus aureus*	64
	Tannic acid-glycine derivatives	*S. aureus* *E. coli* *P. aeruginosa* *B. subtilis*	65
Cu	Dodecyl amine Cationic hexadecyl pyridinium chloride	*E. coli* *P. aeruginosa* *S. faecalis* *S. aureus*	64
	Peptide	*E. coli* *Enterococcus faecalis* *S. aureus*	66
	Dodecyl amine	*B. cereus* *K. pneumoniae*	67
	Cationic cetyl trimethyl ammonium bromide	*Desulfonamonas pigra* *E. coli* *S. aureus*	29

Metal ion	Surfactant/ chelating ligand	Organism tested	Ref.
	Polysaccharide derivatives of sodium alignate	*B. subtilis* *S. aureus* *E. coli* *P. aeruginosa*	68
	Hexadecylpyridinium chloride	*B. polymyxa* *B. cereus* *P. aeruginosa* *K. pneumonae*	69
	Hexadecyltrimethyl ammonium chloride	*E. coli* *S. aureus*	70
	Azobenzene isothiouronium salts	*P. aeruginosa* *S. aureus*	71
	Cationic alkyl acetate benzyl diphenil ammonium salt	*P. aeruginosa* *Sarcina lutea* *Bacillus pumilus* *Miluteus luteus*	20
	Decyl amine hydro chloride Dodecyl amine hydro chloride Tetradecyl amine hydro chloride	*B. subtilis* *E. coli* *S. aureus* *S. faecalis*	72
	Dodecylamine Cetylamine	*S. aureus* *B. subtilis* *E. coli*	73

Given the already studied antibacterial activity of metal species and surfactants, copper- and iron-based metallosurfactant complexes are proposed as complementary agents for incorporation into polymeric matrixes of atomised spray plasma deposition of metallosurfactant–polymer antibacterial coatings. Metallosurfactants precursors Cu-CTAC,[60] Fe-CTAC,[60] and CuDDA,[61] were provided by Dr Gurpreet Kaur, and Dr Preeti Garg from the Department of Chemistry, Panjab University, Chandigarh, India.

For this purpose, atomised spray plasma deposition (ASPD) of antibacterial metallosurfactant/polymer coatings will be performed to obtain stable composite coatings, Scheme 5.2, allowing release of antibacterial metallosurfactant material upon contact with bacterial environments. To date, there are no reports available for the deposition of the proposed type of coatings that host metallosurfactants as antibacterial agents. Thus, the present work proposes ASPD process as an approach to achieve coatings which display high and quick antibacterial activity against *Escherichia coli* and *Staphylococcus aureus* strains.
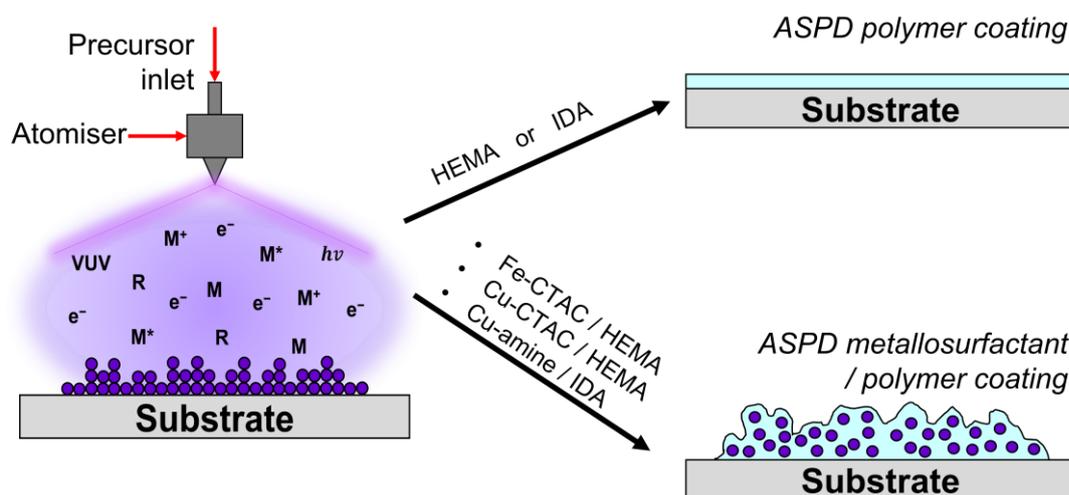
Scheme 5. 1: Fabrication process of atomised spray plasma deposition of polymer- and ASPD metallosurfactant/polymer coatings on surfaces.

5.2. Experimental

5.2.1. Atomised Spray Plasma Deposition (ASPD) of Metallosurfactant–Polymer Coatings

Precursor materials used were 2-hydroxyethyl methacrylate (HEMA, +97%, Sigma-Aldrich Inc.), isodecyl acrylate (IDA, +99.9%, Sigma-Aldrich Inc.), and

metallosurfactants provided by Dr Gupreet Kaur and Dr Preeti Garg, from the Department of Chemistry, Centre of Advanced Studies in Chemistry, Punjab University,[60,61] Scheme 5. 2 and Table 5. 2. Metallosurfactants were mixed with precursor monomers at 2% w/v concentration and shaken (VXR Vibrax orbital shaker, IKA® Works Inc.) until fully dissolved to form stable suspensions; precursor monomers were chosen to be combined with a particular metallosurfactant depending on their solubility. Each metallosurfactant/precursor mixture was loaded into a sealable glass delivery tube and degassed using multiple freeze–pump–thaw cycles. Before the ASPD treatment, the Cu-amine/IDA suspension was stirred with a custom-built portable magnetic stirrer (designed, developed and built by Dr Bryan Denton, Durham University) during plasma deposition (operation conditions: 15 V, 25 mA; 2–20 Hz).
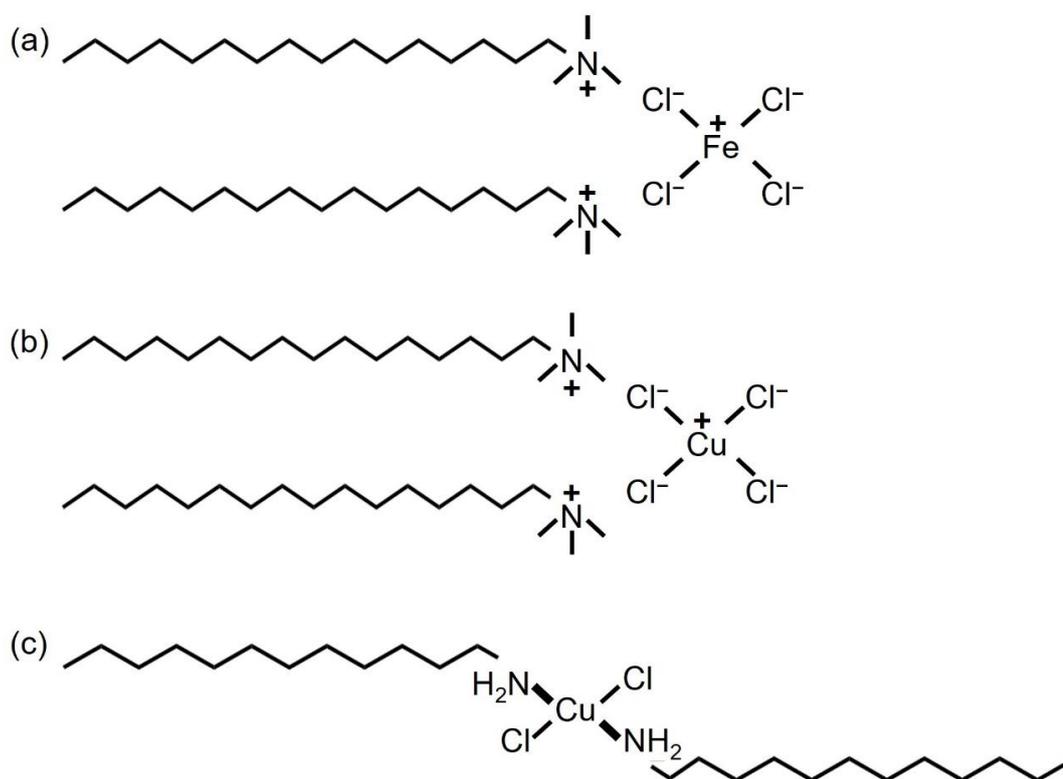
Scheme 5. 2: Metallosurfactants: (a) bishexadecyl trimethyl ammonium iron (II) tetrachloride (Fe-CTAC); (b) bishexadecyl trimethyl ammonium copper (II) tetrachloride (Cu-CTAC); (c) bisdodecylamine copper (II) chloride (Cu-amine); where thicker lines denote coordinated copper–nitrogen bonds.

Table 5. 2: 2% w/v metallosurfactant-monomer precursor combinations used for atomised spray plasma deposition.

Coating	Metallosurfactant	Monomer
Fe-CTAC / HEMA	Bishexadecyl trimethyl ammonium iron (II) tetrachloride (Fe-CTAC)	2-Hydroxyethyl methacrylate
Cu-CTAC / HEMA	Bishexadecyl trimethyl ammonium copper (II) tetrachloride (Cu-CTAC)	2-Hydroxyethyl methacrylate
Cu-amine / IDA	Bisdodecylamine copper(II) dichloride (Cu-amine)	Isodecyl acrylate

Substrates used for coating were silicon (100) wafer (14–24 mΩ cm resistivity, Silicon Valley Microelectronics Inc.), and hierarchical-coarse non-woven polypropylene cloth (0.4 mm thick, 22.7 ± 4.4 µm fibre diameter, and dimpled structure 0.7 ± 0.2 mm separation, Spunbond, 70 g m^{-2}, Avoca Technical Ltd., UK[74]). Silicon wafers were sonicated in a 1:1 v/v mixture of propan-2-ol (+99.5 wt %, Fisher Scientific Ltd.) / cyclohexane (+99.7%, Sigma-Aldrich Ltd.) for 10 min, air-dried, followed by UV-ozone cleaning for 10 min (model ProCleaner UV.TC.EU.003, BioForce Nanosciences Inc.), then sonicated in 1:1 v/v solvent mixture of propan-2-ol / cyclohexane for 5 min and air dried. The hierarchichal-coarse non-woven polypropylene cloth substrates were washed with ethanol (+99.8%, Fisher Scientific Ltd., UK) for 20 min, and any excess ethanol removed with absorbent paper tissue wipes (Kimtech Science, Kimberly-Clark Europe Ltd.) and vacuum dried. Substrates were placed downstream in line-of-sight from the atomiser prior surface treatment.

Ambient temperature ASPD was carried out as described in Chapter 2 Section 1.2 Atomised Spray Plasma Deposition, using a 50 W continuous wave plasma in conjunction with atomisation of each solid–liquid slurry into the reaction chamber employing an optimised flow rate of 8 ± 1×10^{-4} mL s^{-1} for poly(HEMA) and (metallosurfactant/HEMA) coatings, and 11 ± 1×10^{-4} mL s^{-1} for poly(IDA) and (metallosurfactant/IDA) coatings (higher flow rates produce unstable films due to incomplete polymerisation). Upon plasma

extinction, the atomiser was switched off and the system was evacuated to base pressure, followed by venting to atmosphere, Scheme 5.2.[75]

5.2.2. Film Characterisation

Infrared spectroscopy, water contact angle analysis, scanning electron microscopy, and antibacterial test, were employed as characterisation techniques to determine the physicochemical features and antibacterial properties of the ASPD polymer- and 2% w/v ASPD (metallosurfactant/polymer) coatings. The corresponding characterisation procedures were carried out as described in Chapter 2 Experimental Techniques.

5.2.3. Antibacterial Testing

Antibacterial activity testing was performed against representative Gram-positive and Gram-negative bacteria to evaluate their sensitivity towards the coatings produced in this work, as well as to check their reusability, and finally tested against 12 different *E. coli* mutant strains to provide insight into possible antibacterial modes of action.

For testing, the cloth samples were cut into pieces of 5 mm x 5 mm size. Both Gram-positive *Staphylococcus aureus* (FDA209P, an MSSA strain; ATCC 6538P) and Gram-negative wild-type *Escherichia coli* BW25113 (CGSC 7636; *rrnB3 ΔlacZ4787 hsdR514 Δ(araBAD)567 Δ(rhaBAD)568 rph-1*) were tested. Bacterial cultures were grown to optical densities OD_{600nm} = 0.4 (0.4 ± 0.0 for *S. aureus*, and 0.4 ± 0.0 for *E. coli*), measured using a spectrophotometer (model DS-11, DeNovix Inc.) to provide bacterial cultures in the mid-log phase of growth.[76] 10 µL from each bacterial culture was applied to the surface of each cloth sample for 16 h at 30 °C. For recycling experiments, bacteria were exposed to samples for 4 h

at 30 °C, which were taken out from the 10^{-1} solution, which is the prepared bacterial culture that interacted with each sample for a fixed time, then topped up with 90 µL LB, and mixed properly (refer to Section 2.7.3 Antibacterial Test: Dilution Method, for 100 µL scale); next, rinsed with autoclaved Milli-Q® water for 1 min, and completely dried in preparation for the next antibacterial activity test cycle.

Additional antibacterial testing was carried out using Gram-negative *Escherichia coli* mutant bacteria strains (*ahpC*, *copA*, *cueO*, *feoB*, *fepA*, *katG*, *lpxL*, *mutM*, *rfaC*, *sodA*, *sodB*, and *sodC*), Table 5. 3. These strains have various defects in outer membrane intergrity, copper and iron tolerance and oxidative damage repair and offer insights into the mechanism of action of metallosurfactants. Optical densities $OD_{600nm} = 0.4$ (0.4 ± 0.0 for *E. coli* mutant strains), were measured as before. For this set of experiments, 100 µL bacterial culture from each mutant strain interacted with the surface of each testing sample for 2 min at room temperature.

Table 5. 3: *E. coli* K12 Keio collection mutants used in this study; *E. coli* BW25113 is their wild-type background. List provided by Dr Gary Sharples, Department of Biosciences, Durham University.

Strain	Gene	Protein	Functional role
Lipopolysaccharide biosynthesis			
JW3596[77]	*rfaC* (*waaC*)	Lipopolysaccharide heptosyltransferase 1	Heptose transfer to the lipopolysaccharide core; it transfers the innermost heptose to [4'-P](3-deoxy-D-manno-octulosonic acid)2-IVA.
JW1041[78]	*lpxL*	Lipid A biosynthesis lauroyltransferase	Catalyzes transfer of laurate from lauroyl-acyl carrier protein (ACP) to Kdo_2-lipid IV(A) to form Kdo_2-(lauroyl)-lipid IV(A).
Metal homeostasis			
JW0119[79]	*cueO*	Blue copper oxidase CueO	Periplasmic detoxification of copper by oxidizing Cu^+ to Cu^{2+}; prevents uptake into the cytoplasm; role in copper efflux

Strain	Gene	Protein	Functional role
			under aerobic conditions.
JW0473[80]	*copA*	Copper-exporting P-type ATPase A	Involved in copper export; may also be involved in silver export.
JW3372[81]	*feoB*	Fe^{2+} transporter FeoB	Transporter of a GTP-driven Fe^{2+} uptake system, probably couples GTP-binding to channel opening and Fe^{2+} uptake.
JW5086[82]	*fepA*	Ferrienterobactin receptor	Involved in the initial step of iron uptake by binding ferrienterobactin (Fe-ENT), an iron chelatin siderophore.
Oxidative damage repair and tolerance			
JW3610[83]	*mutM* (*fpg*)	Formamidopyrimidine-DNA glycosylase	Acts as a DNA glycosylase that recognises and removes damaged bases; has a preference for oxidized purines.
JW3879[84]	*sodA*	Superoxide dismutase [Mn]	Destroys superoxide anion radicals.
JW1648[85]	*sodB*	Superoxide dismutase [Fe]	Destroys superoxide anion radicals.
JW1638[86]	*sodC*	Superoxide dismutase [Cu-Zn]	Bacteriocuprein; destroys superoxide anion radicals in the periplasmic space.
JW0598[87]	*ahpC*	Alkyl hydroperoxide reductase subunit C	Directly reduces organic hydroperoxides in its reduced dithiol form; antioxidant.
JW3914[88]	*katG*	Catalase-peroxidase	Bifunctional enzyme with both catalase and broad-spectrum peroxidase activity; detoxifies hydrogen peroxide; binds iron.

All bacterial cultures were prepared as described in Chapter 2 Section 2.7.2 Preparation of Bacterial Cultures. Then, antibacterial sensitivity and

reusability, tests were performed by the dilution method at 100 µL scale and required interaction times between bacteria and samples, followed by colony-forming unit (CFU) plate counting, as described in Chapter 2 Section 2.7.3 Antibacterial Test: Dilution Method.

5.3. Results

5.3.1. ASPD Metallosurfactant–Polymer and ASPD Polymer coatings

The infrared spectrum of substrate polypropylene cloth includes the following absorbances: CH_3 and CH_2 antisymmetric stretchings at 2953 cm^{-1} and 2917 cm^{-1}, respectively; CH_3 and CH_2 symmetric stretchings at 2867 cm^{-1} and 2831 cm^{-1}, respectively; $-CH_2-$ stretching at 1459 cm^{-1}; and $-C(CH_3)$ symmetric bending at 1382 cm^{-1},[89,90] Figure 5. 1, Table 5. 4, and Table 5. 5.
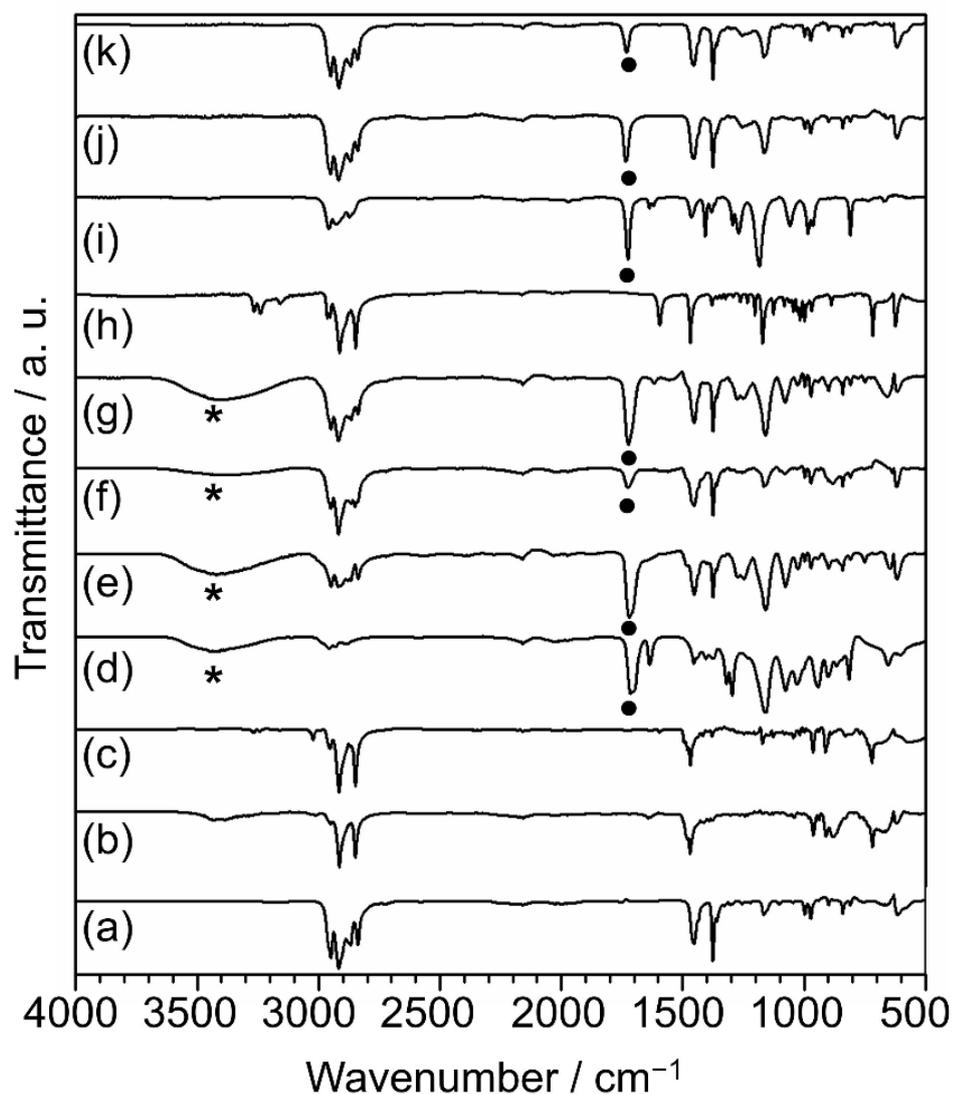
Figure 5. 1: ATR infrared spectra of: (a) non-woven polypropylene cloth substrate; (b) Fe-CTAC powder; (c) Cu-CTAC powder; (d) HEMA liquid monomer; (e) ASPD poly(HEMA) on polypropylene cloth; (f) 2% w/v ASPD Fe-CTAC/HEMA on polypropylene cloth; (g) 2% w/v ASPD Cu-CTAC/HEMA on polypropylene cloth; (h) Cu-amine powder; (i) IDA liquid monomer; (j) ASPD poly(IDA) on polypropylene cloth; (k) 2% w/v ASPD Cu-amine/IDA on polypropylene cloth. ✱ and ⬤ denote characteristic infrared absorbances for O–H stretching (liquid HEMA precursor and corresponding ASPD coatings) and C=O stretching (liquid HEMA and IDA monomers, and corresponding ASPD coatings) respectively, Table 5. 4 and Table 5. 5.

Table 5. 4: Infrared spectra absorbances of: non-woven polypropylene (PP) substrate; HEMA and IDA liquid monomers; Fe-CTAC, Cu-CTAC, and Cu-amine metallosurfactant powder precursors.[60,61,89,90]

Assignment	Absorption Frequency / cm^{-1}					
	Substrate	Liquid Monomers		Metallosurfactant Powders		
	PP	HEMA	IDA	Fe-CTAC	Cu-CTAC	Cu-amine
O–H stretching	–	3400	–	–	–	–
R–NH$_2$ symmetric stretching	–	–	–	–	–	3240
CH$_3$ antisymmetric stretching	2953	2957	2960	2952	2953	2960
CH$_2$ antisymmetric stretching	2917	2931	2924	2914	2915	2914
CH$_3$ symmetric stretching	2867	2887	2870	2849	2849	2848
CH$_2$ symmetric stretching	2831	–	2860–2830	2840–2830	2840–2830	2840–2830
C=O stretching	–	1714	1727	–	–	–
C=C stretching	–	1637	1632	–	–	–
R–NH$_2$ bending	–	–	–	–	–	1595
–CH$_2$– stretching	1459	1454	1463	1470	1469	1463
=CH$_2$ bending	–	1403	1402	–	–	–
–C(CH$_3$) symmetric bending	1382	1375	1377	–	–	1380
C–O stretching	–	1293, 1158	1260, 1181	–	–	–
C–N stretching	–	–	–	–	–	1174
–CH(CH$_3$)$_2$ stretching	1175–1140 1060–1040	1175–1140	1175–1140	–	–	1175–1140
=CH$_2$ bending	–	942	983	962	963	–

143

Table 5. 5: Infrared spectra absorbances of: ASPD polymer coatings poly(HEMA) and poly(IDA); and 2% w/v ASPD (metallosurfactant/polymer) coatings on PP substrate, i.e. Fe-CTAC/HEMA, Cu-CTAC/HEMA, and Cu-amine/IDA.[60,61,89,90.]

Assignment	Absorption Frequency / cm^{-1}				
	ASPD polymer coatings		2% w/v (ASPD metallosurfactant/polymer) coatings		
	Poly (HEMA)	Poly (IDA)	Fe-CTAC/ HEMA	Cu-CTAC/ HEMA	Cu-amine/ IDA
O–H stretching	3400	–	3400	3400	–
R–NH$_2$ symmetric stretching	–	–	–	–	–
CH$_3$ antisymmetric stretching	2949	2953	2950	2950	2953
CH$_2$ antisymmetric stretching	2918	2921	2917	2917	2917
CH$_3$ symmetric stretching	2869	2864	2851	2870	2867
CH$_2$ symmetric stretching	2837	2838	2839	2832	2838
C=O stretching	1721	1731	1725	1724	1731
C=C stretching	–	–	–	–	–
R–NH$_2$ bending	–	–	–	–	1595
–CH$_2$– stretching	1452	1456	1453	1452	1456
=CH$_2$ bending	–	–			–
–C(CH$_3$) symmetric bending	1374	1377	1374	1374	1377
C–O stretching	1257	1260	1260	1263	1260
C–N stretching	–	–	–	–	–
–CH(CH$_3$)$_2$ stretching	1175–1140	1175–1140	1175–1140	1175–1140	1175–1140
=CH$_2$ bending	942	983	960	969	983

Infrared absorbances for hexadecyltrimethylammonium chloride (CTAC)-based metallosurfactant powder precursors, Fe-CTAC and Cu-CTAC, include: CH_3 and CH_2 antisymmetric stretching at 2952–2953 cm^{-1} and 2914–2915 cm^{-1}, respectively; CH_3 and CH_2 symmetric stretching at 2849 cm^{-1} and 2840–2830 cm^{-1}, respectively; and $-CH_2-$ stretching at 1469–1470 cm^{-1}. For dodecyl amine-based metallosurfactant powder precursor, Cu-amine, infrared absorbances include: $R-NH_2$ symmetric stretching at 3240 cm^{-1}; CH_3 and CH_2 antisymmetric stretching at 2960 cm^{-1} and 2914 cm^{-1}, respectively; CH_3 and CH_2 symmetric stretching at 2848 cm^{-1} and 2840–2830 cm^{-1}, respectively; $R-NH_2$ bending at 1595 cm^{-1}; $-CH_2-$ stretching at 1463 cm^{-1}; $-C(CH_3)$ symmetric bending at 1380 cm^{-1}; and C–N stretching at 1174 cm^{-1},[60,61,89,90] Figure 5. 1, Table 5. 4 and Table 5. 5.

The infrared spectrum of liquid HEMA monomer include the following absorbances: O–H stretching at 3400 cm^{-1}; CH_3 and CH_2 antisymmetric stretching at 2957 cm^{-1} and 2931 cm^{-1}, respectively; CH_3 symmetric stretching at 2887 cm^{-1}; C=O stretching at 1714 cm^{-1}; C=C stretching at 1637 cm^{-1}; $-CH_2-$ stretching at 1454 cm^{-1}; $=CH_2$ bending at 1403 cm^{-1}; $-C(CH_3)$ symmetric bending at 1375 cm^{-1}; and C–O stretching at 1293 cm^{-1} and 1158 cm^{-1}. These absorbances were also found for the ASPD poly(HEMA) coating infrared spectrum, however the disappearance of carbon–carbon double bond stretch at 1637 cm^{-1} and $=CH_2$ bending at 1403 cm^{-1} absorbances can be attributed to polymerisation occurring during the ASPD process,[89,90] Figure 5. 1, Table 5. 4 and Table 5. 5.

The infrared spectrum of liquid IDA monomer include the following absorbances: CH_3 and CH_2 antisymmetric stretching at 2960 cm^{-1} and 2924 cm^{-1}, respectively; CH_3 and CH_2 symmetric stretching at 2870 cm^{-1} and 2860–2830 cm^{-1}, respectively; C=O stretching at 1727 cm^{-1}; C=C stretching at 1632 cm^{-1}; $-CH_2-$ stretching at 1463 cm^{-1}; $=CH_2$ bending at 1402 cm^{-1}; $-C(CH_3)$ symmetric bending at 1377 cm^{-1}; and C–O stretching at 1260 cm^{-1} and 1181 cm^{-1}. These absorbances were also found for the ASPD poly(IDA) coating infrared spectrum, however the disappearance of carbon–carbon double bond stretch at 1632 cm^{-1} and $=CH_2$ bending at 1402 cm^{-1}

absorbances can be attributed to polymerisation occurring during the ASPD process,[89,90] Figure 5. 1, Table 5. 4 and Table 5. 5.

Infrared absorption spectra for 2% w/v ASPD Fe-CTAC/HEMA, Cu-CTAC/HEMA, and Cu-amine/IDA coatings, did not show any significant differences with their corresponding ASPD poly(HEMA) and ASPD poly(IDA) coatings, Figure 5. 1 and Table 5. 4. This is probably due to the low (2% w/v) metallosurfactant concentration in the precursor mixture, and the ATR infrared characterisation is not a sensitive surface analysis (depth penetration of 0.5–5 µm[91]). However, these metallosurfactant powder precursors and their corresponding metallosurfactant / polymer coatings are visually different in colour (i.e. metallosurfactants colours for ASPD coatings were: orange Fe-CTAC, yellow Cu-CTAC,[60] and blue Cu-amine[61]).

5.3.2. Water Contact Angle

Static water contact angle measurements indicated different levels of wettability for the ASPD coatings deposited onto silicon wafers. 2% w/v ASPD Fe-CTAC/HEMA and Cu-CTAC/HEMA coatings showed hydrophilic behaviour (~30°), whereas the 2% w/v ASPD Cu-amine/IDA coatings are hydrophobic (~105°), Table 5. 6.

Table 5. 6: Static water contact angle values for silicon wafer substrate and ASPD coatings. Contact angle measurements performed by A. W. Ritchie and I. Castaneda-Montes, accordingly.

Surface	Water Contact Angle / °
Uncoated silicon wafer	36 ± 4
ASPD poly(HEMA)	51 ± 3
2% w/v ASPD Fe-CTAC/HEMA	32 ± 5
2% w/v ASPD HEMA/Cu-CTAC	30 ± 4
ASPD poly(IDA)	98 ± 4
2% w/v ASPD Cu-amine/IDA	105 ± 4

5.3.3. Scanning Electron Microscopy

SEM cross-section analysis of ASPD coated silicon wafers at different points along the sample was used to estimate thickness and deposition rate, by relating the measured thickness with the deposition time, for each ASPD coating type, Table 5. 7.

Table 5. 7: Thickness and deposition rate for ASPD coatings on silicon wafers.

Surface	Thickness / μm	Deposition Rate / μm min⁻¹
ASPD poly(HEMA)	5.6 ± 3.2	0.7 ± 0.3
2% w/v ASPD Fe-CTAC/HEMA	22.3 ± 5.0	2.5 ± 0.6
2% w/v ASPD Cu-CTAC/HEMA	29.4 ± 8.1	3.0 ± 0.9
IDA	8.4 ± 2.9	1.0 ± 0.3
2% ASPD Cu-amine/IDA	9.9 ± 4.7	1.5 ± 0.8

Furthermore, the surface topography of untreated and treated samples was also analysed by SEM. The untreated non-woven polypropylene cloth fibres exhibited a smooth appearance. The ASPD poly(HEMA) and poly(IDA) coatings on non-woven polypropylene cloth, showed a very similar appearance, whereas the 2% w/v ASPD metallosurfactant/polymer coatings (i.e., Fe-CTAC/HEMA, Cu-CTAC/HEMA, and Cu-amine/IDA) all showed a roughened surface topography attributed to the presence of solid metallosurfactant particles within the polymeric matrix, Figure 5. 2.
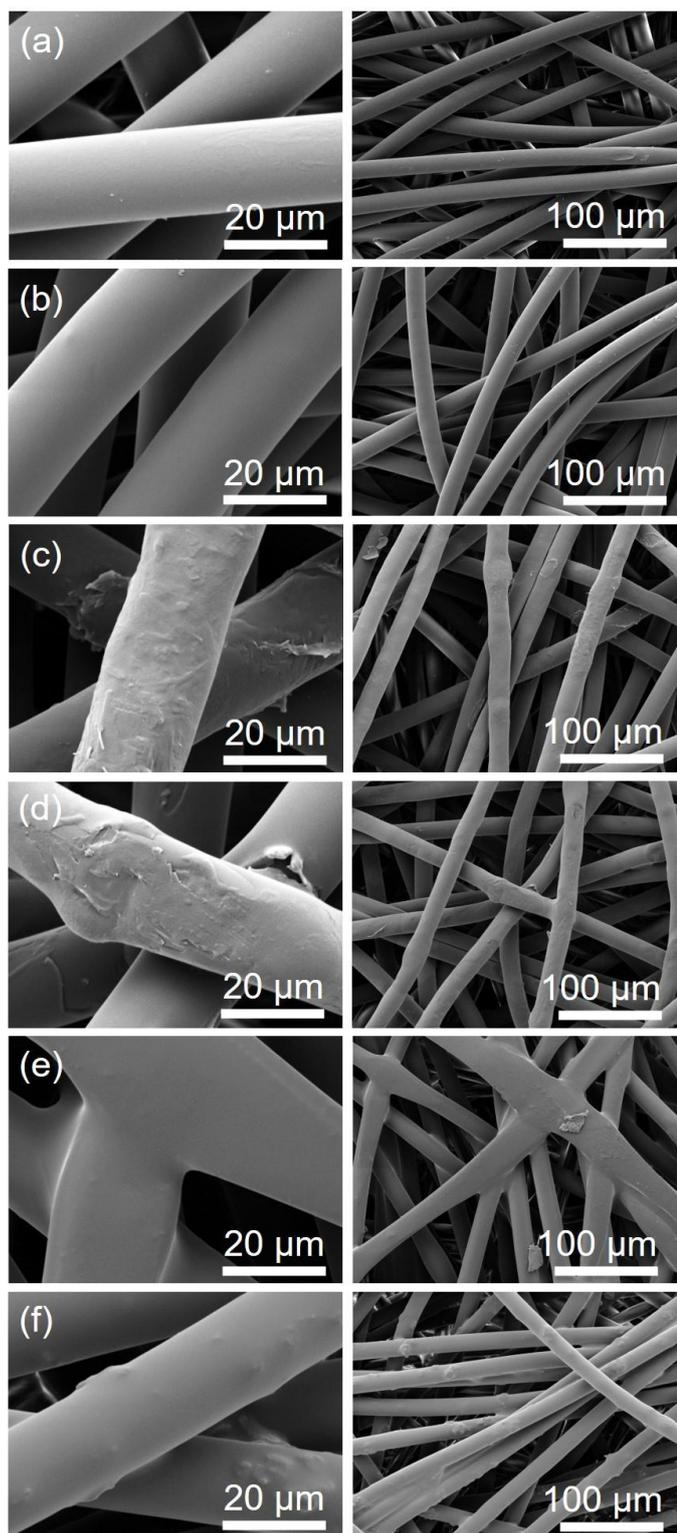
Figure 5. 2: SEM images non-woven polypropylene cloth: (a) untreated; (b) ASPD poly(HEMA); (c) 2% w/v ASPD FeCTAC/HEMA; (d) 2% w/v ASPD CuCTAC/HEMA; (e) ASPD poly(IDA); and (f) 2% w/v ASPD Cu-amine/IDA coatings.

5.3.4. Antibacterial Activity

ASPD (metallosurfactant/polymer) coatings display highly-efficient antibacterial activities against *E. coli* and *S. aureus*, Figure 5. 3. Antibacterial activities of the optimum 2% w/v ASPD (metallosurfactant/polymer) coatings exceed the minimal clinical standard (log reduction > 3),[92] against wild-type *E. coli* and *S. aureus* following exposure of 1–10 min at room temperature. 2% w/v ASPD Fe-CTAC/HEMA and Cu-CTAC/HEMA coatings completely killed *S. aureus* from 1 min, however these coatings were about 2.5 times thicker than ASPD Cu-amine/IDA coatings, Table 5. 7. 1% w/v ASPD (metallosurfactant/polymer) coatings were found to be less effective. Control antibacterial tests for ASPD poly(HEMA) and poly(IDA) coatings did not show antibacterial activity when tested against *E. coli* wild-type and *S. aureus* for 16 h.

Figure 5. 3: Antibacterial activity of 2% w/v ASPD (metallosurfactant/polymer) coatings on PP substrate against (a) *E. coli*, and (b) *S. aureus* at 1 min, 2 min, 5 min, and 10 min at room temperature, and 4 h and 16 h at 30 °C interacting times and temperature. At different interaction times, ■, ●, and ▲ denote 100% antibacterial efficiency of 2% w/v ASPD Fe-CTAC/HEMA, Cu-CTAC/HEMA, and Cu-amine/IDA coatings, respectively. Appendix 1: Table A1. 1.
.

5.3.4.1. Sensitivity of *E. coli* mutant strains

In order to probe the antimicrobial mechanism, *E. coli* mutants with defects in different cellular activities were examined. It was anticpated that increased sensitivity of strains carrying such defects would provide insight into the cellular targets of the metallosurfactants.. From the *E. coli* wild-type studies, 2 min was chosen as the optimum interaction time for the mutant strain experiments due to the significant log reduction rate and the differences that could be observed among the results from each sample, whilst these differences could not be differentiated readily at shorter or longer interaction times. For example, for a 1 min interaction period, the bacterial log reduction rate was insufficient to differentiate from untreated cloths samples. In contrast, for longer times (i.e., above 5 min), 2% w/v ASPD Cu-CTAC/HEMA coated samples showed high antibacterial activity, killing all bacteria; thus, not allowing to compare to the antibacterial activity of 2% w/v ASPD Fe-CTAC/HEMA and Cu-amine/IDA coated samples towards *E. coli* mutant strains, that could be useful for the experiments with mutants which would likely show increased susceptibility.

Each mutant strain has a slightly different functionality, Table 5. 3. For the case of 2% w/v ASPD (metallosurfactant/polymer) coatings, the most striking result is with *rfaC* which displays increased sensitivity with the Fe-CTAC/HEMA and Cu-CTAC/HEMA coatings but not Cu-amine/IDA. The *E. coli rfaC* gene encodes a function for lipopolysaccharide core biosynthesis and O-antigen attachment but is defective in the addition of heptose to the lipid A acceptor and thus accumulates much more of the donor substrate than the wild-type.[93,94] There is a modest effect with the *lpxL* strain, with 2% w/v ASPD Fe-CTAC/HEMA and Cu-CTAC/HEMA coatings, which also fits with increased sensitivity when the outer membrane is compromised. However, it is not possible to readily distinguish membrane damage being the primary problem or a combination of membrane damage and increased permeability of metal ions and reactive oxygen species, but it is a good clue to what is happening. The *mutM* mutant shows a slight increase in sensitivity to 2% w/v ASPD Fe-CTAC/HEMA coating. Other mutants are generally

similar to the wild-type for 2% w/v ASPD Fe-CTAC/HEMA and Cu-CTAC/HEMA coatings, Figure 5. 4.

In contrast, some mutants are distinctly more resistant to the 2% w/v ASPD Cu-Amine/IDA coating, including *copA*, *cueO*, *fepA*, *sodA*, and *sodB*. It is likely that the hydrophobic behaviour of the 2% ASPD Cu-amine/IDA coating affects bacterial–coating interaction, whereas for the 2% w/v ASPD Fe-CTAC/HEMA and Cu-CTAC/HEMA coatings have hydrophilic behaviour which facilitates the bacterial–coating interaction, Figure 5. 4. It is not clear why these mutants, affected in metal homeostasis and oxidative damage tolerance, all tend to show improved survival, although it may indicate toxicity associated with reactive oxygen species production.
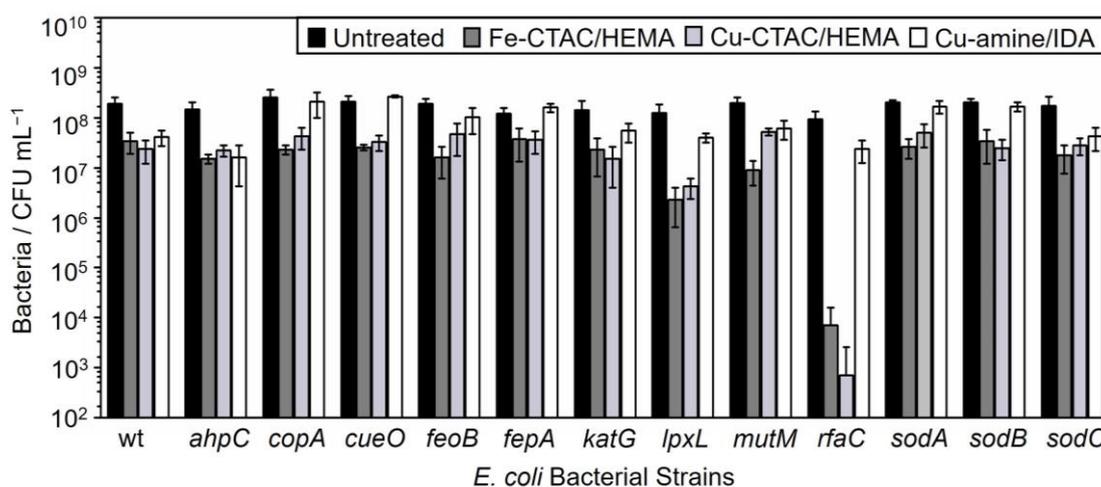
Figure 5. 4: Antibacterial activity for 2 min contact time, for ASPD Fe-CTAC/HEMA, Cu-CTAC/HEMA, and Cu-amine/IDA coatings on PP substrate, against wild-type *E. coli* and different mutant strains; wt denotes *E. coli* wild-type strain. Appendix 1: Table A1. 2.

5.3.4.2. Recycling Results

Recycling experiments were performed for 2% w/v ASPD (metallosurfactant/polymer) coatings, Figure 5. 5. The results show that the 2% w/v ASPD Cu-amine/IDA coatings have better recycling responses against *E. coli*, whilst 2% w/v ASPD Fe-CTAC/HEMA and Cu-CTAC/HEMA coatings have a better recycling rate when interacting with *S. aureus*, and

are expected to leach higher amounts of metallosurfactant material since they are about 2.5 times thicker than 2% w/v ASPD Cu-amine/IDA coatings, Table 5. 7.
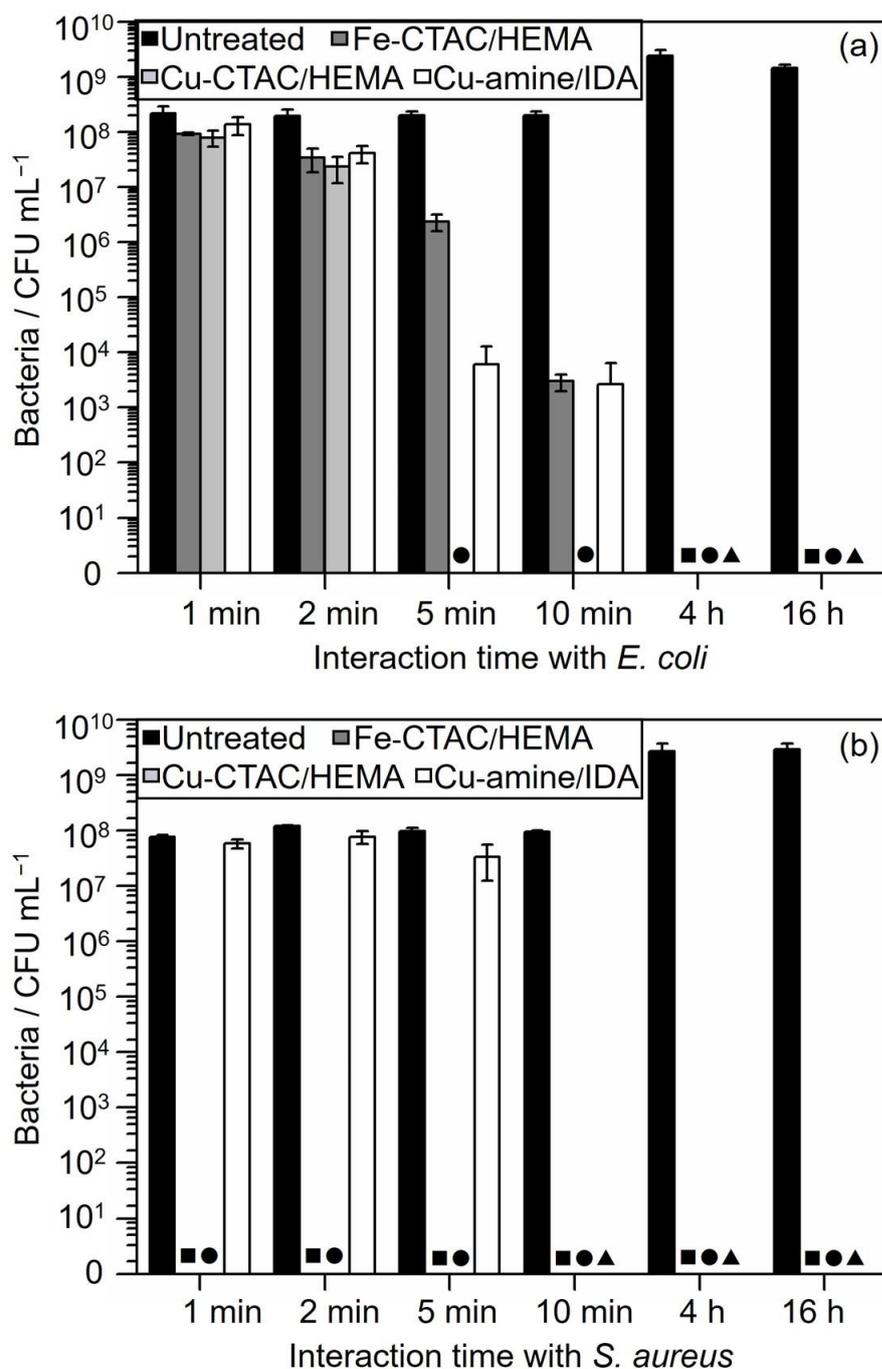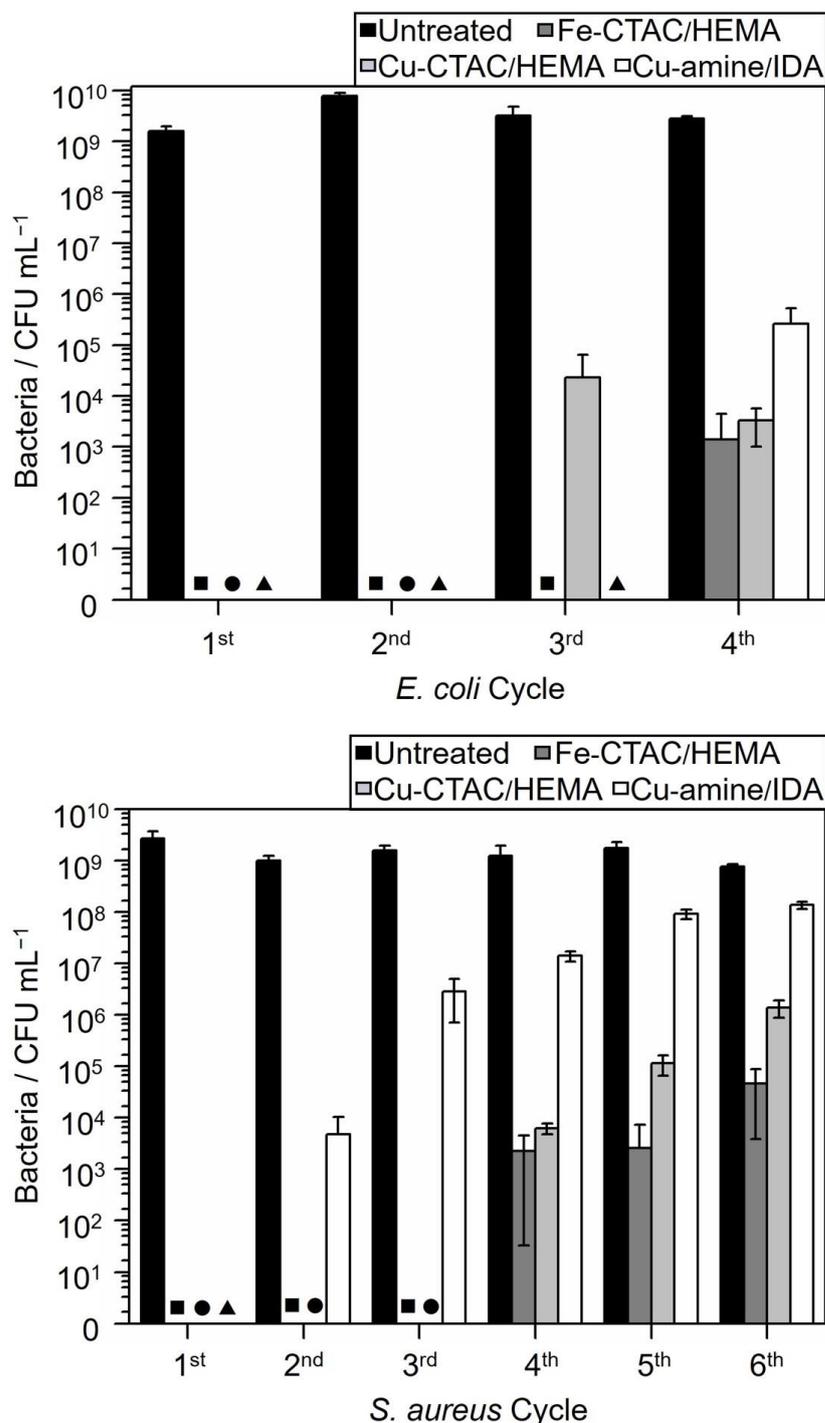

Figure 5. 5: Recycling test for 2% w/v ASPD (metallosurfactant/polymer) coatings on PP substrate against (a) *E. coli* and (b) *S. aureus*. ■, ●, and ▲ denote 100% antibacterial efficiency of 2% w/v ASPD Fe-CTAC/HEMA, Cu-CTAC/HEMA, and Cu-amine/IDA coatings, respectively. Appendix 1: Table A1. 3 and Table A1. 4.

5.4. Discussion

The fabrication of 2% w/v ASPD (metallosurfactant/polymer) coatings yielded excellent antibacterial activity against *E. coli* and *S. aureus*, where the metallosurfactants Fe-CTAC, Cu-CTAC, and Cu-amine, acted as antibacterial agents in mixtures with HEMA and IDA precursors, Table 5. 2.

Infrared characterisation showed that the reactive plasma species present when the metallosurfactant–polymer suspension droplets were exposed to the electrical discharge, activate the precursor C=C vinyl group in the plasma phase and continue the deposition of the plasma metallosurfactant–polymer coating onto the substrate surface via conventional free-radical polymerisation. On the other hand, SEM analysis confirmed this approach is suitable to treat textile substrates, ensuring an even coating of the fibres, tuning their chemical and physical features without massively modifying the cloth at the microscale, Figure 5. 2. It is likely that the metallosurfactants interacted with the host polymer matrix through hydrophilic and hydrophobic interactions forming random micelles during the atomisation.

High antibacterial efficacy was found for metallosurfactant–polymer coatings prepared at the optimum concentration of 2% w/v metallosurfactant in mixture with HEMA or IDA precursors, Table 5. 2. This antibacterial activity was tested against Gram-positive *S. aureus* and Gram-negative *E. coli*, where all three (metallosurfactant/polymer) coatings displayed antibacterial activity (log reduction > 3[95,96]) within a few minutes of exposing them to the testing bacteria, Figure 5. 3. Furthermore, these 2% w/v ASPD (metallosurfactant/polymer) coatings showed good reusability after rinsing samples for 1 min in water.

The antibacterial activity of 2% w/v ASPD (Cu-amine/IDA) coatings is attributed to the Cu-amine metallosurfactant being released when exposing the coating to the liquid bacterial culture, where the released metallosurfactant component interacts with bacteria causing bacterial cell wall disruption and bacterial cell death. Supporting this, there are reports of metallosurfactants in microemulsion displaying antibacterial activity by

154

disrupting bacterial cell membrane, damaging DNA, and provoking bacteria lysis due to the synergistic interaction of the corresponding metal ion and surfactant chain components in the metallosurfactant complex.[61,97] Furthermore, surfactant alkyl chain length is reported to have an effect in the antibacterial activity of alkylamines,[98] due to hydrophobic interactions taking place between the alklyl chains and hydrophobic lipids and proteins composing the bacterial cell wall, causing additional bacterial cell membrane damage, and consequent bacterial cell death.[20,99] These hydrophobic interactions between alkyl chains and bacteria walls tend to physically affect more to *E. coli* than *S. aureus* because of the thinner hydrophobic cell wall of *E. coli*.[20,100–103] This observation is in agreement with the present antibacterial test results, Figure 5. 3. Overall, features present in this hydrophobic antibacterial material allow both, killing and repelling of bacteria.

For the case of 2% w/v ASPD hydrophilic Cu-CTAC/HEMA and Fe-CTAC/HEMA coatings, it is suggested that the cationic metallosurfactants, Cu-CTAC and Fe-CTAC, are released from the polymeric matrix and interact with bacteria when the coating is in contact with liquid bacterial culture. However, in this case, Cu-CTAC and Fe-CTAC are cationic surfactants, whose antibacterial activity is mainly attributed to electrostatic interactions between positive charged metallosurfactants and the negatively charged bacteria cell wall.[60] Furthemore, copper ions present in Cu-CTAC metallosurfactant complex are capable of generating reactive oxygen species which would damage the outer bacterial cell membrane, and for the case of *E. coli*, interact with the periplasmic space causing oxidative stress, faster membrane disruption compared with Gram-positive bacterial membranes, and bacterial cell death, [97,104] which is in agreement with the faster bacterial reduction of *S. aureus* in this work, Figure 5. 3.

Given the general characteristics of ASPD metallosurfactant–polymer coatings, the metallosurfactant was hosted in the polymeric matrix of the coating, and released when in contact with liquid, suggesting a uncontrolled leaching behaviour. This could explain the good but limited reusability of the 2% w/v ASPD (metallosurfactant/polymer) coatings after continuous rinsing in water.

However, looking at each particular 2% w/v ASPD (metallosurfactant/polymer) coating, there are specific characteristics that may have an impact on their individual antibacterial activities. The first to consider are the chemical characteristics of each metallosurfactant–precursor mixture—their corresponding active metal ion,[104] surfactant alkyl chain, and base monomer precursor; and second, their physical features such as wettability and thickness, which in consequence affect interaction with liquid bacterial solution on the surface, and the leaching rate/load of metallosurfactant component when exposed to liquid media.

In the *E. coli* mutant tests, 2% w/v ASPD Fe-CTAC/HEMA, Cu-CTAC/HEMA, and Cu-amine/IDA coatings were compared against the *E. coli* mutant strains to provide insight into their possible antibacterial mechanism, Table 5. 3. From this, hydrophilic 2% w/v ASPD (metallosurfactant/HEMA) coatings did show a considerable log reduction of *E. coli rfaC* compared to the wild-type strain, suggesting bacterial membrane damage.[105] In contrast, the hydrophobic 2% w/v ASPD Cu-amine/IDA coatings several mutants showed improved resistance, however this may be due to the short time that the coatings were exposed to liquid bacterial cultures. The experiment was performed in order to show a comparison among the three coatings. However, wettability could affect the results obtained from the hydrophobic coatings and limit what can be concluded concerning the antibacterial mechanism. The test should be repeated with an alternative interaction time so bacterial mutant strains could be compared accurately under hydrophobic conditions; furthermore, 2% w/v ASPD (metallosurfactant/HEMA) coatings were considerably thicker than 2% w/v ASPD Cu-amine/IDA coatings, Table 5. 7, meaning that a higher load of metallosurfactant is released when in contact with liquid bacterial culture.

Nevertheless, in terms of the metallosurfactants chemistry, Scheme 5. 2, Fe-CTAC and Cu-CTAC complexes are cationic metallosurfactants whose positive charge is known to electrostatically interact with negatively charged bacterial cell walls,[60,106] while the hydrophilic poly(HEMA) matrix where they are hosted offers ideal conditions for the bacteria to spread on the whole coating, Table 5. 6. This is in good agreement with results obtained from the mutant experiments where *E. coli rfaC* displayed greater sensitivity to these

coatings in comparison with other mutant strains, Figure 5. 4. On the other hand, Cu-amine complex is a non-ionic metallosurfactant whose alkyl amine chains undertake hydrophobic interactions with bacterial cell wall components and damage it,[98] while the hydrophobic nature of poly(IDA) polymeric matrix, where Cu-amine is hosted, does not allow the liquid bacterial culture to spread evenly on the surface, Table 5. 6. Therefore, it would be appropriate to perform further tests for each type of coating to get an accurate comparison among mutant strains, rather than among the coatings.

5.5. Conclusions

ASPD metallosurfactant/polymer coatings on polypropylene cloth display antibacterial activity against Gram-positive *Staphylococcus aureus* and Gram-negative *Escherichia coli* bacteria. A correlation is found between the concentration of metal ions contained in the metallosurfactant molecules and highly efficient antibacterial activity (log reduction > 9). The antibacterial coatings presented in this chapter, can be used multiple times by rising them in water. However, further studies on the cytotoxicity against healthy mammalian cells should be made to determine the usability of these antibacterial coatings, because biomedical applications may be limited if high toxicity displayed against bacterial cells also occurs with human cell membranes.

5.6. References

(1) Scrimin, P.; Tecilla, P.; Tonellato, U.; Vendrame, T. Aggregate Structure and Ligand Location Strongly Influence Cu^{2+} Binding Ability of Cationic Metallosurfactants. *J. Org. Chem.* **1989**, *54*, 5988–5991.

(2) Griffiths, P. C; Fallis, I. A.; Chuenpratoom, T.; Watanesk, R. Metallosurfactants: Interfaces and Micelles. *Adv. Colloid Interface Sci*. **2006**, *122*, 107–117.

(3) Owen, T.; Butler, A. Metallosurfactants of Bioinorganic Interest: Coordination‐Induced Self Assembly. *Coord. Chem. Rev*. **2011**, *255*, 678–687.

(4) Lemire, J. A.; Harrison, J. J.; Turner, R. J. Antimicrobial Activity of Metals: Mechanisms, Molecular Targets and Applications. *Nat. Rev. Microbiol.* **2013**, *11*, 371–384.

(5) Vaidya, M. Y.; McBain, A. J.; Butler, J. A.; Banks, C. E.; Whitehead, K. A. Antimicrobial Efficacy and Synergy of etal Ions Against *Enterococcus faecium*, *Klebsiella pneumoniae* and *Acinetobacter baumanii* in Planktonic and Biofilm Phenotypes. *Sci. Rep.* **2017**, *7*, 5911.

(6) Akhidime, I. D.; Saubade, F.; Benson, P. S.; Butler, J. A.; Oliver, S.; Kelly, P.; Verran, J.; Whitehead, K. A. The Antimicrobial Effect of Metal Substrates on Food Pathogens. *Food Bioprod. Process.* **2019**, *113*, 68–76.

(7) Ishida, T. Mechanism of Antibacterial Activities of Cu(II) Ions Against *Staphylococcus aureus* and *Escherichia coli* on The Ground of Results Obtained from Dilution Medium Method. *Virol. Immunol. J.* **2017**, *1*, 000117.

(8) Vimbela, G. V.; Ngo, S. M.; Fraze, C.; Yang, L.; Stout, D. A. Antibacterial Properties and Toxicity from Metallic Nanomaterials. *Int. J. Nanomed.* **2017**, *12*, 3941–3965.

(9) Brycki, B.; Koziróg, A.; Kowalczyk, I.; Pospieszny, T.; Materna, P.; Marciniak, J. Synthesis, Structure, Surface and Antimicrobial Properties of New Oligomeric Quaternary Ammonium Salts with Aromatic Spacers. *Mol.* **2017**, *22*, 1810.

(10) Falk, N. A. Surfactants as Antimicrobials: A Brief Overview of Microbial Interfacial Chemistry ans Surfactant Antimicrobial Activity. *J. Surfactants Deterg.* **2019**, *22*, 1119–1127.

(11) Zhang, S.; Ding, S.; Yu, J.; Chen, X.; Lei, Q.; Fang, W. Antibacterial Activity *in vitro* Cytotoxicity, and Cell Cycle Arrest of Gemini Quaternary Ammonium Surfactants. *Langmuir* **2015**, *31*,12161–12169.

(12) Zhou, C.; Wang, F.; Chen, H.; Li, M.; Qiao, F.; Liu, Z.; Hou, Y.; Wu, C.; Fan, Y.; Liu, L.;Wang, S.; Wang, Y. Selective Antimicrobial Activities and Action Mechanism of Micelles Self-Assembled by Cationic Oligomeric Surfactants. *ACS Appl. Mater. Interfaces* **2016**, *8*, 4242–4249.

(13) Zhou, C.; Wang, D.; Cao, M.; Chen, Y.; Liu, Z.; Wu, C.; Xu, H.; Wang, S.; Wang, Y. Self-Aggregation, Antibacterial Activity, and Mildness of Cyclodextrin/Cationic Trimeric Surfactant Complexes. *ACS Appl. Mater. Interfaces* **2016**, *8*, 30811–30823.

(14) Tobe, S.; Majima, T.; Tadenuma, H.; Suekuni, T.; Sakai, K.; Sakai, H.; Abe, M. Nonionic Surfactants Enhancing Bactericidal Activity at Their Critical Micelle Concentrations. *J. Oleo Sci.* **2015**, *64*, 61–68.

(15) Aiad, I.; Riya, M. A.; Tawfik, S. M.; Abousehly, M. A. Synthesis, Surface Properties and Biological Activity of N, N,N,-Tris(Hydroxymethyl)-2-Oxo-2-(2-(2-(Alkanoyloxy) Ethoxy)Ethoxy) Ethanaminium Chloride Surfactants. *Egypt. J. Pet.* **2016**, *25*, 299–307.

(16) Zhang, L.; Jiao, L.; Zhong, J.; Guan, W.; Lu, C. Lighting Up the Interactions Between Bacteria and Surfactants with Aggregation-Induced Emission Characteristics. *Mater. Chem. Front.* **2017**, *1*, 1829–1835.

(17) Morsi, R. E.; El-Salamony, R. A. Effect of Cationic, Anionic and Non-Ionic Polymeric Surfactantss on the Stability, Photo-Catalytic and Antimicrobial Activities of Yttrium Oxide Nanofluids. *J. Mol. Liq.* **2020**, *297*, 111848.

(18) Liu, K.; Yang, L.; Peng, X.; Gong, H.; Wang, J. Effects of Conventional Surfactans on The Activity of Desifned Antimicrobial Peptide. *Langmuir* **2020**, *36*, 3531–3539.

(19) Azzam, E. M. S.; Zaki, M. F. Surface and Antibacterial Activity of Synthesized Nonionic Surfactant Assembled on Metal Nanoparticles. *Egypt. J. Pet.* **2016**, *25*, 153–159.

(20) Adawy, A. I.; Khowdiary, M. M. Structure and Biological Behaviors of Some Metallo Cationic Surfactants. *J. Surfact. Deterg.* **2013,** *16,* 709–715.

(21) Garg, P.; Kaur, G.; Chaudhary, G. R. Transition Metal Based Single Chained Surfactant: Synthesis, Agglomeration, Aggregation Behaviour and Enhanced Photoluminescence Properties of Fluorescein. *RSC Adv.* **2016**, *6*, 108573–108582.

(22) Garg, P.; Kaur, G.; Chaudhary, G. R. Chromium-Based Metallosurfactants: Synthesis, Physicochemical Characterization and Probing of Their Interactions With Xanthene Dyes. *New J. Chem.* **2018**, *42*, 1141–1150.

(23) Garg, P.; Kaur, G.; Chaudhary, G. R.; Gawali, S. L.; Hassan, P. A. Fabrication of Metalosomes (Metal Contaiining Cationic Liposomes) Using Single Chain Surfactants as a Precursor Via Formation of Inorganic Hybrids. *Phys. Chem. Chem. Phys.* **2017**, *19*, 25764–25773.

(24) Kaur, G.; Garg, P.; Chaudhary, G. R. Role of Manganese-Based Surfactant Towards Solubilization and Photophysical Properties of Fluorescein. *RSC Adv.* **2016**, *6*, 7066–7077.

(25) Sharma, N. K.; Singh, M. Multifunctional Supramolecular Ionic Metallosurfactants (SMIMs) for Antimicrobial, Anticancer and Serum Albumins Binding. *J. Mol Liq.* **2018**, *263*, 463–471.

(26) Sharma, N. K.; Singh, M.; Bhattarai, A. Hydrophobic Study of Increasing Alkyl Chain Length of Platinum Surfactant Complexes: Synthesis, Characterization, Micellization, Thermodynamics, Thermogravimetrics and Surface Morphology. *RSC Adv.* **2016**, *6*, 90607–90623.

(27) Sharma, N. K.; Singh, M. New Class of Platinum Based Metallosurfactant: Synthesis, Micellization, Surface, Thermal Modelling and *in vitro* Biological Properties. *J. Mol. Liq.* **2018**, *268*, 55–65.

(28) Chandar, S.C. N.; Santhakumar, K.; Arumugham, M. N. Metallosurfactant Schiff Base Cobalt (III) Coordination Complexes, Synthesis, Characterization, Determination of CMC Values and Biological Activities. *Transition Met. Chem.* **2009**, *34*, 841–848.

(29) Badawi, A. M.; Zakhary, N. I.; Morsy, S. M. I.; Sabry, G. M.; Fouad, M. M.; Mousa, A. M. Biochemical Study on the Effect of Metallo-Surfactant and Its Loaded Nano-Analogue as Anticancer Drug. *J. Am. Sci.* **2012**, *8*, 763–772.

(30) Chandar, S. C. N.; Sangeetha, D.; Arumugham, M. N. Synthesis, Structure, CMC Values, Thermodynamics of Micellization, Steady-State Photolysis and Biological Activities of Hexadecylamine Cobalt(III) Dimethyl Glyoximato Complexes. *Transition Met. Chem.* **2011**, *36*, 211–216.

(31) Chaudhary, G. R.; Singh, P.; Kaur, G.; Mehta, S. K.; Kumar, S.; Dilbaghi, N. Multifaceted Approach for the Fabrication of Metallomicelles and Metallic Nanoparticles Using Solvophobic Bisdodecylaminepalladium (II) Chloride as Precursor. *Inorg. Chem.* **2015**, *54*, 9002−9012.

(32) Sasikala, K.; Arunachalam, S. Antimicrobial Activity, Spectral Studies and Micellar Properties of Some Surfactant-Cobalt(III) Complexes. *Chem. Sci. Trans.* **2013,** *2,* S157–S166.

(33) Kumaraguru, N.; Santhakumar, K. Synthesis, Characterization, Critical Micelle Concentration Determination, and Antimicrobial Studies of Some Complexes of Chromium(III) Metallosurfactants. *J. Coord. Chem.* **2009,** *62,* 3500–3511.

(34) Hawllett, A. J.; Placet, E.; Prieux, R.; McCafferty, D.; Platts, J. A.; Lloud, D.; Isaacs, M.; Hayes, A. J.; Coles, S. J.; Pitak, M. B.; Marchant, S.; Marriott, S. N.; Allemann, R. K.; Dervisi, A.; Fallis, I. A. Exploring The Cellular Uptake and Localisation of Phosphorescent Rhenium Fac-Tricarbonyl Metallosurfactants as a Function of Lipophilicity. *Dalton Trans.* **2018**, *47*, 14241–14253.

(35) Gonawala, S.; Leopoldino, V. R.; Kpogo, K.; Verani, C. N. Langmuir–Blodgett Films of Salophen-Based Metallosurfactans as Surface Pretreatment Coatings for Corrosion Mitigation. *Chem. Commun.* **2016**, *52*, 11155–11158.

(36) Taira, T.; Yanagimoto, T.; Sakai, K.; Sakai, H.; Endo, A.; Imura, T. Self-Assembling Properties of An N-Heterocyclic Carbene-Based Metallosurfactant: Pd-Coordination Induced Formation of Reactive Interfaces in Water. *J. Oleo Sci.* **2018**, *67*, 1107–1115.

(37) Hafiz, A. A. Metallosurfactants of Cu(II) and Fe(III) Complexes as Catalysts for The Destruction of Paraoxon. *J. Surfactants Deterg.* **2005**, *8*, 359–363.

(38) Ghirlanda, G. Self-Assembled Monolayers of Cu(II) Metallosurfactants on GC and HOPG. *Langmuir* **1996**, *12*, 3695–3701.

(39) Bowers, J.; Danks, M. J.; Bruce, D. W. Surface and Aggregation Behavior of Aqueous Solutions of Ru(II) Metallosurfactants: 1. Micellization of [Ru(Bipy)$_2$(Bipy')][Cl]$_2$ Complexes. *Langmuir* **2003**, *19*, 292–298.

(40) Kaur, N.; Kaur, G.; Bhalla, A.; Dhau, J. S., Chaudhary, G. R. Metallosurfactant Based Pd-Ni Alloy Nanoparticles as Proficient Catalyst in Mizoroki Heck Coupling Reaction. *Green Chem.* **2018**, *20*, 1506–1514.

(41) Pradeep; Kaur, G.; Chaudhary, G. R.; Batra, U. Investigating Affordable Cobalt Based Metallosurfactants as an Efficient Electrocatalyst for Hydrogen Evolution Reaction. *J. Colloid Interface Sci.* **2020**, 598–607.

(42) Kagalwala, H. N.; Chirdon, D. N.; Mills, I. N.; budwal, N.; Bernhard, S. Light-Driven Hydrogen Generation from Microemulsions Using Metallosurfactant Catalyst and Oxalic Acid. *Inorg. Chem.* **2017**, *56*, 10162–10171.

(43) Do Pim, W. D.; Ribeiro-Santos, T. A.; Jardim, I. S.; De Castro, M. C. M., Braga, A. H.; Do Nascimento, G. M.; Binatti, I.; Stumpf, H. O.; Lorençon, E. Bistable Copper(II) Metallosurfactant as Molecular Machine for The Preparation of Hybrid Silica-Based Porous Materials. *Mater. Des.* **2018**, *160*, 876–885.

(44) Hondow, N.; Harowfield, J.; Koutsantonis, G.; Nealon, G.; Saunders, M. Metallosurfactants in The Preparation of Mesoporous Silicas. *Microporous Mesoporous Mater.* **2012**, *151*, 264–270.

(45) Berro, Y.; Gueddida, S.; Bouizi, Y.; Bellouard, C.; Bendeif, E.-E.; Gansmuller, A.; Celzard, A.; Fierro, V.; Ihiawakrim, D.; Ersen, O.; Kassir, M.; Hassan, F. E. H.; Lebegue, S.; Badawi, M.; Canilho, N.; Pasc, A. Imprinting Isolated Single Iron Atoms onto Mesoporous Silica by Templating with Metallosurfactants. *J. Colloid Interface Sci.* **2020**, *573*, 193–203.

(46) Chen, Y.; Zhu, Q.; Cui, X.; Tang, W.; Yang, H.; Yuan, Y.; Hu, A. Preparation of Highly Efficient MRI Contrast Agents through Complexation of Cationic Gd^{III}-Containing Metallosurfactant with Biocompatible Polyelectrolytes. *Chem. Eur. J.* **2014**, *20*, 12477–12482.

(47) Gong, P.; Chen, Z.; Chen, Y.; Wang, W.; Wang, X.; Hu, A. High-Relaxivity MRI Contrast Agents Prepared from Miniemulsion Polymerization Using Gadolinium(III)-based Metallosurfactants. *Chem. Commun.* **2017**, *47*, 4240–4242.

(48) Xu, K.; Wang, M.; Tang, W.; Ding, Y.; Hu, A. Flash Nanoprecipitation with Gd(III)-Based Metallosurfactants to Fabricate Polylactic Acid Nanoparticles as Highly Efficient Contrast Agents for Magnetic Resonance Imaging. *Chem. - Asian J.* **2020**, *15*, 2475–2479.

(49) Zhu, Q.; Pan, F.; Tian, Y.; Tang, W.; Yuan, Y.; Hu, A. Facile Synthesis of Gd(III)-Metallosurfactant Functionalized Carbon Nanorods with High Relaxivity as Bimodal Imaging Probes. *RSC Adv.* **2016**, *6*, 29441–29447.

(50) Parera, E.; Marín-García, M.; Pons, R.; Comelles, F.; Suades, J.; Barnadas-Rodríguez, R. Supramolecular Arrangement of Molybdenum Carbonyl Metallosurfactants with CO-Releasing Properties. *Organometallics* **2016**, *35*, 484–493.

(51) Trickett, K.; Xing, D.; Eastoe, J.; Enick, R.; Mohamed, A.; Hollamby, M. J.; Cummings, S.; Rogers, S. E.; Heenan, R. K. Hydrocarbon Metallosurfactants for CO_2. *Langmuir*, **2010**, *26*, 4732–4737.

(52) Abdosalam, K. R.; Mohamed, A. Synthesis and Characterisation of Metallosurfactants as Carbon Dioxide Viscosity Modifier. *EDUCATUM JSMT* **2017**, *4*, 16–28.

(53) Chu, B W.-K.; Yam, V W.-W. Synthesis, Characterization, Langmuir–Blodgett Film-forming Properties, and Second-Harmonic-Generation Studies of Ruthenium(II) Complexes with Long Hydrocarbong Chains. *Inorg. Chem.* **2001**, *40*, 3324–3329.

(54) Bowers, J.; Danks, M. J.; Bruce, D. W. Surface Aggregation Behavior of Aqueous Solutions of Ru(II) Metallosurfactants. 2. Adsorbed Films of [Ru(BIpy)$_2$(Bipy')][Cl]$_2$ Complexes. *Langmuir* **2003**, *19*, 299–305.

(55) Donnio, B. Lyotropic Metallosmesogens. *Curr. Opin. Colloid Interface Sci.* **2002**, *7*, 371–394.

(56) Borras, J.; Mesa, V., Suades, J.; Barnadas-Rodríguez, R. Direct Synthesis of Rhenium and Technetium-99m Metallosurfactants by a Transmetallation Reaction of Lipophilic Groups: Potential Applications in the Radiolabeling of Liposomes. *Langmuir* **2020**, *36*, 1993–2002.

(57) Kaur, R.; Mehta, S. K. Self Aggregating Metal Surfactant Complexes: Precursors for Nanostructures. *Coord. Chem. Rev.* **2014**, *262*, 37–54.

(58) Kaur, N.; Sood, A.; Bhasin, K. K.; Kaur, G.; Bhalla, A.; Dhau, J. S.; Chaudhary, G. R. Metallosurfactants Derived Pd-NiO Nanocomposite for Remediation of Nitrophenol in Water. *J. Mol. Liq.* **2019**, *288*, 111018.

(59) Mazumder, A.; Chowdhury, Z.; Sen, D.; Bhattacharjee, C. Study on Application of Novel Synthesized Silver Metallosurfactant for Membrane Cleaning. In *Advances in Bioprocess Engineering and Technology. Lecture Notes in Bioengineering*. Springer, Singapore: 2021.

(60) Garg, P.; Kaur, G.; Chaudhary, G. R.; Kaur, S.; Gawali, S. L.; Hassan, P. A. Investigating the Structural Integrity of Bovine Serum Albumin in Presence of Newly Synthesized Metallosurfactants. *Colloids Surf., B* **2018**, *164*, 116–124.

(61) Kaur, G.; Dogra, V.; Kumar, R.; Kumar, S.; Bhanjana, G.; Dilbaghi, N.; Singhal, N. K. DNA Interaction, Anti-Proliferative Effect of Copper Oxide Nanocollids

Prepared from Metallosurfactant Based Microemulsions Acting as Precursor, Template and Reducing Agent. *Int. J. Pharm.* **2018**, *535*, 95–105.

(62) Aiad, I.; Ahmed, M. H. M.; Hessein, A.; Ali, M. Preparation, Surface, and Biological Activities of Some Novel Metallosurfactants. *J. Disper. Sci. Technol.* **2012**, *33*, 1144–1153.

(63) Kaur, G.; Garg, P.; Kaur, B.; Chaudhary, G. R.; Kumar, S.; Dilbaghi, N.; Gawali, S. L. Cationic Double Chained Metallosurfactants: Syntheis, Aggregation, Cytotoxicity, Antimicrobial Activity, and Their Impact on the Structure of Bovine Serum Albumin. *Soft Matter.* **2018**, *14*, 5306–5318.

(64) Hafiz, A. A. Crystal Structure of Benzyl Triphenyl Phosphonium Chlorometallate: Some Surface and Biological Properties of Their Metallosurfactant Derivatives. *JICS* **2008,** *5,* 106–114.

(65) Negm, N. A.; Farargy, A. F. E; Mohammad, I. A.; Zaki, M. F.; Khowdiary, M. M. Synthesis and Inhibitory Activity of Schiff Base Surfactants Derived from Tannic Acid grassand Their Cobalt (II), Manganese (II) and Iron (III) Complexes Against Bacteria and Fungi. *J. Surfactants Deterg.* **2013,** *16,* 767–777

(66) Loboda, D.; Kozlowski, H.; Rowinska-Zyrek, M. Antimicrobial Peptide–Metal Ion Interactions – A Potential Way of Activity Enhancement. *New. J. Chem.* **2018**, *42*, 7560–7568.

(67) Kaur, G.; Singh, P.; Mehta, S. K.; Kumar, S.; Dilbaghi, N.; Chaudhary, G. R. A Facile Route for the Syntheis of Co, Ni, and Cu Metallic Nanoparticles with Potential Antimicrobial Activity Using Novel Metallosurfactants. *Appl. Surf. Sci.* **2017**, *404*, 254–262.

(68) Tawfik, S. M.; Hefni, H. H. Synthesis and Antimicrobial Activity of Polysaccharide Alginate Derived Cationic Surfactant–Metal(II) Complexes. *Int. J. Biol. Macromol.* **2016,** *82,* 562–572.

(69) Kaur, G.; Kumar, S.; Dilbaghi, N.; Bhanjana, G.; Guru, S. K.; Bhushan, S.; Jaglan, S.; Hassan, P. A.; Aswal, V. K. Hybrid Surfactants Decorated with Copper

Ions: Aggregation Behavior, Antimicrobial Activity and Anti-Proliferative Effect. *Phys. Chem. Chem. Phys.* **2016,** *18,* 23961–23970.

(70) Kaur, G.; Kumar, S.; Dilbaghi, N.; Kaur, B.; Kant, R.; Guru, S. K.; Bhushan, S.; Jaglan, S. Evaluation of Bishexadecyltrimethyl Ammonium Palladium Tetrachloride Based Dual Functional Colloidal Carrier as an Antimicrobial and Anticancer Agent. *Dalton Trans.* **2016,** *45,* 6582–6591.

(71) Badawi, A. M.; Azzam, E. M. S.; Morsy, S. M. I. Surface and Biocidal Activity of Some Synthesized Metallo Azobenzene Isothiouronium Salts. *Bioorg. Med. Chem.* **2006,** *14,* 8661–8665

(72) Badawi, A. M.; Mekawi, M. A.; Mohamed, A. S.; Mohamed, M. Z.; Khowdairy, M. M. Surface and Biological Activity of Some Novel Cationic Surfactants. *J. Surfact. Deterg.* **2007**, *10*, 243–255.

(73) Sasikala, K.; Arunachalam, S. Antimicrobial Activity, Spectral Studies and CMC Determinatioon of Some Surfactant-Copper (II) Complexes. *J. Chem. Bio. Phy. Sci. Sec. A* **2012**, *2*, 708–718.

(74) Gürsoy, M.; Harris, M. T.; Downing, J. O.; Barrientos-Palomo, S. N.; Carletto, A.; Yaprak, A. E.; Karaman, M.; Badyal, J. P. S. Bioinspired Fog Capture and Channel Mechanism Based on the Arid Climate Plant *Salsola crassa*. *Colloids Surf., A* **2017**, *529*, 195–202.

(75) Castaneda-Montes, I.; Ritchie, A. W.; Badyal, J. P. S. Atomised Spray Plasma Deposition of Hierarchical Superhydrophobic Nanocomposite Surfaces. *Colloids Surf., A* **2018**, *558*, 192–199.

(76) Bot, C. T.; Prodan, C. Quantifying the Membrane Potential During *E. coli* Growth Stages. *Biophys. Chem.* **2010**, 146, 133–137.

(77) UniprotKB-P24173 (RFAC_ECOLI). https://www.uniprot.org/uniprot/P24173 (accessed: August 12, 2020).

(78) UniprotKB-P0ACV0 (LPXL_ECOLI). https://www.uniprot.org/uniprot/P0ACV0 (accessed: August 12, 2020).

(79)   UniprotKB-P36649   (CUEO_ECOLI).   https://www.uniprot.org/uniprot/P36649 (accessed: August 12, 2020).

(80)   UniprotKB-Q59385   (COPA_ECOLI).   https://www.uniprot.org/uniprot/Q59385 (accesssed: August 12, 2020).

(81)   UniprotKB-P33650   (FEOB_ECOLI).   https://www.uniprot.org/uniprot/P33650 (accessed: August 12, 2020).

(82)   UniprotKB-P05825   (FEPA_ECOLI).   https://www.uniprot.org/uniprot/P05825 (accessed: August 12, 2020).

(83)   UniprotKB-P05523   (FPG_ECOLI).   https://www.uniprot.org/uniprot/P05523 (accessed: August 12, 2020).

(84)   UniprotKB-P00448   (SODM_ECOLI).   https://www.uniprot.org/uniprot/P00448 (accessed: August 12, 2020).

(85) UniprotKB-P0AGD3 (SODF_ECOLI).   https://www.uniprot.org/uniprot/P0AGD3 (accessed: August 12, 2020).

(86) UniprotKB-P0AGD1 (SODC_ECOLI). https://www.uniprot.org/uniprot/P0AGD1 (accessed: August 12, 2020).

(87)   UniprotKB-P0AE08   (AHPC_ECOLI).   https://www.uniprot.org/uniprot/P0AE08 (accessed: August 12, 2020).

(88)   UniprotKB-P13029   (KATG_ECOLI).   https://www.uniprot.org/uniprot/P13029 (accessed: August 12, 2020).

(89) Lin-Vien, D; Colthup, N. B.; Fateley, W. G.; Grasselli, J. G. *The Handbook of Infrared and Raman Characteristic Frequencies of Organic Molecules*; Academic Press, Inc.: San Diego, 1991.

(90) Bellamy, L. J. *The Infra-Red Spectra of Complex Molecules*; Vol. 2; Chapman and Hall, Ltd.; London, 1975.

(91) Stuart, B. *Infrared Spectroscopy: Fundamentals and Applications*; John Wiley & Sons: Sydney, 2004.

(92) Schoffield, W. C. E.; Badyal, J. P. S. A Substrate-Independent Approach for Bactericidal Surfaces. *ACS Appl. Mater. Interfaces* **2009**, *1,* 2763–2767.

(93) Kadrmas, J. L.; Raetz, C. R. H. Enzymatic Synthesis of Lipopolysaccharide in *Escherichia coli*. *J. Biol. Chem.* **1998**, *273*, 2799–2807.

(94) Schnaitman, C. A.; Klena, J. D. Genetics of Lipopolysaccharide Biosynthesis in Enteric Bacteria. Microbiol. Rev. 1993, 57, 655–682.

(95) FTTS-AA-001 *Specified Requirements of Antibacterial Textiles for General Use*. The Committee for Conformity Assessment of Accreditation and Certification on Functional and Technical Textiles: Taiwan, 2005.

(96) Harrison, J. J.; Turner, R. J.; Ceri, H. Persister Cells, The Biofilm Matrix and Tolerance to Metal Cations in Biofilm and Planktonic *Pseudomonas aeruginosa*. *Environ. Microbiol.* **2005**, *7*, 981–994.

(97) Grass, G.; Rensing, C.; Solioz, M. Metallic Copper as an Antimicrobial Surface. *Appl. Environ. Microbiol.* **2011**, *77*, 1541–1547.

(98) Kosmowska, N.; Łuczak, W.; Gwiazdowska, D.; Michocka, K.; Wieczorek, D. Antibacterial Activity of Chemical Compounds Used as Surfactants. *Current Trends in Commodity Science. Dvelopment and Assessment of Non-Food Products*. Uniwersytet Ekonomiczny w Poznaniu, Wydział Towaroznawstwa, Poznań. 2015.

(99) Kabara, J. J.; Conley, A. J.; Truant, J. P. Relationship of Chemical Structure and Antimicrobial Activity of Alkyl Amides and Amines. *Antimicrob. Agents Chemother.* **1972**, *2*, 492–498.

(100) Tortora, G. J.; Funke, B. R; Case, C. L. *Microbiology An Introduction*, 12th ed.; Pearson Education, Inc.: New York, 2016.

(101) Ljungh, Å.; Yanagisawa, N.; Wadström, T. Using the Principle of Hydrophobic Interaction to Bind and Remove Wound Bacteria. *J. Wound Care* **2006**, *15*, 175–180.

(102) Kaur, G.; Kumar, S.; Kant, R.; Bhanjana, G.; Dibaghi, N.; Guru, S. K.; Bhushan, S.; Jaglan, S. One-Step Synthesis of Silver Metallosurfactnat as an Efficient Antibacterial and Anticancer Material. *RSC Adv.* **2016**, *6*, 57084–57097.

(103) Mai-Prochnow, M.; Clauson, M.; Hong, J.; Murphy, A. B. Gram Positive and Gram Negative Bacteria Differ in Their Sensitivity to Cold Plasma. *Sci. Rep.* **2016**, *6*, 38610.

(104) Solioz, M.; Abicht, H. K.; Mermod, M.; Mancini, S. Response of Gram-Positive Bacteria to Copper Stress. *J. Biol. Inorg. Chem.* **2010**, *15*, 3–14.

(105) Moreau, F.; Desroy, N.; Genevard, J. M.; Vongsouthi, V.; Gerusz, V.; Le Fralliec, G.; Oliveira, C.; Floquet, S.; Denis, A.; Escaich, S.; Wolf, K.; Busemann, M.; Aschenbrenner, A. Discovery of New Gram-Negative Antivirulence Drugs: Structure and Properties of Novel *E. coli* WaaC Inhibitors.

(106) Hobman, J. L.; Crossman, L. C. Bacterial Antimicrobial Metal Ion Resistance. *J. Med. Microbiol.* **2014**, *64*, 471–497.

6. General Conclusion and Comments

6.1. Conclusions

In this thesis, different approaches based on plasma polymerisation were used to fabricate antibacterial coatings. These included chitosan immobilised coatings onto pulsed plasma-enhanced chemical vapour deposited (PECVD) poly(glycidyl methacrylate) (poly(GMA)) films, atomised spray plasma deposited (ASPD) poly(acrylic acid), and ASPD polymer coatings using metallosurfactants as antibacterial release agents (Table 6. 1). The antibacterial coatings generated in this thesis were tested to evaluate their antibacterial activity, and experimentally characterised to analyse their physicochemical features to suggest a possible relationship between them, as described in the respective conclusion sections of each experimental chapter.

Table 6. 1: Key features and antibacterial efficacy of optimum antibacterial coatings in this thesis.

Technique	Type of Coating	Antibacterial Coating	Optimum Sample Conditions	Bacterial Reduction - 16 h *E. coli* / %	Bacterial Reduction - 16 h *S. aureus* / %
Pulsed PECVD + Dip Coating	Contact killing	Poly(GMA) + Chitosan	3% w/v Chitosan–2% v/v acetic acid aqueous solution	100	99.9
ASPD	Contact killing	Poly(Acrylic Acid)	Acrylic acid 99%, as received	100	Not tested
	Antibacterial agent release	Cu-CTAC / HEMA	2% w/v metallosurfactant/ precursor	100	100
		Fe-CTAC / HEMA	2% w/v metallosurfactant/ precursor	100	100
		Cu-amine / IDA	2% w/v metallosurfactant/ precursor	100	100

For the approach proposed in Chapter 3 Surface Immobilisation of Chitosan, chitosan was immobilised via covalent linkage to epoxide groups of pulsed plasma deposited poly(GMA). The 3% w/v chitosan–2% v/v acetic acid aqueous solution coating proved the best based on reductions in bacterial viability against both *Staphylococcus aureus* and *Escherichia coli* by contact killing, Table 6. 1. Overall, as mentioned in Chapter 1, contact killing coatings offer the advantage of directly interacting with bacteria without releasing antibacterial agents to the surrounding environment. Furthermore, the approach proposed in Chapter 3 implies a 2-step process where the pulsed PECVD is easy to apply and gives high quality results with minimum requirements of precursor as long as reaction parameters are controlled with precision, and the dip coating step is cheap and quick to apply. However, because the dip coating step requires a solution to be prepared, a large quantity of precursors may be needed; furthermore, durable post-treatment effects are not guaranteed since chitosan readily biodegrades and its antibacterial efficacy may vary depending on factors such as the deacetylation degree and commercial source. For these reasons, bacterial biofilm formation may occur when the chitosan on the surface degrades or is no longer available due to limitations in the dip coating technique. In general, this substrate-independent approach offers a simple way to obtain biodegradable antibacterial coatings.

In Chapter 4 Antibacterial Atomised Spray Plasma Deposited Poly(Acrylic Acid) Coatings, poly(acrylic acid) coatings were synthesised and processed in a solventless single ASPD step, displaying 100% of antibacterial activity by contact killing against *E. coli* over a 16 h-period, Table 6. 1. Apart from the general advantages of contact killing coatings mentioned above, the acidic nature of the proposed ASPD poly(acrylic acid) coating surface may offer additional adverse conditions to restrict bacterial proliferation and thus prevent biofilm formation, Chapter 4. However, further antibacterial testing against Gram-positive species and physicochemical characterisation are recommended to provide a greater understanding of how this coating might prevent biofilm formation and also optimise the conditions to avoid bacterial adaptation to the acidic environment of the coating.

Finally, in Chapter 5 Antibacterial Atomised Spray Plasma Deposited (Metallosurfactant/Polymer) Coatings, antibacterial agent release coatings were obtained using the ASPD approach and loading 2% w/v metallosurfactant/precursor solutions as the optimum concentration in all cases, Table 6. 1. Although all ASPD metallosurfactant/polymer coatings displayed rapid antibacterial activity by completely killing bacteria within minutes, their individual performance varied from coating to coating. For example, ASPD Cu-CTAC/HEMA and ASPD Cu-amine/IDA coatings showed antibacterial activity against *E. coli* from 5 minutes, while ASPD Fe-CTAC/HEMA showed antibacterial activity from 10 minutes. In contrast, ASPD Fe-CTAC/HEMA and ASPD Cu-CTAC/HEMA coatings killed all bacteria from the first minute when tested against *S. aureus*, whereas ASPD Cu-amine/IDA coatings displayed full antibacterial activity from 10 minutes, Chapter 5. Overall, the antibacterial activity of the ASPD metallosurfactant/polymer coatings investigated in this chapter is attributed to the impact of the metallosurfactant agents; however, the high toxicity of these coatings may also mean they are cytotoxic for mammalian cells. The characteristic agent-release antibacterial action (i.e., uncontrolled leaching) of these ASPD metallosurfactant/polymer coatings is indicative of robust but limited reusability after continuous rinsing steps, Chapter 5.

The development of antibacterial coatings is one of the multiple strategies that should be continuously innovated and improved to prevent bacterial infections and limit their spread, while attempting to avoid bacterial resistance to coating chemistry and limit the accumulation of bacterial debris on surfaces over time that may provide a protective layer for biofilm formation. Therefore, while the substrate-independent approaches proposed in this thesis to fabricate antibacterial coatings require further innovation and tests to fulfil all requirements in order not to be a risk for antibacterial resistance, they represent an alternative to overcome bacterial infections by limiting the spread of bacteria in the surrounding environment and are, therefore, amenable for multipurpose applications.

7. Appendix 1

7.1. Tables

Table A1. 1: Antibacterial activity of 2% w/v ASPD against *Escherichia coli* and *Staphylococcus aureus* at 1 min, 2 min, 5 min, and 10 min at room temperature, and 4 h and 16 h at 30 °C interacting times and temperature.

Time	Description	Bacterial Concentration / CFU mL^{-1}	
		E. coli	*S. aureus*
1 min	Untreated	$2.17 \times 10^8 \pm 7.57 \times 10^7$	$7.60 \times 10^7 \pm 7.94 \times 10^6$
	2% w/v ASPD Fe-CTAC/HEMA	$9.33 \times 10^7 \pm 5.77 \times 10^6$	0
	2% w/v ASPD Cu-CTAC/HEMA	$8.00 \times 10^7 \pm 2.65 \times 10^7$	0
	2% w/v ASPD Cu-amine/IDA	$1.37 \times 10^8 \pm 4.93 \times 10^7$	$5.82 \times 10^7 \pm 1.10 \times 10^7$
2 min	Untreated	$1.94 \times 10^8 \pm 5.98 \times 10^7$	$1.21 \times 10^8 \pm 2.31 \times 10^6$
	2% w/v ASPD Fe-CTAC/HEMA	$3.43 \times 10^7 \pm 1.54 \times 10^7$	0
	2% w/v ASPD Cu-CTAC/HEMA	$2.37 \times 10^7 \pm 1.18 \times 10^7$	0
	2% w/v ASPD Cu-amine/IDA	$4.17 \times 10^7 \pm 1.43 \times 10^7$	$7.72 \times 10^7 \pm 1.99 \times 10^7$
5 min	Untreated	$2.03 \times 10^8 \pm 3.40 \times 10^7$	$9.90 \times 10^7 \pm 1.40 \times 10^7$
	2% w/v ASPD Fe-CTAC/HEMA	$2.40 \times 10^6 \pm 8.21 \times 10^5$	0
	2% w/v ASPD Cu-CTAC/HEMA	$6.00 \times 10^2 \pm 1.34 \times 10^3$	0
	2% w/v ASPD Cu-amine/IDA	$6.00 \times 10^3 \pm 6.98 \times 10^3$	$3.40 \times 10^7 \pm 2.15 \times 10^7$
10 min	Untreated	$2.03 \times 10^8 \pm 3.40 \times 10^7$	$9.53 \times 10^7 \pm 5.03 \times 10^6$
	2% w/v ASPD Fe-CTAC/HEMA	$3.00 \times 10^3 \pm 1.00 \times 10^3$	0
	2% w/v ASPD Cu-CTAC/HEMA	0	0

Time	Description	Bacterial Concentration / CFU mL^{-1}	
		E. coli	*S. aureus*
	2% w/v ASPD Cu-amine/IDA	$2.67 \times 10^3 \pm 3.79 \times 10^3$	0
4 h	Untreated	$1.60 \times 10^9 \pm 3.61 \times 10^8$	$2.73 \times 10^9 \pm 1.03 \times 10^9$
	2% w/v ASPD Fe-CTAC/HEMA	0	0
	2% w/v ASPD Cu-CTAC/HEMA	0	0
	2% w/v ASPD Cu-amine/IDA	0	0
16 h	Untreated	$5.03 \times 10^9 \pm 5.51 \times 10^8$	$2.93 \times 10^9 \pm 8.08 \times 10^8$
	2% w/v ASPD Fe-CTAC/HEMA	0	0
	2% w/v ASPD Cu-CTAC/HEMA	0	0
	2% w/v ASPD Cu-amine/IDA	0	0

Table A1. 2: Antibacterial activity for 2 min contact time for 2% w/v ASPD Fe-CTAC/HEMA, Cu-CTAC/HEMA, and Cu-amine/IDA coatings, against *E. coli* wild-type and different mutant strains.

Bacterial strain	Description	Bacterial Concentration / CFU mL^{-1}
E. coli wild-type	Untreated	$1.94 \times 10^8 \pm 5.98 \times 10^7$
	2% w/v ASPD Fe-CTAC/HEMA	$3.43 \times 10^7 \pm 1.54 \times 10^7$
	2% w/v ASPD Cu-CTAC/HEMA	$2.37 \times 10^7 \pm 1.18 \times 10^7$
	2% w/v ASPD Cu-amine/IDA	$4.17 \times 10^7 \pm 1.43 \times 10^7$
E. coli ahpC	Untreated	$1.48 \times 10^8 \pm 5.26 \times 10^7$
	2% w/v ASPD Fe-CTAC/HEMA	$1.54 \ 10^7 \pm 3.21 \times 10^6$
	2% w/v ASPD Cu-CTAC/HEMA	$2.24 \times 10^7 \pm 5.77 \times 10^6$
	2% w/v ASPD Cu-amine/IDA	$1.63 \times 10^7 \pm 1.21 \times 10^7$
E. coli copA	Untreated	$2.58 \times 10^8 \pm 1.08 \times 10^8$
	2% w/v ASPD Fe-CTAC/HEMA	$2.33 \times 10^7 \pm 4.73 \times 10^6$
	2% w/v ASPD Cu-CTAC/HEMA	$4.30 \times 10^7 \pm 1.97 \times 10^7$
	2% w/v ASPD Cu-amine/IDA	$2.11 \times 10^8 \pm 1.12 \times 10^8$
E. coli cueO	Untreated	$2.13 \times 10^8 \pm 6.44 \times 10^7$
	2% w/v ASPD Fe-CTAC/HEMA	$2.57 \times 10^7 \pm 3.21 \times 10^6$
	2% w/v ASPD Cu-CTAC/HEMA	$3.33 \times 10^7 \pm 1.13 \times 10^7$
	2% w/v ASPD Cu-amine/IDA	$2.67 \times 10^8 \pm 1.53 \times 10^7$
E. coli feoB	Untreated	$1.90 \times 10^8 \pm 4.82 \times 10^7$

Bacterial strain	Description	Bacterial Concentration / CFU mL^{-1}
	2% w/v ASPD Fe-CTAC/HEMA	$1.60E \times 10^7 \pm 1.00 \times 10^7$
	2% w/v ASPD Cu-CTAC/HEMA	$4.72 \times 10^7 \pm 2.99 \times 10^7$
	2% w/v ASPD Cu-amine/IDA	$1.02 \times 10^8 \pm 5.49 \times 10^7$
E. coli fepA	Untreated	$1.20 \times 10^8 \pm 3.69 \times 10^7$
	2% w/v ASPD Fe-CTAC/HEMA	$3.73 \times 10^7 \pm 2.41 \times 10^7$
	2% w/v ASPD Cu-CTAC/HEMA	$3.62 \times 10^7 \pm 1.71 \times 10^7$
	2% w/v ASPD Cu-amine/IDA	$1.61 \times 10^8 \pm 3.08 \times 10^7$
E. coli katG	Untreated	$1.43 \times 10^8 \pm 7.63 \times 10^7$
	2% w/v ASPD Fe-CTAC/HEMA	$2.29 \times 10^7 \pm 1.62 \times 10^7$
	2% w/v ASPD Cu-CTAC/HEMA	$1.53 \times 10^7 \pm 1.13 \times 10^7$
	2% w/v ASPD Cu-amine/IDA	$5.48 \times 10^7 \pm 2.32 \times 10^7$
E. coli lpxL	Untreated	$1.26 \times 10^8 \pm 6.19 \times 10^7$
	2% w/v ASPD Fe-CTAC/HEMA	$2.32 \times 10^6 \pm 1.68 \times 10^6$
	2% w/v ASPD Cu-CTAC/HEMA	$4.20 \times 10^6 \pm 1.85 \times 10^6$
	2% w/v ASPD Cu-amine/IDA	$4.06 \times 10^7 \pm 8.41 \times 10^6$
E. coli mutM	Untreated	$1.97 \times 10^8 \pm 6.02 \times 10^7$
	2% w/v ASPD Fe-CTAC/HEMA	$9.00 \times 10^6 \pm 4.58 \times 10^6$
	2% w/v ASPD Cu-CTAC/HEMA	$5.23 \times 10^7 \pm 8.26 \times 10^6$
	2% w/v ASPD Cu-amine/IDA	$6.12 \times 10^7 \pm 2.52 \times 10^7$

Bacterial strain	Description	Bacterial Concentration / CFU mL^{-1}
E. coli rfaC	Untreated	$9.25 \times 10^7 \pm 4.07 \times 10^7$
	2% w/v ASPD Fe-CTAC/HEMA	$7.00 \times 10^3 \pm 8.79 \times 10^3$
	2% w/v ASPD Cu-CTAC/HEMA	$7.14 \times 10^2 \pm 1.86 \times 10^3$
	2% w/v ASPD Cu-amine/IDA	$2.36 \times 10^7 \pm 1.13 \times 10^7$
E. coli sodA	Untreated	$2.02 \times 10^8 \pm 2.40 \times 10^7$
	2% w/v ASPD Fe-CTAC/HEMA	$2.63 \times 10^7 \pm 1.10 \times 10^7$
	2% w/v ASPD Cu-CTAC/HEMA	$5.05 \times 10^7 \pm 2.47 \times 10^7$
	2% w/v ASPD Cu-amine/IDA	$1.67 \times 10^8 \pm 4.73 \times 10^7$
E. coli sodB	Untreated	$2.04 \times 10^8 \pm 3.58 \times 10^7$
	2% w/v ASPD Fe-CTAC/HEMA	$3.47 \times 10^7 \pm 2.27 \times 10^7$
	2% w/v ASPD Cu-CTAC/HEMA	$2.50 \times 10^7 \pm 1.09 \times 10^7$
	2% w/v ASPD Cu-amine/IDA	$1.70 \times 10^8 \pm 3.61 \times 10^7$
E. coli sodC	Untreated	$1.73 \times 10^8 \pm 9.22 \times 10^7$
	2% w/v ASPD Fe-CTAC/HEMA	$1.80 \times 10^7 \pm 1.04 \times 10^7$
	2% w/v ASPD Cu-CTAC/HEMA	$2.83 \times 10^7 \pm 1.04 \times 10^7$
	2% w/v ASPD Cu-amine/IDA	$4.25 \times 10^7 \pm 2.06 \times 10^7$

Table A1. 3: Recycling test for 2% w/v ASPD (metallosurfactant/polymer) coatings against *E. coli*.

	Recycling test against *E. coli*			
	Untreated	2% w/v ASPD Fe-CTAC/HEMA	2% w/v ASPD Cu-CTAC/HEMA	2% w/v ASPD Cu-amine/IDA
Initial	$1.60 \times 10^9 \pm 3.61 \times 10^8$	0	0	0
1st	$7.75 \times 10^9 \pm 1.06 \times 10^9$	0	0	0
2nd	$3.23 \times 10^9 \pm 1.59 \times 10^9$	0	$2.33 \times 10^4 \pm 4.04 \times 10^4$	0
3rd	$2.83 \times 10^9 \pm 2.89 \times 10^8$	$1.40 \times 10^3 \pm 3.13 \times 10^3$	$3.33 \times 10^3 \pm 2.31 \times 10^3$	$2.60 \times 10^5 \pm 2.60 \times 10^5$

Table A1. 4: Recycling test for 2% w/v ASPD (metallosurfactant/polymer) coatings against *S. aureus*.

	Recycling test against *S. aureus*			
	Untreated	2% w/v ASPD Fe-CTAC/HEMA	2% w/v ASPD Cu-CTAC/HEMA	2% w/v ASPD Cu-amine/IDA
Initial	$2.73 \times 10^9 \pm 1.03 \times 10^9$	0	0	0
1st	$9.93 \times 10^8 \pm 2.66 \times 10^8$	0	0	$4.80 \times 10^3 \pm 5.54 \times 10^3$
2nd	$1.57 \times 10^9 \pm 3.79 \times 10^8$	0	0	$2.86 \times 10^6 \pm 2.15 \times 10^6$
3rd	$1.23 \times 10^9 \pm 7.09 \times 10^8$	$2.25 \times 10^3 \pm 2.22 \times 10^3$	$6.20 \times 10^3 \pm 1.48 \times 10^3$	$1.41 \times 10^7 \pm 3.33 \times 10^6$
4th	$1.77 \times 10^9 \pm 5.03 \times 10^8$	$2.60 \times 10^3 \pm 4.72 \times 10^3$	$1.15 \times 10^5 \pm 4.96 \times 10^4$	$9.30 \times 10^7 \pm 1.99 \times 10^7$
5th	$7.63 \times 10^8 \pm 8.50 \times 10^7$	$4.60 \times 10^4 \pm 4.22 \times 10^4$	$1.39 \times 10^6 \pm 5.14 \times 10^5$	$1.37 \times 10^8 \pm 2.18 \times 10^7$